ISTANBUL TECHNICAL UNIVERSITY ★ GRADUATE SCHOOL

INVESTIGATING OLIVE TREES BY MONITORING PHENOLOGICAL STAGES USING MULTI-MODAL SATELLITE SENSOR DATA

Ph.D. THESIS

Haydar Muhammed AKÇAY

Department of Geomatics Engineering

Geomatics Engineering Programme

FEBRUARY 2024

ISTANBUL TECHNICAL UNIVERSITY ★ GRADUATE SCHOOL

INVESTIGATING OLIVE TREES BY MONITORING PHENOLOGICAL STAGES USING MULTI-MODAL SATELLITE SENSOR DATA

Ph.D. THESIS

Haydar Muhammed AKÇAY
(501172602)

Department of Geomatics Engineering

Geomatics Engineering Programme

Thesis Advisor: Prof. Dr. Şinasi KAYA

FEBRUARY 2024

İSTANBUL TEKNİK ÜNİVERSİTESİ ★ LİSANSÜSTÜ EĞİTİM ENSTİTÜSÜ

ÇOK-MODLU UYDU SENSÖR VERİLERİ KULLANILARAK FENOLOJİK AŞAMALARININ İZLENMESİYLE ZEYTİN AĞAÇLARININ ARAŞTIRILMASI

DOKTORA TEZİ

Haydar Muhammed AKÇAY
(501172602)

Geomatik Mühendisliği Anabilim Dalı

Geomatik Mühendisliği Programı

Tez Danışmanı: Prof. Dr. Şinasi KAYA

ŞUBAT 2024

Haydar Muhammed AKÇAY, a Ph.D. student of ITU Graduate School student ID 501172602, successfully defended the thesis entitled "INVESTIGATING OLIVE TREES BY MONITORING PHENOLOGICAL STAGES USING MULTI-MODAL SATELLITE SENSOR DATA", which he prepared after fulfilling the requirements specified in the associated legislations, before the jury whose signatures are below.

Thesis Advisor :	**Prof. Dr. Şinasi KAYA** Istanbul Technical University	....
Jury Members :	**Prof. Dr. Elif SERTEL** Istanbul Technical University	....
	Prof. Dr. Cem GAZİOĞLU Istanbul University	....
	Prof. Dr. Bülent BAYRAM Yıldız Technical University	....
	Assoc. Prof. Dr. Uğur ALGANCI Istanbul Technical University	....

Date of Submission : 07 December 2023
Date of Defense : 09 February 2024

To the 100th anniversary of the Turkish Republic,

FOREWORD

I would like to thank Prof. Dr. Şinasi KAYA for his invaluable support, patience, guidance and encouragement throughout my thesis and academic work. I also would like to thank Prof. Dr. Elif SERTEL for her invaluable contributions and guidance during my thesis and academic progress. I would like to thank as well Prof. Dr. Cem GAZİOĞLU and Assoc. Prof. Dr. Uğur ALGANCI for their contributions and guidances.

I would particularly like to thank Prof. Dr. Jadu DASH for his hospitality, patience, academic advises and unique character during and after my visit to the Unversity of Southampton.

I would like to thank Izmir Olive Research Institute staff, particularly Dr. Ünal KAYA and Metin ALTINDAĞ, for sharing knowledge and data.

I would like to thank my colleague Samet AKSOY for his help in programming.

I would like to thank my brother Dr. Fuzuli Ağrı AKÇAY for his encouragement, support and guidance during my entire academic and personal life.

I would like to thank my wife Saliha and my parents for their continuous patience and support in this journey.

I appreciate the financial support of the Scientific and Technological Council of Türkiye (TÜBİTAK) during my one-year visit to the University of Southampton via the International Research Fellowship Programme for Ph.D. Students 2214-A with application number 1059B142000675.

December 2023

Haydar Muhammed AKÇAY
(Geomatics Engineer, M.Sc.)

TABLE OF CONTENTS

Page

ABBREVIATIONS

ACE	**:** Arbor Crown Enumeration
API	**:** Application Prograxmming Interface
AR	**:** Autoregressive
ASTER	**:** Advanced Spaceborne Thermal Emission and Reflection Radiometer
AVHRR	**:** Advanced Very High Resolution Radiometer
BSI	**:** Bare Soil Index
CHIRPS	**:** Climate Hazards Group InfraRed Precipitation with Station
CHT	**:** Circular Hough Transform
CLMS	**:** Copernicus Land Monitoring Service
CLUAS	**:** Clustering Assessment
dB	**:** Decibel
DEM	**:** Digital Elevation Model
DIAS	**:** Data and Information Access Services
DN	**:** Digital Number
DOY	**:** Day of Year
DSM	**:** Digital Surface Model
DVI	**:** Difference Vegetation Index
DVIR	**:** Difference Vegetation Red Index
ECV	**:** Essential Climate Variable
EEA	**:** European Economic Area
EOS	**:** End of Season
EOSD	**:** End of Season Date
ESA	**:** European Space Angency
ETM	**:** Enhanced Thematic Mapper
EU-DEM	**:** European Digital Elevation Model
EVI	**:** Enhanced Vegetation Index
GCOS	**:** Global Climate Observing System
GDEM	**:** Global Digital Elevation Map
GEE	**:** Google Earth Engine
GEOBIA	**:** Geographic Object-Based Image Analysis

GLCM	: Grey-Level Co-occurrence Matrix
GPM	: Global Precipitation Measurement
GPP	: Gross Primary Productivity
GRD	: Ground Range Detected
HR-VPP	: High-Resolution Vegetation Phenology and Productivity
L2A	: Level 2A
LC	: Land Cover
LST	: Land Surface Temperature
MAF	: Ministry of Agriculture and Forestry
MERIS	: Medium Resolution Imaging Spectrometer
MODIS	: Moderate Resolution Imaging Spectroradiometer
MTCI	: MERIS Terrestrial Chlorophyll Index
NDBI	: Normalized Difference Built-up Index
NDTI	: Normalized Difference Tillage Index
NDVI	: Normalized Difference Vegetation Index
NDVIre	: The Red-Edge NDVI
NPP	: Net Primary Productivity
NRMSE	: Normalized Root Mean Square Error
PPI	: Plant Phenology ındex
PVI	: Perpendicular Vegetation Index
RGB	: Red Green Blue
RMSE	: Root Mean Square Error
RVI	: Radar Vegetation Index
S2A	: Sentinel-2A
S2B	: Sentinel-2B
SAR	: Synthetic Aperture Radar
SAVI	: Soil Adjusted Vegetation Index
SOS	: Start of Season
SOSD	: Start of Season Date
SRTM	: Shuttle Radar Topography Mission
SSM	: Surface Soil Moisture
TPROD	: Total Productivity
TRMM	: Tropical Rainfall Measuring Mission
TUIK	: Turkish Statistical Institute
TÜİK	: Türkiye İstatistik Kurumu (TÜİK)

VHR	**:** Very High Resolution
VI	**:** Vegetation Indices
VPP	**:** Vegetation Phenology and Productivity
WEkEO	**:** WE knowledge Earth Observation
WV	**:** Water Vapour

SYMBOLS

B1 – B12	**:** Band numbers
DVI	**:** Difference vegetation index
DVI_S	**:** DVI of the soil
K	**:** Gain factor
M	**:** Site-specific canopy maximum DVI
n	**:** Number of observations
$\sigma°$	**:** Backscatter coefficient (sigma nought)
VH	**:** Polarization mode vertical/horizontal
VV	**:** Polarization mode vertical/vertical
P_i	**:** Expected value
O_i	**:** Observed value
$\bar{O}$	**:** Mean value

LIST OF TABLES

Page

LIST OF FIGURES

Page

INVESTIGATING OLIVE TREES BY MONITORING PHENOLOGICAL STAGES USING MULTI-MODAL SATELLITE SENSOR DATA

SUMMARY

Olive tree is crucial due to its social, cultural and economical values to the Mediterranean society. The demand for olive oil and other products produced from olives is constantly increasing with the global trend of healthy lifestyle. To meet this demand, olive trees are grown in different regions as long as climatic conditions allow. However, global warming and the environmental disasters adversely affect olive trees. As a result, during the past 20 years, several studies on olive trees have been carried out utilising a variety of remote sensing techniques and platforms for diverse agronomic aims, including tree identification, fertilisation, irrigation etc. However, researches on olive trees in Türkiye is limited and to the best knowledge, no studies on olive trees have been performed using remote sensing techniques on regional scale in Türkiye. Therefore, the aim of this research is to map olive trees of Izmir Province, one of the main olive growing regions, for the first time using Sentinel-1 and Sentinel-2 data. The phenology and productivity of olive trees of Izmir are investigated as well, using CLMS HR-VPP products on a regional scale for the first time.

The effectiveness of multitemporal Sentinel-1 and -2 data for olive tree classification is evaluated in Chapter 2. Datasets consist of May and October composites of each year between 2017 and 2021 are used in order to capture the different phenological stages of olive trees. Random forest classfier is implemented to datasets. Classification map of Izmir province is produced and number of classes are reduced to two classes “olive” and “non-olive” to create binary olive tree map. Results are validated using both K-fold cross validation and confusion matrix methods. The results show that Sentinel-1 data can map olive trees with up to 70%, while Sentinel-2 data succed up to 90%. However, the combined usage of Sentinel-1 and Sentinel-2 datasets show the best classification accuracy for olive trees. This is a clear example of the advantage of mapping tree crops using radar and optical data fusion. In addition, this is the first olive tree distribution map of Izmir Province, and it's essential for creating a successful management plan. Using data from Sentinel-1 and Sentinel-2, this research assessed the possibilities of mapping olive trees regionally.

The phenology and productivity of olive trees of Izmir Province are investigated in Chapter 3. Copernicus Land Monitoring Sevices’s High-Resolution Vegetation Phenology and Productivity (HR-VPP) metrics are used. Interannual variability of phenology metrics (SOSD, EOSD) of olive trees are evaluated and the effects of climatic conditions such as precipitation and surface soil mositure as well as elevation to the productivity of olive trees are investigated. Results demonstrate that precipitation have a significant effect on EOSD. Additionally, a strong correlation between total productivity and elevation and climatic conditions, such as precipitation and surface soil moisture, is observed. The strong corrrelation between productivity of olive trees and TUIK crop yield data (R^2 = 0.77) verifies the efficiency of CLMS HR-

VPP metrics to be used on a regional and global scale. This is one of the first attempts to utilise the power and potential of WEkEO and GEE cloud infrastructures using Sentinel-1 and Sentinel-2 data as well as CLMS HR-VPP products. Moreover, this is the first regional satellite-based phenology and productivity research on olive trees in Türkiye.

Field trips to the districts of Bergama and Bayındır are explained in Chapter 4, to look into the reasons of the overestimation and underestimation issues that are discussed in the Chapter 2 and Chapter 3. As olive forests in hillsides are mixed with different types of trees and the other background vegetation around olive trees, olive trees are more likely to be misclassified in hilly regions.

In conclusion, this research encourages the use of the cloud infrastructure capabilities of GEE in order to develop a scalable methodology for studies on tree crops at regional to global scales. If this method is expanded to other parts of Türkiye, it will allow for the first country-scale research on olive trees.

ÇOK-MODLU UYDU SENSÖR VERİLERİ KULLANILARAK FENOLOJİK AŞAMALARININ İZLENMESİYLE ZEYTİN AĞAÇLARININ ARAŞTIRILMASI

ÖZET

Zeytin ağacı, Akdeniz bölgesi ve halkı için önemli bir yere sahiptir. Kuraklığa dayanıklı bir tür olması sebebiyle toprağı erozyondan korur. Akdeniz halkı için sosyal, kültürel ve mutfak açısında vazgeçilmezdir. Zeytin yağı bölgenin kalkınması için temel ekonomik değer taşır. Küresel olarak artan sağlıklı beslenme trendiyle zeytin yağına ve zeytinden üretilen diğer ürünlere talep sürekli olarak artmaktadır. Bu talebi karşılamak için zeytin ağaçları iklim koşullarının el verdiği farklı bölgelerde de yetiştirilmektedir. Fakat, küresel ısınma ve onun etkisiyle yaşanan çevre felaketleri zeytin ağaçalarını olumsuz etkilemektedir. Bu yüzden son 20 yılda zeytin ağaçları üzerine çok sayıda araştırma yapılmıştır. Fakat bu araştırmaların çoğu yerel ölçekte kalmış ve genellikle tek sensörlü uzaktan algılama verileri kullanılarak gerçekleştirilmiştir. Örnek vermek geekirse, yapılan çalışmaların büyük çoğunluğunda optik uydu görüntülerinden faydalanılmıştır. Bu durum bulutlu geçen sonbahar ve özellikle kış aylarında araştırmaların kesintiye uğramasına sebep olmaktadır. Bunun üstesinden gelmek için İnsansız Hava Araçlarıyla (İHA) yapılan araştırmaların sayısı artmaktadır. Fakat İHA ile yapılan çalışmalar masraflı olduğu için yerel ölçekte kalmaktadır. Bölgesel ve ülke çapında çalışmalarda uydu götüntülerinin kullanımı kaçınılmaz olmaktadır. Bulutlu geçen kış aylarında çalışmaların kesintiye uğramaması için radar görüntüleri büyük önem arz etmektedir. Fakat yapılan çalışmalar çok ufak bir kısmı radar görüntülerinden faydalanmıştır.

Zeytin yetiştiriciliği diğer Akdeniz ülkelerinde olduğu gibi Türkiye’de de hayati öneme sahiptir. Kayda değer sayıda aile işletmesi geçimini zeytincilikten sağlamaktadır. Buna karşın, zeytin ağacı üzerine yapılan çalışmalar diğer Akdeniz ülkelerine nazaran kısıtlı kalmıştır. Fakat uzaktan algılama teknikleriyle yapılan bazı yerel ölçekte çalışmalar zeytin ağaçlarının konum ve miktarında dalgalanmalar olduğunu belirtmişlerdir. Bunun ötesinde zeytin ağacı genetik olarak var yılı yok yılı olan bir bitkidir ve zeytin ve zeytin yağı üretiminde yıllara bağlı olarak önemli dalgalanmalar yaşanmaktadır. Bunların yanı sıra güncel zeytin haritalarının eksikliği zeytin ağaçlarının takip edilmesini zorlaştırmaktadır.

Yukarıda belirtilen sebepler dikkate alınarak bu çalışmada Sentinel-1 ve Sentinel-2 uydu verileri kullanılarak (i) zeytin ağaçlarının bölgesel olarak haritalanması ve (ii) bu harita kullanılarak zeytin ağaçlarının 2017 ile 2021 yılları zamansal fenolojisinin incelenmesi ve iklim koşulları ile rakımın zeytin ağaçlarının üretkenliğine olan etkisi araştırılmıştır. Türkiye’nin en önemli zeytincilik şehirlerinden biri olan İzmir bu tezin çalışma bölgesi olarak belirlenmiştir.

Tezin ikinci bölümünde İzmir’in güncel zeytin ağacı haritasının çıkarılması amaçlanmıştır. Bu kapsamda Sentinel-1 ve Sentinel-2 verileri kullanılmış ve örnekleme için Google Haritalardan alınan yüksek çözünürlüklü uydu görüntülerinden

faydalanılmıştır. Zeytin haritası oluşturmadan önce, çalışma alanını temsil eden sınıf sayısını belirlemek amacıyla ESA WorldCover 2020 v100 sınıfları referans alınmıştır. Bunlar: "ekili alan", "ağaç örtüsü", "çıplak/seyrek bitki örtüsü", "yerleşim", "çayır", "çalılık", "kar/buz" ve "su". "Kar/buz" ve "su" sınıfları daha önce maskelenmiş oldukları için sınıflandırmadan hariç tutulmuştur. Ayrıca "zeytin" sınıfı dahil edilmiş ve "çıplak/seyrek bitki örtüsü" sınıfının zeytin sınıfıyla karışmasını önlemek amacıyla "toprak" ve "seyrek bitki örtüsü" olarak iki sınıfa ayrılmıştır. Sonuç olarak zeytin sınıfı da dahil olmak üzere 7 sınıf belirlenmiştir. Zeytin ağaçlarını daha yüksek doğrulukta sınıflandırmak için, farklı fenolojik aşamalar olan Mayıs, Temmuz ve Ekim aylarının görüntüleri seçilmiştir. Zeytin fenolojisi rakım ve enleme göre değişiklik göstermekle birlikte Mayıs ayı çiçeklenme, Temmuz ayı yaprakların hafif sararıp meyvenin büyüdüğü ve çekirdeğin sertleştiği dönem, Ekim ayı ise meyve olgunlaşma ve renklenme aşaması olarak kaul edilmiştir. Mayıs, Temmuz ve Ekim aylarına ait aylık kompozit görüntüler oluşturularak bunların farklı kombinasyonları (Mayıs + Temmuz, Mayıs + Temmuz + Ekim ve Temmuz + Ekim) test edilmiştir. Bunlar arasından en yüksek doğruluğu veren Temmuz + Ekim kombinasyonu ("g" veri seti) nihai sınıflandırma için seçilmiştir. Bu veri setlerine rastgele orman (random forest) sınıflandırması uygulanmıştır. Rastgele orman sınıflandırıcısı, yüksek doğruluk ve düşük bias göstermesi sebebiyle özellikle büyük veri kümelerinin sınıflandırılmasında tercih edilmektedir. Doğruluk değerlendirmesi, K-fold çapraz doğrulama ve hata matrisi kullanılarak gerçekleştirilmiştir. Sonuçlar, Sentinel-1'in tek başına zeytin ağaçlarının haritalanması için orta düzeyde bir sınıflandırma doğruluğu sağladığını göstermiştir (%70'e kadar). Buna karşılık, Sentinel-2'den üretilen optik verilerin kullanılması zeytin ağacı sınıflandırmasını önemli ölçüde iyileştirmiştir (%90'a kadar). Bununla birlikte, Sentinel-1 ve Sentinel-2 veri kümelerinin birleşimi, İzmir İlinde zeytin ağacı sınıflandırması için en iyi sonucu vermiştir. Son aşamada, zeytin dışındaki sınıflar maskelenerek "zeytin" ve "zeytin değil" olmak üzere iki sınıflı nihai zeytin haritası üretilmiştir. Bu harita %98 genel doğruluk ve %93 üretici doğruluğu ile elde edilmiştir. K-fold çapraz doğrulama sonuçları da %90 üzerinde çıkmıştır. Bu sonuçlar, çok yüksek çözünürlüklü görüntülerle yapılan çalışmaların %89 ile %99 arasında doğruluk verdiği dikkate alındığında cesaret vericidir. TÜİK'ten elde edilen 5 yıllık ortalama zeytin alanı, sınıflandırılan alan ile kıyaslanmıştır. Bayındır ve Bergama ilçelerinde korelasyonu bozan eksik ve fazla kestirimler olduğu (underestimation, overestimation) gözlemlenmiştir. Eksik ve fazla kestirimlerin nedenlerini araştırmak üzere saha gözlemleri gerçekleştirilmiştir. Saha gözlemleri sonucu bu iki ilçe karşılaştırmadan hariç tutulmuş ve TÜİK verileriyle oldukça iyi uyumluluk yakalanmıştır (R^2 = 0.77). Bu sonuçlar, meyve ağaçlarının haritalanmasında optik ve radar verilerinin sinerjik kullanımının avantajını açıkça ortaya koymaktadır. Ayrıca, bir bulut altyapılı hesaplama platformu olan Google Earth Engine'in gücü kullanılaarak meyve ağaçlarının bölgesel ve küresel çapta ölçeklenebilirliği mümkün kulunmıştır.

Tezin üçüncü bölümünde, ikinci bölümde üretilen İzmir'in güncel zeytin haritası kullanılarak zeytin ağaçlarının 2017-2021 yılları arasında fenolojik değişkenliği incelenmiş, iklim ve rakımın zeytin ağacının üretkenliğine (productivity) olan etkisi araştırlımıştır. Copernicus Yer İzleme Servisi (Copernicus Land Monitoring Service)'nin yüksek çözünürlüklü bitki fenoloji ve üretkenlik parametreleri (High-Resolution Phenology and Productivity) olan büyüme sezonu başlangıç günü (start of season date), büyüme sezonu bitiş günü (end of season date) ve toplam üretkenlik (total productivity - TPROD) parametreleri kullanılmıştır. Bitki fenoloji indeksi (plant phenology index) kullanılarak yıllık olarak üretilen bu parametreler Copernicus'un veri sağlayıcısı WEkEO'dan elde edilmiştir. Bunların yanında, Climate Hazards Group InfraRed Precipitation with Station (CHIRPS) tarafından sunulan yağış verisi, Moderate Resolution Imaging Spectroradiometer (MODIS) tarafından sunulan yer yüzeyi sıcaklığı verisine ek olarak Corpernicus'un sağladığı toprak yüzey nemliliği (surface soil moisture) ve sayısal arazi modeli (EU-DEM) verilerinden faydalanılmıştır. Zeytin ağaçlarının üretkenliğini karşılaştırmak için TÜİK zeytin rekolte verileri baz alınmıştır. Sonuçlara göre, 2017-2021 yılları arasında SOSD trendi, EOSD'ye göre daha az değişkenlik göstermiştir. 2018 yılına ait SOSD diğer yıllarla benzerlik göstermesine rağmen EOSD oldukça erken gerçekleşmiştir. Bunun potansiyel nedenleri araştırıldığında 2018 yılında EOSD tarihinden önceki üç ayda toplam yağış mikatarının diğer yıllara göre oldukça yüksek olduğu tespit edilmiştir. Buna göre EOSD öncesi yoğun yağışın büyüme mevsimini önemli ölçüde kısalttığı gözlemlenmiştir. Bunun dışında, sonuçlar SOSD ve EOSD'nin 1000 m rakıma kadar tutarlı bir şekilde geciktiğini göstermiştir. Bununla birlikte, EOSD gecikmesi 1000 m üzerindeki rakımda yavaş devam etmiştir. SOSD trendi 2000 m rakıma kadar düzenli olarak gecikmiştir. Gecikme trendi 2000 m yükseklikten sonra yavaşlamıştır. Buna göre, rakım arttıkça zeytin ağaçlarının SOSD ve EOSD'si gecikmiş ve mevsim uzunluğu bir miktar kısalmıştır. Ayrıca, SOSD ile rakım arasındaki korelasyonun (R^2 = 0.43) EOSD ile rakım arasındaki korelasyondan (R^2 = 0.22) önemli ölçüde yüksek olduğu görülmüştür. Rakım arttıkça zeytin ağaçlarının toplam verimliliği azalmıştır. Bununla birlikte, 500-800 m rakım arasındaki ortalama toplam üretkenlik değerinda hafif bir dalgalanma gözlemlenmiştir. 800 m rakımın üzerinde ortalama toplam üretkenlik tutarlı bir şekilde azalmaya devam etmiştir. Kümülatif toplam üretkenlikise 600 metre yüksekliğe kadar büyük bir hızla azalmış, daha sonra, düşüş eğilimi devam etmesine karşın düşüş hızı yavaşlamıştır. Toplam üretkenlik ile TÜİK zeytin rekolte verileri kıyaslandığında güçlü bir korelasyon (R^2 = 0.77) elde edilmiştir. Yağışın farklı fenolojik dönemlerde toplam üretkenlik üzerindeki etkilerini araştırmak için ilkbahar, yaz, sonbahar ve yıllık yağışlar dikkate alınmıştır. Sonuçlar, yağışın toplam üretkenlikle güçlü bir şekilde ilişkili olduğunu göstermiştir. Ayrıca, ilkbahar ve sonbahar yağışlarının toplam verimliliğe etkisi yaz yağışlarına nazaran daha fazla olmuştur. İlkbahar, yaz, sonbahar ve yıllık yüzey toprak nemliliğinin zeytin ağaçlarının toplam verimliliğine etkileri incelenmiştir. Sonuçlar, üretkenliğin yüzey toprak nemi ile güçlü bir korelasyona sahip olduğunu göstermiştir. İlkbahardaki yüzey toprak nemi ile toplam üretkenlik arasındaki korelasyon (R^2 =0.62), yaz (R^2 =0.51) ve sonbahardaki toprak yüzey nemliğinden (R^2 =0.51) arasındaki korelasyondan yüksek çıkmıştır. Son olarak, 2017-2021 yılları arasını kapsayan yıllık SOSD, EOSD ve TPROD haritaları üretilmiştir.

Tezin ikinci ve üçüncü bölümlerinde elde edilen sonuçlar Bayındır ver Bergama ilçelerinde sırasıyla düşük ve yüksek kestirim olduğunu göstermiştir. Bu yüzden bu iki ilçede saha gözlemleri gerçekleştirilmiştir. Tezin dördüncü bölümü bu saha gözlemlerini açıklamaktadır. Zeytin ağaçları tepelik alanlarda karışık bitki örtüsü sebebiyle yanlış sınıflandırmaya daha meyilli olmaktadır. Yapılan saha ziyaretlerinde bu durum göz önünde bulundurulmuştur. Bayındır'da yapılan saha gözlemleri göstermiştir ki bazı bölgelerde ormanlar zeytinliğe dönüştürülmüştür. Bu bölgelerde zeytinlikler seyrek bitki kanopisi sergilediği için yanlış sınıflandırılmalar gözlemlenmiştir. Buna ek olarak, bazı bölgelerde yoğun bitki örtüsü sebebiyle yine yanlış sınıflandırmalar gözlemlenmiştir. Her iki sebeple zeytin olan kısımlar zeytin değil olarak sınıflandırıldığından Bayındır ilçesinde düşük kestirim gerçekleşmiştir. Bergama ilçesnin bazı yüksek rakımlı bölgelerinde meşe ağaçlarının (holm oak) zeytin olarak yanlış sınıflandırıldığı gözlemlenmiştir. Meşe ağacının morfolojik yapısı, kanopi şekli ve yaprak renginin zeytinle benzerlik gösterdiği anlaşılmıştır. Buna ek olarak, çam ormanın seyrek olduğu bazı yerlerde zeytin olarak yanlış sınıflandırılma olduğu gözlemlenmiştir. Bu sonuçlar, Bergama ilçesinde fazla kestirime yol açmıştır.

Sonuç olarak, Sentinel-1 ve Sentinel-2 verileri kullanılarak zeytin ağaçlarının bölgesel ve küresel ölçekte iyi bir doğrulukla sınıflandırılabilir olduğu gösterilmiştir. Ayrıca, Copernicus tarafından sunulan HR-VPP parametreleri kullanılarak zeytin ağaçlarının fenoloji ve üretkenliklerinin bölgesel ve küresel ölçekte iyi bir doğrulukla takip edilmesinin mümkün olduğu sonucuna varılmıştır. Bu tezde sunulan yöntem Türkiye'nin diğer bölgelerinde de uygulanırsa, zeytin ağaçlarının ülke çapında haritalanarak fenolojik ve üretkenlik analizi gerçekleştirilebilir.

1. INTRODUCTION

Monitoring the distribution and production from agricultural fields is more important than ever before due to the global challenges such as climate change and rising food demand from the world's growing population (Heupel et al., 2018). Globally, significant conservation and resource-use efficiency improvements are required to meet the food demand while also halting and reversing ecological degradation (Vos and Bellu, 2019). As a result, continuously updated information on food production is critical because near-real time monitoring is essential for responding to catastrophic occurrences induced by changing climatic conditions such as extreme events, and therefore, minimising their impact on the global food supply (Weiss et al., 2020). In this regard, crop type mapping and continuously monitoring the phenology and productivity of crops are crucial.

Olive trees (*Olea europaea*) are very important to environment and human culture in Mediterranean region. They play a key role to conserve soil and prevent erosion, functioning as a protector. In addition, olive crop is vital as an economical resource. Olive cultivation has been one of the main economical incomes for the Meditarranean society. With increasing healthy life style trend globally, demand on olive and olive-derived products, particularly olive oil increases. However, as climate change and environmental issues become more severe, olive trees need more attention. Therefore, the current distribution of olive trees need to be mapped and monitored continuously.

The seasonality of olive trees plays a crucial role in the growth, development, and productivity of the crop, understanding the exact time of flowering is crucial for successful pollination. In order to select the appropriate harvest time, it is essential to monitor the seasonal trend of fruit growth. Harvest time is vital to determine the ideal quality of the crop such as size, colour, oil and nutritional content, and flavour. Apart these, a proper irrigation plan and pest management in certain phenological stages are also important. For these reasons, the phenology and productivity of olive trees need to be monitored continuously. This can help farmers and decision makers to develop methods to sustain & improve the efficiency and the quality of the crop.

Consequently, many studies have been conducted over the past 20 years on olive trees using various remote sensing methods and platforms on different agronomic purposes such as tree identification/classification, fertilization, irrigation, disease management and phenophase estimation among others (Messina et al., 2022; Anastasiou et al., 2023). The literature research on “classification & tree detection” and “phenology and productivity” which are the interest of this thesis are presented in Chapter 2 and Chapter 3, respectively.

Türkiye is one of the most olive producer countries in the world and was ranked fifth in 2020 with 1 316 000 tons of olive production (FAO, 2022). Olive is the fourth most produced fruit (TUIK, 2019) and olive production is primarily a traditional family business of which around 320 000 families live off (General Directorate of Traders, Artists and Cooperatives of Türkiye, 2020). However, even though olive cultivation is strategically important for the economy of Türkiye, studies reported temporal alterations of spatial distribution of olive trees in regards of damaging and growing practices (Doygun 2009; Efe et al., 2013; Gulcin, 2019). Besides, olive oil production shows high periodicity (75%) year by year which is between 170 000 and 200 000 tons in highly efficient years and 40 000 – 60 000 tons in low efficient years in the country. This ratio is reported 35% - 40% in Spain, which is the leader of the industry. Furthermore, yield estimation in Türkiye is carried out by experts, based on their self-experiences and observations. According to the “Olive and Olive Oil Report” of General Directorate of Traders, Artists and Cooperatives of Türkiye (2020) a database and geographical information system using remote sensing techniques is proposed as a solution to determine the number of olive trees precisely and have reliable data. However, researches on olive trees in Türkiye is limited. In addition, no province-level and country-level olive tree map have been produced, yet. For this reason, a province-level olive tree investigation is decided to conduct in this research. Izmir Province, one of the main olive producer provinces in Türkiye, is selected as the study area of this research.

In Chapter 2 of the thesis, olive tree distribution of Izmir province was aimed to be determined. The performance of combined usage of Sentinel-1 and -2 data was evaluated for the first time, in a regional mapping of olive trees. The k-fold cross-validation method was used to evaluate the results, and the final olive tree map of Izmir was created. The area covered by olive trees at the district-level was determined and validated using official data from the Turkish Statistical Institute (TUIK).

In Chapter 3, the inter-annual variability of phenology of olive trees of Izmir and the relationships between productivity and climatic conditions and elevation were investigated covering a five-year period between 2017 and 2021. The results demonstrated that precipitation and elevation had a substantial impact on the phenology of olive trees. Furthermore, findings showed that total productivity is closely related to external factors such as meteorological conditions (i.e. precipitation and surface soil moisture) and elevation.

In Chapter 4 of the thesis, the results of field observations to the Bayındır and Bergama districts were explained. Field visits to Bayndır and Bergama districts were decided based on the findings in the Chapter 2 and Chapter 3. According to field observations, underestimation in Bayındır and overestimation in Bergama caused by misclassifications due to the mixed vegetation among olive trees in the hillsides of these districts, were observed.

2. EVALUATING THE POTENTIAL OF MULTI-TEMPORAL SENTINEL-1 AND SENTINEL-2 DATA FOR REGIONAL MAPPING OF OLIVE TREES[1]

2.1 Introduction

Crop type mapping is important for agricultural practices, such as crop management and yield estimation (Haboudane et al., 2002; Doraiswamy et al., 2004; Thenkabail et al., 2009; Zhong et al., 2011; Ren et al., 2022a) because different agronomic practices are required for efficient crop production (Roma and Catania, 2022) under varying climatic conditions. For example, comprehensive current agricultural maps of arid and semi-arid regions such as the Mediterranean are essential for water planning and irrigation management (El-Magd and Tanton, 2003; Xie et al., 2007; Zhong et al., 2011; Qader et al., 2018). However, crop-type mapping using traditional methods generally requires routine ground visits to small fields with limited access, which may result in inconsistent outputs owing to the lack of standardised reporting protocols (Peña et al., 2014). Additionally, this field-based procedure is expensive, time-consuming (Peña et al., 2014; Maponya et al., 2020) and biased (Gilbertson et al., 2017).

Remote sensing provides an alternative method for crop monitoring which is more reliable and cost-effective (Peña-Barragán et al., 2008; Peña et al., 2014; Gilbertson et al., 2017) and offers freely available Earth Observation satellite data over large areas (Maponya et al., 2020) at different spectral, spatial, and temporal resolutions. Nevertheless, spatial and temporal resolutions are generally complementary characteristics of satellite data (Ranghetti et al., 2020). At this point, Sentinel missions, in particular the Sentinel-2 mission (ESA, 2015), marked a milestone by meeting expectations for both high spatial (i.e. 10 m to 60 m) and temporal resolutions (i.e. ≤ 5 days). This becomes significant considering there was international consensus for

[1] This chapter is based on: Akcay, H., Kaya, S., Sertel, E., Aksoy, S., and Dash, J. (2023) Evaluating the Potential of Multi-temporal Sentinel-1 and Sentinel-2 Data for Regional Mapping of Olive Trees, International Journal of Remote Sensing, 44(23), 7338-7364, DOI: 10.1080/01431161.2023.2282404

the need for systematic 50 m resolution global mapping of vegetation biophysical variables at ≤ 10 days revisit time (GCOS, 2016; Djamai et al., 2019).

The olive tree (*Olea europaea*), an indigenous Mediterranean plant, is cultivated in approximately 40 countries globally, covering over 10.5 million hectares of land. Over 98% of this olive crop is grown in Mediterranean countries (Roma and Catania, 2022). Besides their economic benefits, olives are indispensable to Mediterranean society for their social and cultural influence as well as their aesthetic and culinary values (Gulcin, 2019), with olive oil being the main ingredient of Mediterranean cuisine (Khan et al., 2018). Moreover, olive-derived products such as olive oil are considered healthy alternatives, causing an increase in global demand. For example, olive oil and table olive consumption increased worldwide by 96% and 79%, respectively, between 1990 and 2020 (International Olive Council, 2022). For these reasons, sustainable olive cultivation based on sound management plans is crucial for the future of the olive industry. First, updated and consistent high-resolution mapping showing the spatial distribution of olive trees is useful for oliviculture applications, such as crop monitoring, irrigation planning, disease management and yield estimation (Roma and Catania 2022). Furthermore, to help inform the agricultural policies of local and central government institutions, it is necessary to verify farmer yield claims and planning subsidies (Alganci et al., 2018). Accordingly, over the past 20 years, numerous studies have focused on providing information on olive tree distribution using various remote sensing data and image analysis techniques (Messina et al., 2022; Anastasiou et al., 2023); these include blob detection, template matching, image segmentation, unsupervised and supervised classification using machine learning algorithms, and deep learning (Messina et al., 2022).

However, the majority of these studies on olive tree detection/classification focused on small-scale practices and utilised object-based techniques using very high resolution (VHR) images (see Table 2.1). Owing to the extensive distribution of olive trees throughout the Mediterranean region, working on a regional scale makes managing the high volume of VHR data costly, time-consuming and challenging. Furthermore, most studies on olive tree identification rely on data from only one sensor, particularly optical remote sensing data. Only 5% of the studies included radar data (Anastasiou et al., 2023), despite satellite radar data being crucial for uninterrupted large-scale observations of olive trees during cloudy periods, particularly in winter. To address this gap, we evaluated the performance of a multitemporal fusion of Sentinel-1 and Sentinel-2 data for the first time in regional olive tree mapping. Izmir, an ancient olive cultivation region in Türkiye, was selected as the study area because there was no detailed map of olive tree distribution across the province which could be used to identify specific areas of low production. Additionally, it could be used as a base map for other applications. Consequently, the objectives of this study were: (i) to evaluate the capability of integrating Sentinel-1 and Sentinel-2 data for olive tree classification at the regional scale and (ii) to produce an olive tree distribution map of Izmir Province for the first time, an essential step before developing any regional crop management plan or intervention.

Table 2.1 : Olive tree classification references. The platform and sensor type are indicated along with methods used and size of the study area.

Platform	Sensor type	Method	Size of the study area	Reference
Aircraft	RGB	Modified morphological texture segmentation	6.25 km^2	Barata and Pina (2003)
Quickbird	MS	Machine learning classification algorithms	0.69 km^2	Castillejo-González (2018)
Quickbird	MS	Arbor Crown Enumeration (ACE) algorithm	218 km^2	Daliakopoulos et al. (2009)
Aircraft CESSNA 421, Quickbird	MS	Clustering Assessment (CLUAS)	87.25 km^2	García Torres et al. (2008)
Quickbird	PAN	Template matching	6982 trees	Gonzalez et al. (2007)
UAV eBee	MS	Geographic Object-Based Image Analysis (GEOBIA)	0.578 km^2	Karydas et al. (2017)
Quickbird	RGB	Circular Hough Transform (CHT)	1167 trees	Khan et al. (2018)
PlanetScope, WorldView-2 and 3	MS, RGB	Grid sampling and region sampling based deep learning	Nine sites with areas ranging from 11 to 25 km^2	Lin et al. (2021)
Aircraft -ADS40 camera, Quickbird andIKONOS	RGB, PAN, MS	Regional minima method	877 km^2	Masson et al. (2004)
UAV Multirotor G4Surveying-Robot	MS	Geographic Object-Based Image Analysis (GEOBIA)	0.169 km^2	Modica et al. (2020)
UAV Multirotor G4Surveying-Robot	MS	Geographic Object-Based Image Analysis (GEOBIA)	0.051 km^2	Modica et al. (2021)
Quickbird	PAN	OLICOUNT	298 km^2	Nihal et al. (2009)
Quickbird	MS	Comparison of OLICOUNT, M-OLICOUNT, a template method, and the Geographic Object-Based Image Analysis (GEOBIA) approach	1.5 km^2	Ozen and Bolca (2020)
RAMSES SAR and TerraSAR-X, Aircraft	SAR and MS	Multi resolution segmentation	1.206 km^2	Peters et al. (2011)
Aircraft	-	Geometrical squared-grid pattern	1022 olive trees	Robbez-Masson and Foltête (2005)

Table 2.1 (continued) : Olive tree classification references. The platform and sensor type are indicated along with methods used and size of the study area.

Platform	Sensor type	Method	Size of the study area	Reference
UAV DJI Phantom 4	RGB	Color-based and stereo vision-based segmentation (Deep Learning)	0.5 km^2	Salamí et al. (2019)
UAV DJI Matrice 100	MS	Digital Surface Model (DSM) based tree detection	0.175 km^2	Sarabia et al. (2020)
UAV DJI Matrice210 RTKV2, UAV DJI Matrice 600 Pro	RGB, MS	Pixel-based and GEOBIA-based classification	2.021 km^2	Šiljeg et al. (2020)
Worldview-3	PAN, MS	Geographic Object-Based Image Analysis (GEOBIA)	0.357 km^2	Solano et al. (2019)
Quickbird	RGB	K-means clustering	-	Waleed et al. (2020b)
Quickbird	Red	Multi-step image processing technique using Circular Hough Transform (CHT)	1167 trees	Waleed et al. (2020a)
UAV DJI Phantom 4	RGB	Semantic segmentation model U2-Ne	751 trees	Ye et al. (2022)

Note: PAN = panchromatic; MS = multispectral; RGB = red-green-blue; SAR = synthetic aperture radar; GEOBIA = geographic object-based image analysis; VHR = very high resolution; - = missing information

2.2 Materials and Methods

2.2.1 Study area

Izmir Province is located on the west coast of Türkiye, bordering on the Aegean Sea, located between latitudes 26°15′ – 28°20′E and 37°45′ – 39°15′N and covering an area of 12 012 km^2. The Gediz River flows through the province ending in the Gediz Delta on the Aegean coast. The country's third-largest city, Izmir, is situated on a small coastal plain south of the Gediz delta. Although there are hills and mountains in the interior of the province, the area is mostly flat. Izmir has a Mediterranean climate with hot, dry summers and mild winters (Izmir Governorship, n.d.). Because the Mediterranean region was unaffected by the last Ice Age, its wildlife and habitats are quite distinct, and the rate of endemism is unusually high (European Commission, n.d.). Olive forests with high biodiversity form part of the mountainous ecosystems, mainly growing in the valleys and basins between the ridges. They are not planted or fenced but are created by grafting wild olives (Delice) inside these basins where olive cultivation occurs (Figure 2.1b). Since these olive forests are also home to other plants and shrubs as well as to natural pasture among the olive trees, beekeeping and large and small livestock farming also occur within these valleys. Apart from mountains and hillsides, olives have also been planted in flatter lowland next to agricultural areas (Izmir Development Agency, 2022).

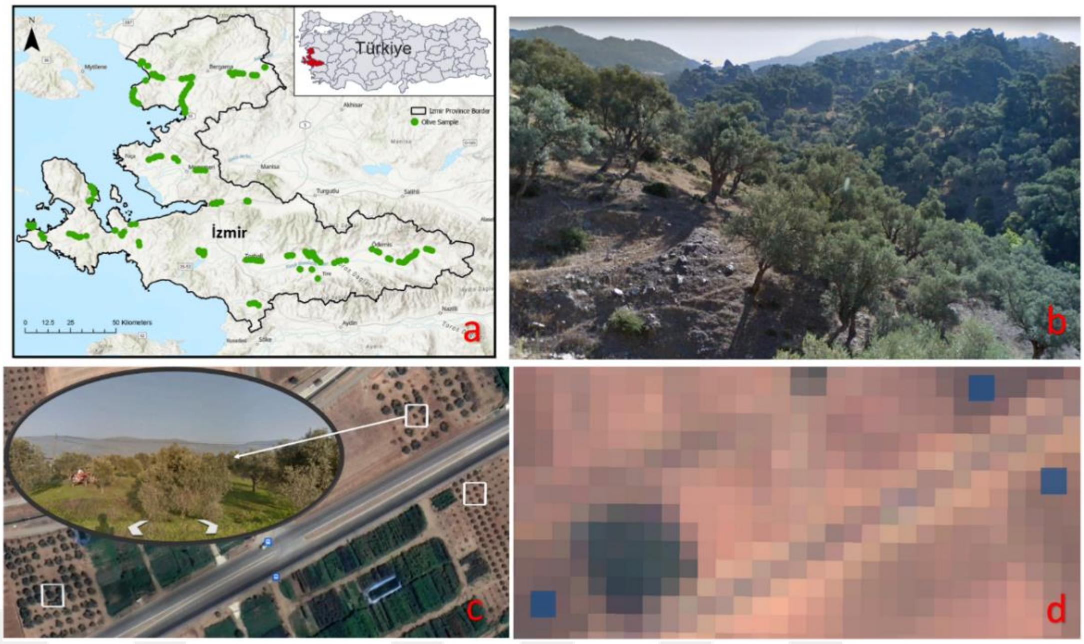

Figure 2.1 : a) The distribution of samples in the study area shown as green dots; b) olive forest with mixed vegetation in Yamanlar Valley, Izmir; c) olive samples on Google Earth with street view and high-resolution image; d) location of olive samples on Sentinel-2 L2A RGB image.

The phenological cycle of olive trees is linked to seasonal weather trends, particularly temperature and precipitation (Efe et al., 2011). Winter and spring precipitation retained in the soil promotes the flowering of olive trees (Ayaz and Varol, 2015). More than 50% of the annual precipitation in Izmir falls in winter (December–February), 40–45% in spring (March–May) and autumn (September–November). The region's annual average temperature ranges from 14 ºC to 18 ºC. The hottest months are July (27.3 ºC) and August (27.6 ºC), while the coldest months are January (8.6 ºC) and February (9.6 ºC) (Izmir Municipality, n.d.). This is significant because these average annual and monthly temperatures are crucial to the phenology of olive trees (Ulaş, 2012). For example, for blossom buds to form, an olive tree needs a chilling period in winter (Temuçin, 1993; Ertin, 2000) between 7 ºC and -7 ºC since olives cannot tolerate temperatures below -7 ºC (Efe et al., 2013). Similarly, high temperatures adversely affect the phenology of olive trees; for example, the intensity of photosynthesis reaches a maximum at 30 ºC and stops entirely at 40–45º C (Ayaz and Varol, 2015).

2.2.2 Data preparation

In this study, we used Sentinel-1 and Sentinel-2 data for regional olive tree mapping. This was complemented by reference data obtained by digitising high-resolution satellite images to train and test the classification algorithm. Finally, official district-level statistics from the Turkish Statistical Institute (TUIK, 2022) (https://www.tuik.gov.tr) were used to validate the total area covered by olive-growing regions. These statistical data included all historical data up to 2022. This study covers five growing seasons from 2017 to 2021.

We used Google Earth Engine (GEE), a cloud-based, planetary-scale geospatial analysis platform (Gorelick et al., 2017) to map the olive trees. The platform is accessed and operated via an internet-accessible application programming interface (API) which enables the processing and analysis of large datasets, allows the identification of changes in the Earth's ecosystem over time (Aksoy et al., 2022) and generates wider-scale land use-land cover maps.

Izmir Province was covered by six Sentinel-2 L2A scenes and two Sentinel-1 ground range detected (GRD) descent scenes. Each satellite dataset was pre-processed separately and then combined to obtain different datasets for the classification step. Random forest classification was applied to the datasets to compare the results and determine the final dataset for classification. Figure 2.2 illustrates our methodological framework.

As explained and detailed subsequently in the “phenological stages” and “phenological datasets” sections, to identify different phenological characteristics of olive trees, we used July and October monthly gap-filled composites of each year (2017–2021) for the classification. However, all monthly gap-filled composites between 2017 and 2021 were used to create monthly gap-filled composites for July and October. It is noted that a single composite of the gap-filled images constituted several Sentinel-2 L2A images. As a result, a substantial number of Sentinel-2 L2A images were used for the gap-filling process. Consequently, several images may have indirectly contributed to the July and/or October monthly gap-filled composite. Therefore, we did not include the exact dates of all the images used.

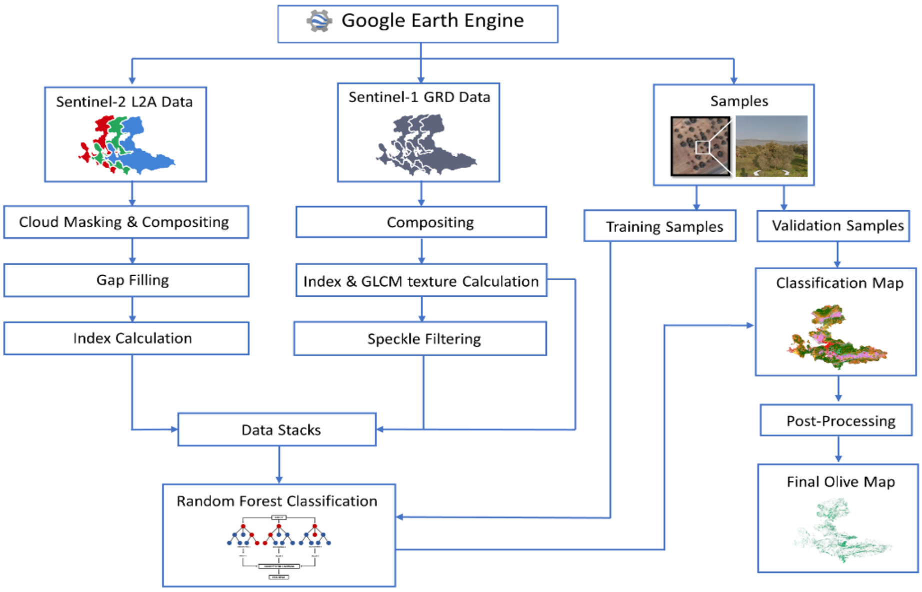

Figure 2.2 : Methodological framework of the study.

2.2.2.1 Sentinel-1 data

Sentinel-1 satellites, which operate in C-band Synthetic Aperture Radar (SAR), provide GRD products with high resolution (10 × 10 m pixel spacing) and dual polarisation (e.g. VH + VH+VV) in interferometric wide-swath acquisition mode (ESA, 2012; Torres et al., 2012). Each satellite has a 12-day revisit capability with a single pass (ascending or descending) in the interferometric wide-swath mode. The two-satellite constellation previously enabled a 6-day revisit cycle. However, in December 2021, a malfunction in Sentinel-1B satellite's instrument electronics power supply rendered it unable to produce data (ESA, 2022). The Sentinel-1 GRD products are available on the GEE platform and are pre-processed as implemented by the Sentinel-1 Toolbox (https://sentinel.esa.int/web/sentinel/toolboxes/sentinel-1) as follows: (i) applying the orbit file; (ii) removing GRD border noise; (iii) removing thermal noise; (iv) applying radiometric calibration; and (v) performing terrain correction (orthorectification) to obtain σ° (sigma nought) value using the SRTM 30-metre DEM (https://developers.google.com/earth-engine/guides/sentinel1).

The Sentinel-1 data in GEE are presented in decibel (dB) units by default, but it is also possible to obtain them in linear units. Logarithmic dB data are preferred because they are closer to normally distributed values and contain more visual contrast (Braun, 2020). Nevertheless, we evaluated the performances of both the dB and linear data using a random forest classifier. This preliminary analysis aimed to compare the classification performance of both units to determine the best data for further analysis.

Consequently, linear data were preferred because they performed slightly better. The data were then pre-processed using two different methods.

The first method involved calculating the VH/VV band, radar vegetation index (RVI) and 18 grey-level co-occurrence matrix (GLCM) textures, 14 of which were proposed by Haralick et al. (1973) and four additional metrics from Conners et al. (1984). The RVI equation follows (Charbonneau et al., 2005):

$$RVI = (4\sigma°VH) / (\sigma°VH + \sigma°VV) \tag{2.1}$$

where σ° is the backscatter coefficient (sigma nought), VH is polarization mode vertical/horizontal, and VV is polarization mode vertical/vertical. The GLCM, also known as the grey-level spatial dependence matrix, is a statistical technique for analysing textures that considers the spatial relationship of pixels. The GLCM functions determine how frequently pairs of pixels with particular values and in a specific spatial relationship occur in an image, building a GLCM, then extracting statistical measures from this matrix to define the texture of an image (Mathworks, 2023). Each GLCM texture was calculated for both the VH and VV bands, resulting in 36 GLCM texture bands in total. Finally, we obtained 40 layers for each monthly median of the Sentinel-1 images.

The second method used the framework presented by Mullissa et al. (2021). The proposed framework was developed to provide Sentinel-1 Analysis-Ready Data comprising three steps: additional border noise correction, speckle filtering and radiometric terrain normalisation. The code is openly available at (https://github.com/adugnag/gee_s1_ard) and each step is provided as an option. We considered only additional border noise correction and speckle filtering because radiometric terrain normalisation did not improve the classification performance of the test case. This framework outputs the VH, VV, VV/VH and angle bands. We sustained all outputs at their default values for comparison with the first method. The two pre-processed datasets described above were used separately and in different combinations during the classification stage.

2.2.2.2 Sentinel-2 data

The first Sentinel-2 satellite (S2A) was launched in 2015, followed by the second (S2B) in 2017, with 13 spectral bands, spatial resolutions of 10, 20 and 60 m (Laurin et al., 2018) and a revisit frequency of five days. The Sentinel-2 L2A products used in this study include 12 orthorectified and atmospherically corrected spectral bands with bottom-of-atmosphere reflectance values. Note that band 10 (SWIR cirrus) was not available for the atmospherically corrected L2A products. Furthermore, three QA bands were present, one of which (QA60) was a bitmask band containing cloud mask information. Additional outputs included quality indicators for cloud and snow probability at 60-metre resolution, an aerosol optical thickness map, a water vapour (WV) map, and a scene classification map (ESA, 2015).

The time series of Sentinel-2 data offer potential for exploring the phenological characteristics of vegetation and, hence, can be used as a basis for distinguishing different cover types. Consequently, we processed monthly Sentinel-2 composites. The pre-processing stage of Sentinel-2 L2A data comprises three steps: cloud masking, gap-filling, and index calculation.

Six Sentinel-2 scenes cover Izmir Province. Owing to the extensive spatial area and varied topography of the province, variable amounts of cloud cover were observed across the scenes. Therefore, S2cloudless (Zupanc, 2020) and Sentinel Hub’s (https://www.sentinel-hub.com/) machine learning-based cloud detector, which is already built-in to GEE, were used. We used the JavaScript API version of S2cloudless which was obtained from gis.stackexchange.com. The algorithm requires eight parameters to be defined. After experimenting with different values, we determined the cloud percentage as 100 and the cloud probability threshold as 40. We maintained the remaining parameters at their default values set by the S2cloudless developers. However, the masking process was inadequate in some places. Therefore, we applied additional masking using the Sentinel-2 scene classification map classes of (i) saturated or defective (class 1), (ii) dark area pixels (class 2), (iii) cloud shadows (class 3), and (iv) water (class 6). At the end of the process, cloud-free Sentinel-2 L2A monthly median composites were produced for Izmir Province. Missing data points in the monthly composites were gap-filled using the mean values of the previous and successive monthly composites (Gandhi, 2021).

Individual bands are generally less sensitive to vegetation features than the combined form of vegetation indices (VIs), which can functionally link crop attributes and spectral reflectance (Avola et al., 2019). Hence, different studies employed vegetation indices to separate olive trees (Pena-Barragan et al., 2004; Avola et al., 2019).

As described earlier, in Izmir, olive forests are mixed with different vegetation types (Figure 2.1b). It is also common to see olive parcels among agricultural lands and in built-up areas. Tiny olive trees are more likely to be classified as barren land or agriculture, mainly because of similar textural characteristics to other row-shaped crops such as vineyards. Therefore, we applied different vegetation indices related to agriculture, soil, and built-up areas (Table 2.2). Accordingly, we evaluated the contributions of the spectral indices to the Sentinel-1 and -2 stand-alone datasets. Using the difference vegetation index (DVI) and red band, DVIR was generated which, we observed, was distinctive when separating olive orchards.

Table 2.2 : Spectral indices.

Index Name	Formula		Reference
NDVI	(B8 − B4) / (B8 + B4)		Rouse et al. (1973)
MTCI	(B6 − B5) / (B5 − B4)		Dash and Curran (2004)
NDBI	(B11 − B8) / (B11 + B8)		Zha et al. (2003)
SAVI	(B8 − B4) × (1 + L) / (B8 + B4 + L)	L = 0.5	Huete (1988)
(B+G+R)/3	(B2 + B3 + B4) / 3		Peña-Barragán et al. (2004)
DVIR	(2 × B4 − B8) / B8)		Akcay et al. (2021)
DVI	B8 − B4		Tucker (1979)
NDVIre	(B5 − B4) / (B5 + B4)		Gitelson and Merzlyak (1994)
BSI	((B11 + B4) − (B8 + B2)) / ((B11 + B4) + (B8 + B2))		Roy et al. (1996)
NDTI	(B11 − B12) / (B11 + B12)		Van Deventer et al. (1997)

2.2.2.3 Reference data

Olive trees in Izmir are distributed throughout province and, considering that the area of Izmir is 12 012 km^2, it would have been challenging and time-consuming to collect representative ground samples. Moreover, such sampling could not be undertaken without landlord permission to enter property. These samples should have been selected from olive groves of different ages and canopy patterns to provide the requisite diversity. Ideally, as the study covered a five-year period between 2017 and 2021, ground samples should have been collected during that period to enable temporal analysis. In this context, Google Earth (Google, 2022), with its high-resolution historical images and street view capability, provided an alternative approach for determining the locations of olive trees across the province in specific time ranges. Accordingly, 602 pure olive samples/grids were randomly selected across Izmir Province (Figure 2.1a). In this step, three important requirements were fulfilled, namely, to ensure that:

- one Sentinel-2 pixel was inside a pure olive orchard sample, with the sample size determined as 15 m × 15 m (Figure 2.1c).
- each sample was selected from orchards with a border on the main road, which enabled us to check for the presence of olive trees using Google Street View (Figure 2.1c).
- each olive sample was checked against a Sentinel-2 background image to ensure that it was entirely inside the sample (Figure 2.1d).

To create an olive map, a detailed land cover (LC) map representing the study area was required to subgroup it into a binary olive/non-olive map. For this purpose, the ESA WorldCover 2020 v100 (Zanaga et al., 2020) classes were referenced to identify the number of classes in the region. The ESA landcover map does not include crop type, and most olive tree regions fall between several classes (e.g. cropland, tree cover, bare/sparse vegetation and shrubland). According to the ESA LC map, the study area includes eight LC classes: cropland, tree cover, bare/sparse vegetation, built-up areas, grassland, shrubland, snow/ice and water. The snow/ice and water classes were excluded because these surfaces were previously masked. Furthermore, the olive class was included, and the bare/sparse vegetation class was separated into two classes to prevent potential overlap with the olive class because it has a canopy structure similar to that of olive orchards. Consequently, seven LC classes, including the olive class, were selected for sampling. In addition to 602 olive samples and taking the total area covered by each class into consideration, 555 cropland, 412 forest, 102 barren land, 260 built-up, 293 grassland and 483 shrubland samples were randomly selected across Izmir Province using the same approach as for the selection of olive tree locations.

2.2.2.4 Validation data

The TUIK publishes all historical data, including annual statistics. Thus, for validation, historical statistics of the area covered by olive trees (in decares) were obtained from the TUIK website (TUIK, 2022). Officials from TUIK confirmed that olive tree statistics were obtained directly from the Republic of Türkiye Ministry of Agriculture and Forestry (MAF) (https://www.tarimorman.gov.tr). Based on information from MAF, the ministry's technical staff conducts field examinations and meetings with producers three times a year, while also considering estimates of proportional increases and decreases based on data analysis from previous years, as well as producing annual reports on official studies estimating olive and olive oil yields. These statistics conducted by them are estimations. We validated our results using the official TUIK statistics.

2.2.3 Classification

2.2.3.1 Phenological stages

The Sentinel-2 scenes of Izmir Province were mostly cloudy between November and March; although a gap-filling procedure was conducted, the data gap was too large in some parts. For this reason, May, July and October, which reflect the different phenological stages of olive trees, were selected for classification. According to information obtained from the Izmir Olive Research Institute (https://arastirma.tarimorman.gov.tr/izmirzae), the phenology of olive trees varies according to the altitude and latitude of the location. In general, May is considered the flowering stage. Due to water scarcity in July, the leaves turn slightly yellow while the fruit grows and the stone hardens. October is the colouration stage of the fruit ripening period. Figure 2.3 shows the normalized difference vegetation index (NDVI) of monthly median composites in 2021 for the different classes.

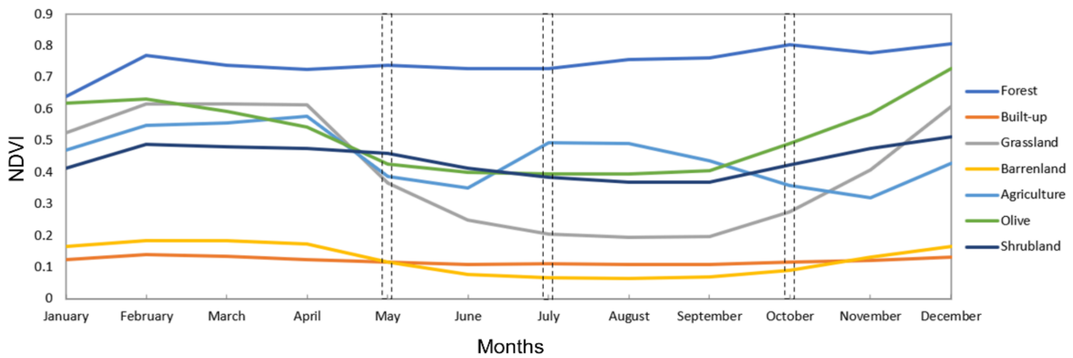

Figure 2.3 : Temporal NDVI chart of seven land cover classes in the study area. The data were obtained from Sentinel-2 Level 2A monthly median composites of 2021. Values represent mean NDVI values of samples from each class. Dotted lines for May, July and October indicate flowering, fruit growing and fruit colouration stages, respectively.

2.2.3.2 Random forests

Random forest (Breiman, 2001), an ensemble learning technique, uses several decision trees to predict the class of a given sample. The term "ensemble technique" refers to methods that build a number of models and then averages them for regression or voting for classification. Each decision tree was constructed by employing a bagging technique to draw a subset of samples by replacement, using only a portion of the randomly chosen characteristics. The random forest classifier demonstrated high accuracy and low bias by voting from several decision trees making it broadly usable (Sun et al., 2021), particularly for extensive and diverse datasets (Bargiel, 2017). The random forest classifier requires certain variables to be defined (i.e. the number of trees, variables per split, minimum leaf population, bag fraction, maximum nodes and seed). Different studies have assessed the performance of random forest classifier parameters for several land cover types. They reported that very small values of k (the number of trees) have a negative impact on classification performance. In contrast, larger values of k have a positive impact on classification stability and variable significance measures. They concluded that there are very few variations in stability after 100 trees, and that the computation time increases for wider ranges of potential values of k (Rodriguez-Galiano et al., 2012; Pelletier et al., 2016; Aksoy et al., 2022). Similarly, in our study, we observed that overall accuracy remained consistent after several iterations, although the producer's accuracy increased slightly after 100 trees. Additionally, the training accuracy reached 100%. Accordingly, we selected 100 trees and kept the other parameters by default, as defined in GEE.

2.2.3.3 Phenological datasets

Monthly May, July, and October gap-filled composites of Sentinel-1 and -2 data were created, as well as their different combinations (i.e. May + July, May + July + October and July + October). A random forest classifier was used to measure performance at each phenological stage. However, it was difficult to classify olive trees using a single phenological stage (e.g. May). To address this, we combined phenological stages to separate olive trees from other vegetation types. The intention was to produce a map for each year using key phenological stages. As a result, the July + October composite combination (dataset "g") was selected for the final classification, which performed at the highest accuracy (see Appendix B.1). Classification procedures were conducted separately for years 2017, 2018, 2019, 2020 and 2021.

2.2.3.4 Cross-validation

Cross-validation uses different portions of the sample dataset in various iterations to train and validate the model and obtain robust results. Many cross-validation methods exist, such as the K-fold, leave-one-out, and Monte Carlo methods. A K-fold cross-validation method was used to validate the final classification results. This method segments the samples into evenly sized K-folds, with one of these folds being left for validation. This process continues until all samples are used for both validation and training, and all results are averaged out (Ramezan et al., 2019). We selected the value of k = 5.

2.2.4 Post-processing

2.2.4.1 Morphological operations

It is common to observe isolated pixels or small isolated regions for a specific class, owing to misclassification by the classifier. We used "focal median" statistics to eliminate the misclassified pixels, a morphological operation built-in GEE. Different parameters, such as kernel type, radius and number of iterations needed to be defined to conduct a morphological operation. Several attempts were made to determine these parameters. First, the pixel size was kept constant and the number of iterations was increased. Subsequently, the number of iterations was kept constant, and the pixel size was increased. Next, both the parameters were increased together for balance. Different kernel types were also included in these trials. After trying several combinations, the selected parameters were as follows: radius, 1.5 pixels; kernel type, square; and number of iterations, 3.

Finally, we masked out the agriculture, forest, barren land, built-up, grassland, and shrubland classes to produce an olive map for each year. Accordingly, olive maps were produced for 2017, 2018, 2019, 2020 and 2021.

2.2.4.2 Final olive map

When we overlapped the olive maps for 2017, 2018, 2019, 2020 and 2021, we observed that each of the two successive years had the most common intersections in terms of spatial coverage. Accordingly, we created four combined intersection maps: 2017–2018, 2018–2019, 2019–2020 and 2020–2021. The combination of the intersecting olive maps resulted in isolated olive pixels. For this reason, olive areas with fewer than five pixels, considered as no-olive orchards, were excluded. Finally, the total area covered by olive trees within the provincial borders of Izmir was calculated on a district basis to validate the official data obtained from TUIK (https://www.tuik.gov.tr). In the statistics from TUIK between 2017 and 2021, there are no data for five of Izmir's 30 districts for some years or for any year (i.e. Balçova, Buca, Çiğli, Konak and Tire). Therefore, we excluded these districts from the validation. As a measure of validation, we applied the normalized root mean square error (NRMSE) equation (Tiktak et al., 1998):

$$NRMSE = \frac{\sqrt{\sum_{i=1}^{n}(P_i - O_i)^2/n}}{\bar{O}} \tag{2.2}$$

where n is the number of observations, $\bar{O}$ is the mean, and P_i and O_i are the expected and observed values, respectively, for i. The optimal NRMSE value is zero.

2.3 Results

Results were assessed using both classification-based accuracy assessment and olive area comparison with TUIK statistics.

2.3.1 Accuracy assessment

Accuracy assessment procedure was conducted in two different ways: K-fold cross validation and confusion matrix.

2.3.1.1 K-fold cross validation

We used the K-fold cross validation method to validate our final classification results, which were composed of dataset "g". The results showed that the models trained with K-fold performed similarly to the no-K-fold version. The K-fold validation accuracy was 6–10% higher than the test performance. However, the test accuracy was nearly identical for both the K-fold and no-K-fold approaches (Table 2.3).

Table 2.3 : Comparison of K-fold accuracies through to study years.

Year	No K-fold Test Accuracy	K-fold	
		Validation Accuracy	Test Accuracy
2017	88%	94%	88%
2018	87%	95%	87%
2019	90%	95%	91%
2020	89%	95%	89%
2021	89%	95%	88%

Note: Test accuracy indicates accuracy of test data (30% of the samples used for validation is referred to as test data). Validation accuracy represented an average accuracy of 5 folds.

2.3.1.2 Confusion matrix

In 2017, 2018 and 2020, the highest producer accuracies for the olive class were achieved (83.6%, 86.5% and 87.2%, respectively) using dataset "g" (see Appendix B.1). Whereas for 2019 and 2021, the highest producer accuracy for the olive class (91.4%) was achieved with datasets "h" and "j", respectively. However, we selected the results of dataset "g" for all years to maintain data consistency between years. Notably, there was a less than 2% difference between the highest-performing dataset and dataset "g".

Sentinel-1

Four different dataset combinations were generated to assess the performance of Sentinel-1 data (see Appendix B.1). Speckle filtering significantly increased the accuracy of the Sentinel-1 stand-alone dataset by up to 12%. However, when speckle filtered VV/VH and an angle band were included, the accuracy decreased significantly because of the adverse effect of the angle band. Additionally, the VV/VH and angle band were included in the experiment based on the performance of the dataset presented by Mulissa et al. (2021). Further, the combination of the VH/VV band, RVI and GLCM textures improved the non-speckle filtered Sentinel-1 stand-alone dataset by up to 23%.

However, it was observed that the Sentinel-1 data generally resulted in low classification accuracy for other land-cover types. Nevertheless, the forest class performed the highest, whereas barren land performed poorly and was completely misclassified (Table 2.4). This result indicates that the soil background of olive trees dramatically decreases the classification performance of SAR data. Table 2.4 describes the confusion matrix of the highest-performing Sentinel-1 dataset combination (dataset "d").

Table 2.4 : Confusion matrix of "Sentinel-1 bands including GLCM textures" dataset.

	Class	Olive	Cropland	Forest	Barren-land	Built-up	Grassland	Shrubland	Producer's Acc.	kappa
2017	Olive	358	95	55	0	0	3	13	68.3%	0.36
	Cropland	242	287	18	0	0	54	4	47.4%	
	Forest	126	7	274	0	9	5	61	56.8%	
	Barren-land	14	18	5	0	4	73	5	0.0%	
	Built-up	36	48	36	0	59	30	67	21.4%	
	Grassland	90	87	14	0	0	158	0	45.3%	
	Shrubland	137	51	100	0	20	9	221	41.1%	
	User's Acc.	35.7%	48.4%	54.6%	0.0%	64.1%	47.6%	59.6%	46.9%	

Sentinel-2

The Sentinel-2 L2A stand-alone classification (12 bands) achieved producer accuracies of 68.9%, 67.4%, 75.0%, 73.7% and 80.9% for 2017, 2018, 2019, 2020 and 2021, respectively (see Appendix B.1). When 10 spectral indices were included, the accuracy of the Sentinel-2 based classification increased significantly by up to 15%. It was also observed that the annual accuracy difference decreased slightly compared to the Sentinel-2 stand-alone classification (see Appendix B.1). Sentinel-2 data also performed very well in classifying classes other than barren land. Forest, built-up and shrubland areas were classified with more than 90% accuracy. The barren-land class had an overall low classification accuracy across all the years. Table 2.5 represents the confusion matrix of the highest-performing Sentinel-2 dataset combination (dataset "f").

Table 2.5 : Confusion matrix of "Sentinel-2 bands including spectral indices" dataset.

	Class	Olive	Cropland	Forest	Barren-land	Built-up	Grassland	Shrubland	Producer's Acc.	kappa
2019	Olive	475	12	8	0	3	3	23	90.6%	0.86
	Cropland	11	496	12	5	17	19	45	82.0%	
	Forest	0	0	480	0	0	0	1	99.8%	
	Barren-land	0	5	0	72	26	11	5	60.5%	
	Built-up	0	4	0	12	258	0	2	93.5%	
	Grassland	0	3	0	0	0	280	66	80.2%	
	Shrubland	31	10	0	0	0	1	496	92.2%	
	User's Acc.	91.9%	93.6%	96.0%	80.09%	84.9%	89.2%	77.7%	88.4%	

Sentinel-1 and-2 combinations

When Sentinel-1 and Sentinel-2 data were combined, there was an overall increase in classification accuracy. In 2019, the Sentinel-1 stand-alone dataset performed at 49% producer accuracy for the olive class, whereas accuracy reached 89.9% when Sentinel-2 bands and 10 spectral indices were included (dataset "g") (see Appendix A2). As shown in Table 2.6, Sentinel-2 derived data significantly improved the classification of the other classes. All classes except barren land were classified with more than 80% producer accuracy. Table 2.6 shows the confusion matrix of the Sentinel-1 and Sentinel-2 datasets, including spectral indices (dataset "g") for 2019, the highest performing year.

Table 2.6 : Confusion matrix of "Sentinel-1 and Sentinel-2 bands including spectral indices" dataset.

		Olive	Cropland	Forest	Barren-land	Built-up	Grassland	Shrubland	Producer's Acc.	kappa
2019	Olive	471	10	13	0	3	2	25	89.9%	0.87
	Cropland	11	516	19	2	0	14	43	85.3%	
	Forest	0	0	479	0	0	0	2	99.6%	
	Barren-land	0	6	0	82	15	13	3	68.9%	
	Built-up	0	3	0	23	248	0	2	89.9%	
	Grassland	0	3	0	0	0	289	57	82.8%	
	Shrubland	25	7	0	0	0	1	505	93.9%	
	User's Acc.	92.9%	94.7%	93.7%	76.6%	93.2%	90.6%	79.3%	89.6%	

Final olive map

The accuracy of the final olive map was assessed as a binary map using two classes, olive and non-olive, resulting in 98% overall accuracy and 93% producer accuracy. Given the scale of the study, the results were encouraging, as they agreed well with the performance of classification that used VHR images whose accuracy ranged between 89% and 99% (Messina et al., 2022). Figure 2.4 shows the classification map and the final olive map of Izmir Province. The land use-land cover map for 2019 is shown in Figure 2.4a because it had the highest overall accuracy (see Appendix A.1) compared with other years.

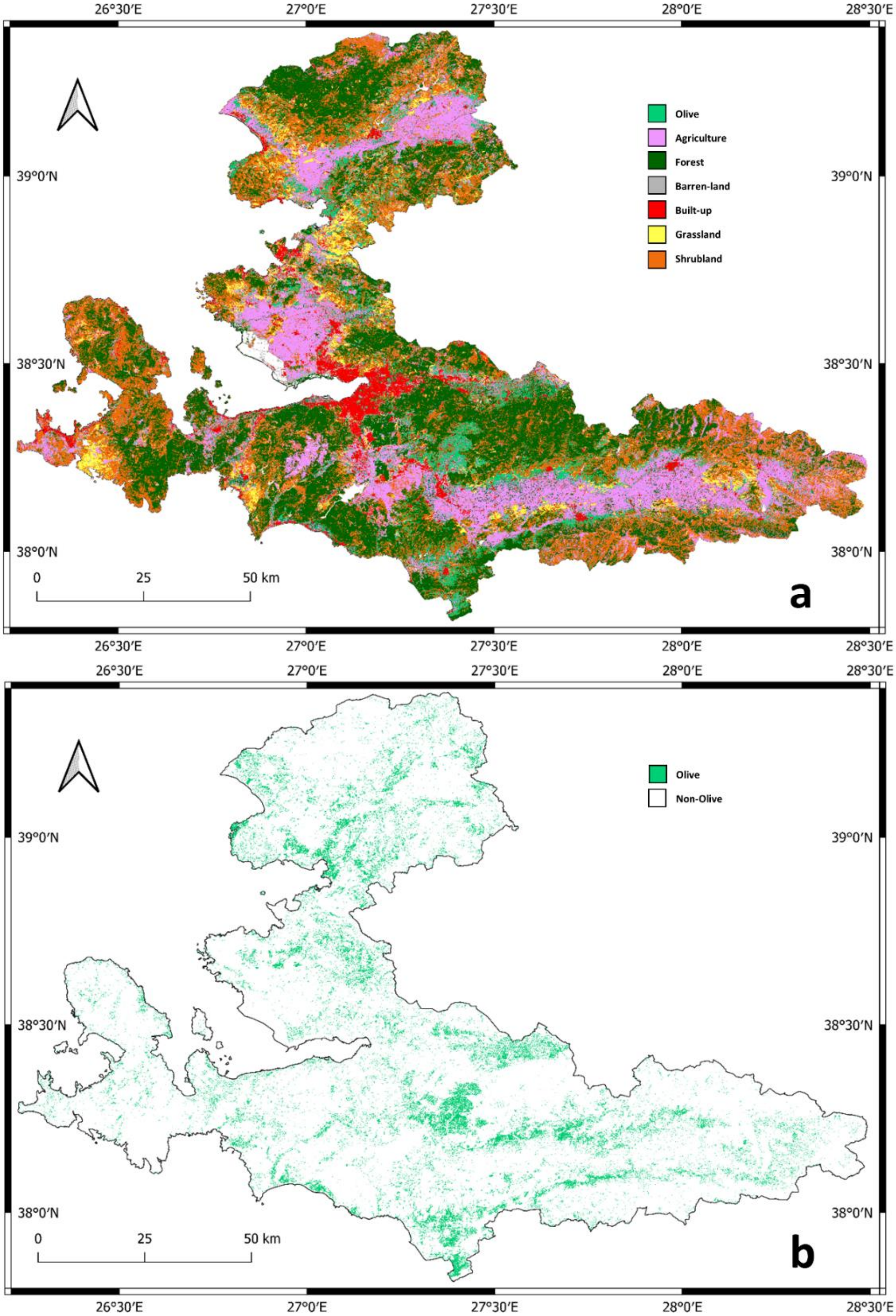

Figure 2.4 : a) Izmir classification map for 2019 at 10-metre spatial resolution produced using Sentinel-1 and -2 data fusion. Olive tree distribution intensified, particularly adjacent to agricultural parcels, forest and shrublands across Izmir province; b) final olive map of Izmir at 10-metre resolution produced from the combination of the intersection of successive olive maps for 2017–2018, 2018–2019, 2019–2020 and 2020–2021.

2.3.2 Validation of final olive map

The total area classified as olive for the 25 districts was 954 872 decares, compared to the 901 761 decares gleaned from the TUIK 5-year mean statistics (2017–2021) with a strong correlation at individual district level (R^2 = 0.60 and NRMSE = 0.64) (Figure 2.5a). However, underestimation and overestimation observed in Bayındır and Bergama districts, respectively, distorted the correlation. In order to understand the drivers of underestimation and overestimation, field observations were conducted in these districts and results were explained in detail in Chapter 4. When these two districts were excluded, the correlation was improved (R^2 = 0.78 and NRMSE = 0.40) (Figure 2.5b) from analysis. We referenced the TUIK 5-year mean statistics to maintain consistency because we produced our final map using images from the last five years. According to the findings, the classification resulted in a slight overestimation. In addition, hilly districts are more likely to be misclassified because of the abovementioned mixed vegetation. Finally, the official data from TUIK, which we used as a reference, were based on estimations.

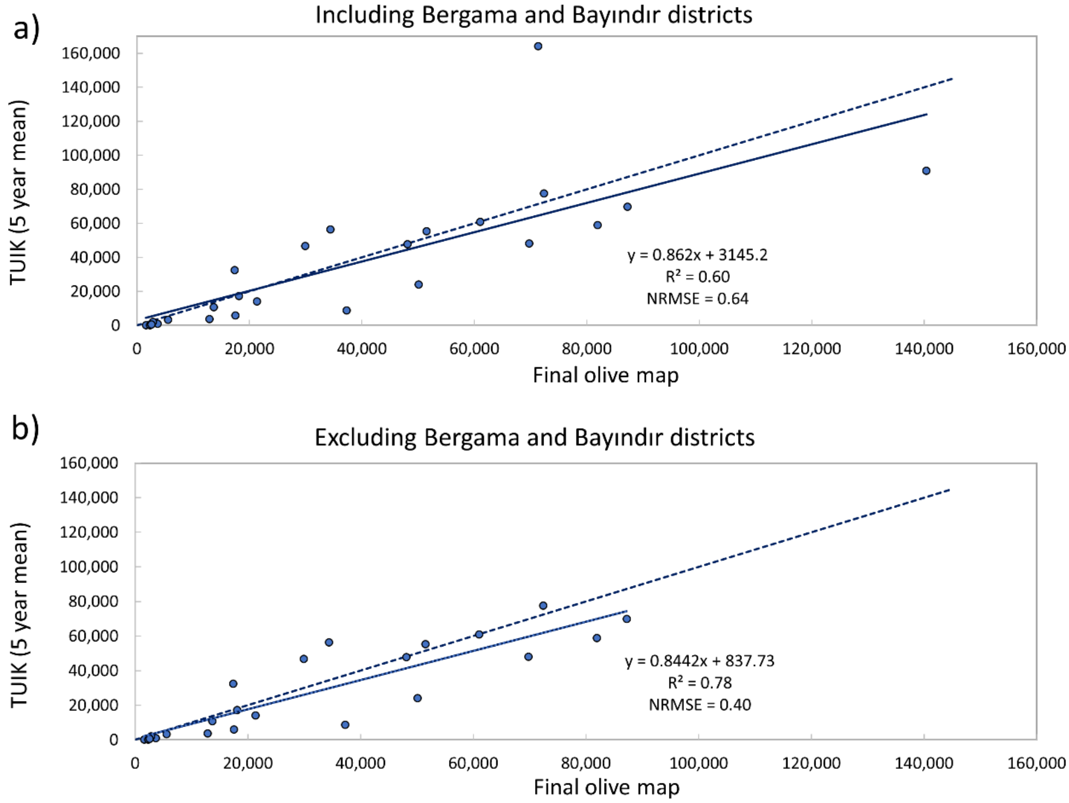

Figure 2.5 : Scatter plot of district level olive area comparison (decares). X axis represents classified olive area while Y axis depicts official statistics of TUIK 5-year mean olive area. Solid line represents correlation trend line while dashed line represents *x* = *y*.

2.4 Discussion

We evaluated the potential of multi-temporal Sentinel-1 and -2 data for large-scale mapping of olive-growing regions. To the best of our knowledge, this work is the first attempt to use a decametric dataset for regional-scale olive tree mapping and is the first olive tree map of the Izmir province of Türkiye. Access to the cloud computing infrastructure of GEE enabled this study to use multitemporal seasonal patterns of optical data, textural information and temporal metrics of radar data (Maskell et al., 2021). Most other large-scale Sentinel-based crop-type mapping studies have primarily focused on annual crops such as maize and wheat (Defourny et al., 2019; Griffiths et al., 2019; Jin et al., 2019). Although studies on perennial trees are limited, research on mapping them using remote sensing imaging is ongoing. For example, Poortinga et al. (2019) mapped oil palms and rubber trees, while Mishra et al. (2019) mapped mango trees. Maskell et al. (2021) focused on mapping coffee in Vietnam using Sentinel-1 and -2 data. We have contributed to this research series with regional olive tree mapping. Because one of the objectives of this study was to evaluate the performance of multi-temporal Sentinel-1 and -2 data, we experimented with their stand-alone and their combined usage. In the following paragraphs, Sentinel-1, Sentinel-2 and their integrated usage are evaluated.

Compared to L-band data, which have a longer wavelength and are frequently used for mapping forests, C-band data, with a shorter wavelength of 3–5 cm, are better suited for mapping lower biomass or sparse tree crops (Maskell et al., 2021). C-band polarimetric SAR data performance was tested for different crop types, and dual polarisation had the highest classification accuracy (McNairn and Brisco, 2014). In our case, we experimented with the contribution of VH/VV and RVI individually to dual polarisation (VV + VH), but observed that GLCM textures and speckle filtering had more positive effects on the accuracy of the classifier. This explains why textural information/differences play a significant role in SAR data (Mishra et al., 2019; Maskell et al., 2021), which could account for the extensive plant structure information contained in SAR backscatter amplitudes (Van Tricht et al., 2018). Nevertheless, none of the Sentinel-1 data combinations exceeded 70% producer accuracy for the olive class in any year, suggesting less textural variability among the different land cover classes. Our results showed a better classification performance than other studies that used Sentinel-1 data for olive tree classification. For example, Maskell et al. (2021)

reported a 46% overall accuracy using Sentinel-1 derived data, including GLCM textures. In comparison, using similar information, our study resulted in a 55% classification accuracy. Our dataset combinations and assessments were based on the olive class; we did not evaluate the classification performance of other classes.

Optical data provide seasonal patterns of vegetation and unique information for classification (Bargiel, 2017). In addition, optical vegetation indices contribute to better discrimination of different classes on heterogeneous land surfaces (Avola et al., 2019). Studies have shown that using Sentinel-2 variables yields classification accuracies varying from 70% to 90% when mapping crops and cropping patterns at a landscape scale (Mudereri et al., 2022). For example, Maskell et al. (2021) reported a 70% overall accuracy using Sentinel-2 derived data to map coffee trees. Our study achieved an overall accuracy of up to 88% using comparable data. In addition, the combination of Sentinel-2 and the spectral indices dataset achieved up to 90% producer accuracy for the olive class, demonstrating the clear advantage of Sentinel-2 derived data for olive tree mapping. Moreover, seasonal patterns in optical data and textural information from radar data complement the classification (Maskell et al., 2021). Several studies have reported the contribution of optical and radar data fusion to crop mapping (Jin et al., 2019; Poortinga et al., 2019). Similarly, in our study, the combination of Sentinel-1 and Sentinel-2 data achieved the best classification accuracy, with an overall accuracy of up to 90% and a producer accuracy of over 90% for the olive class. This is relatively good compared with other studies on perennial trees, such as oil palm and rubber (Poortinga et al., 2019), coffee (Maskell et al., 2021) and mango (Mudereri et al., 2022). Poortinga et al. (2019) reported an overall accuracy of 84–91%. Maskell et al. (2021) reported a user accuracy of 89% and producer accuracy of 66% for coffee trees, whereas Mudereri et al. (2022) reported up to 80% producer accuracy for mango trees.

An interesting outcome of this study is that the inclusion of Sentinel-1 data resulted in a 5% increase in accuracy in 2017, 2018 and 2020 but not in 2019 and 2021. Instead, a slight decrease was observed. The differences in the reflectance and textural characteristics of vegetation between years is a potential cause of this inconsistency. There was up to a 13.5% difference between the lowest and the highest performing years of “Sentinel-2 bands including spectral indices” dataset. This can also be explained by differences in surface reflectance between different years for olive trees.

Moreover, this can be a sign of phenological inconsistency or potential phenological changes in olive trees which need to be validated with further research. Other factors, such as farmer agricultural practices between olive trees, may add further confusion to the classifier. Furthermore, olive trees on hillsides were mixed with different vegetation types (Figure 2.1b). Finally, the phenological changes/differences in other vegetation may be another reason for this inconsistency, as each plant's phenological stage may include unique information (Bargiel, 2017).

Olive trees exhibit different growth stages, with some present as isolated trees or small olive orchards among different land cover types, particularly in built-up areas. Also, young and small olive orchards were more likely to be mixed in with other classes such as agricultural areas of vineyards and row-textured agricultural parcels. Furthermore, a significant extent of deforestation has occurred in Izmir Province during the past five years owing to forest fires and/or human activities. Some forest areas were planted with native trees (Pinus brutia), while others were replaced with olive trees. In either case, these sparsely vegetated, heterogeneous regions are on hillsides and are likely to be classified or misclassified as olives, causing inconsistencies between different years. To eliminate isolated pixels among the classes, a focal median procedure was conducted on the classification maps. This may have removed correctly classified small patches. Although olive trees are distributed on Mediterranean hillsides and are mixed with other vegetation, particularly shrublands, most of the samples for training and validation were confined to the main road, as this is the only data available in Google Street View. This limited the possibility of collecting samples from different geographical areas. In addition, ground vegetation, such as grass, weeds, planted vegetation and bare soil among olive trees, can potentially distort spectral reflectance (Fig 2.1b). This issue has also been reported in object-based classification studies that utilised a blob-detection method using VHR images (Messina et al., 2022). Other vegetation cover within olive trees may vary across regions and years. This results in different spectral/radar signatures and, in turn, different overall classification accuracies. In addition, the spectral reflectance curve of olive trees was similar to that of shrublands (Figure 2.6), which could cause misclassification.

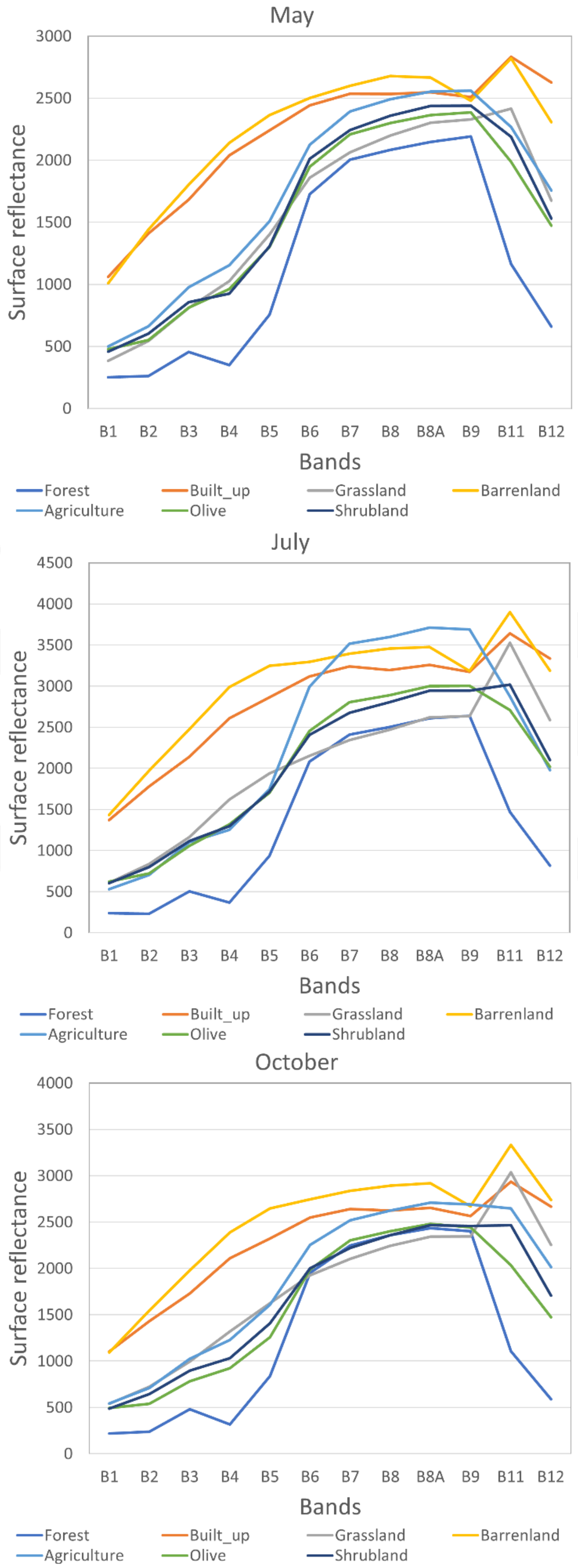

Figure 2.6 : 2017–2021 mean surface reflectance values for different classes according to Sentinel-2 L2A bands.

Figure 2.7 represents a closer look at three regions of classification map. In region a, olive trees were mostly classified as correct. In addition, all cropland and built-up areas were correctly classified. However, some densely vegetated olive areas were misclassified as forest in the second and fourth zones. Also, some olive trees misclassified as shrubland in the second zone. In region b, shrubland, forest and olive areas were classified correctly in the first, second and fourth zones, respectively. However, sparsely distributed olive trees mixed with other trees next to forest area were misclassified as shrubland in the third zone. Note that the elevation of the region increases towards the forest area. In region c, built-up, forest and olive areas were correctly classified in the first, second and fifth zones, respectively. However, olive trees in the third and fourth zones were misclassified as shrubland due to mixed vegetatation.

Despite the limitations described above, good agreement with the TUIK statistics was achieved ($R^2 = 0.78$). Our olive distribution map can thus be a useful resource and base dataset for the Ministry of Agriculture and other institutions and organisations, particularly the Izmir Olive Research Institute. This also fulfils the need for an up-to-date map showing olive tree distribution in Izmir. In addition, it can be used as a basis for other scientific studies on olive trees and for future change detection analyses. Most importantly, this study presents an approach that uses the power of Sentinel data and GEE to produce regional-scale olive distribution mapping which can be replicated across the entire country and elsewhere. This is a step change in geospatial data availability for tree crops, which is less prevalent than annual crop mapping in Earth Observation-based studies.

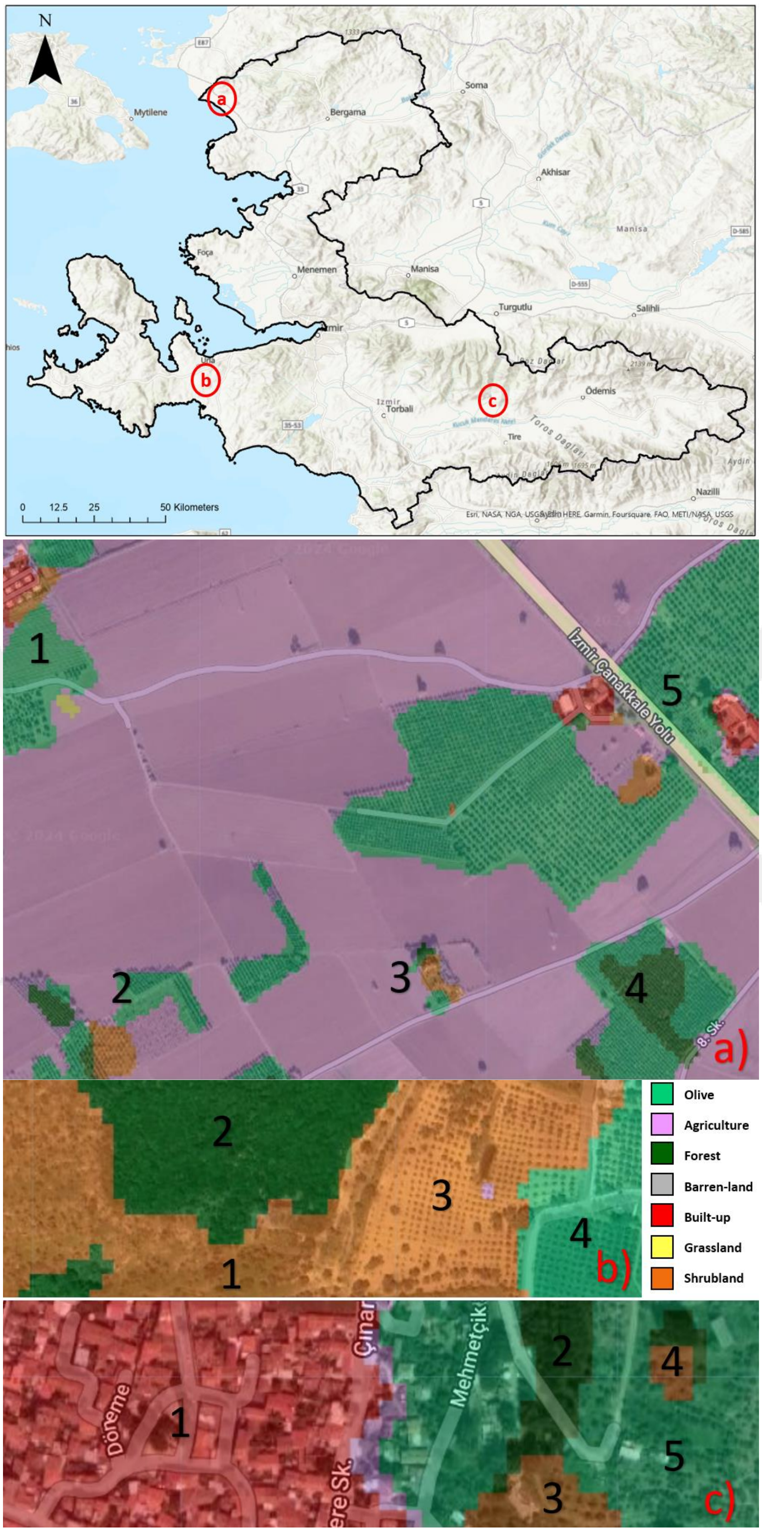

Figure 2.7 : A closer look at three regions of the Izmir classification map for 2019 at 10-metre spatial resolution produced using Sentinel-1 and -2 data fusion overlapping with the Google Earth high-resolution image; a) five zones of region a; b) four zones of region b; c) five zones of region c.

2.5 Conclusion

In this study, we evaluated the performance of multitemporal Sentinel-1 and -2 data for olive tree classification on a regional scale. The results showed that Sentinel-1 alone provides a moderate classification accuracy for mapping olive trees (up to 70%). In comparison, using optical data from Sentinel-2 significantly improves olive tree classification (up to 90%). However, the combination of Sentinel-1 and Sentinel-2 datasets provided the best accuracy for olive tree classification in Izmir Province. This clearly demonstrates the advantage of the synergetic use of optical and radar data in tree crop mapping. This study further develops a scalable approach for mapping tree crops at regional to global scale by using the power of the cloud-computing infrastructure provided by Google Earth Engine. This is the first regional-scale olive tree distribution map for Izmir Province, which is a crucial dataset for the development of an effective management plan. Expanding this method to other regions of Türkiye will pave the way for the first country-scale olive tree mapping exercise.

3. INVESTIGATING THE PHENOLOGY AND PRODUCTIVITY OF OLIVE TREES ON A REGIONAL SCALE USING COPERNICUS LAND MONITORING SERVICE'S HR-VPP PARAMETERS

3.1 Introduction

Vegetation phenology is described as plants' periodic life cycle and the influence of seasonal and inter-annual variations on them (Myneni et al., 1997; Zhang et al., 2003; White et al., 2009; Morisette et al., 2009; Richardson et al., 2013; Wu et al., 2016). It is crucial for water, carbon, and energy cycle of ecosystems (Richardson et al., 2009; Ren et al., 2022b; Zhao et al., 2022). Therefore, in order to understand how ecosystems are adapting to climate change, vegetation phenology is frequently utilised as a strong indicator (Badeck et al., 2004; Parmesan, 2006; White et al., 2009; Ma et al., 2013; Peng et al., 2017). Furthermore, it is an important indicator to capture the short-term changes during the growing season because it is very sensitive to abrupt weather changes (Ren et al., 2022b). Currently, vegetation phenology is mostly monitored in three different ways: (i) traditional visual observations by humans, (ii) ground-based measurements, and (iii) satellite remote sensing (Zeng et al., 2020; Zhao et al., 2022). The visual observation, the traditional method, is very time consuming and not suitable for large-scale applications (Xu et al., 2014; Wu et al., 2021). Ground-based measurements include canopy cameras (e.g. PhenoCam) and flux towers. This method is expensive and mostly used to obtain reference data. The third method, satellite remote sensing presents the optimum option by providing cost-effective, large-scale continuous data (Ivits et al., 2013). However, satellite remote sensing is not able to detect the particular plant events due to its lower spatio-temporal resolution. Therefore, terms like the start of season (SOS) and end of season (EOS) were defined to characterise the vegetation dynamics (Zeng et al., 2020; Zhao et al., 2022). For this purpose, time-series of vegetation indices such as normalized difference vegetation index (NDVI) (Wu et al., 2017), enhanced vegetation index (EVI) (Duarte et al., 2018), and leaf area index (LAI) (Kang et al., 2003) are widely used from satellite sensors such as the Moderate-Resolution Imaging Spectroradiometer (MODIS) and the

Advanced Very High Resolution Radiometer (AVHRR). In addition, vegetation indices such as the perpendicular vegetation index (PVI) (Guyon et al., 2011) and MERIS terrestrial chlorophyll index (MTCI) (Dash et al., 2010; Atkinson et al., 2012) were documented as useful to characterize phenology metrics. Apart these, Copernicus Land Monitoring Service (CLMS) exploits time-series of plant phenology index (PPI) to derive High-Resolution Phenology and Productivity (HR-VPP) metrics. PPI was reported to be linearly related with green LAI, and superior to NDVI and EVI2 (European Union, 2022). HR-VPP metrics are produced annually starting in 2017 and covers all the European Economic Area (EEA39) consisting of 33 member and 6 collaborating countries (European Union, 2022; Borgogno-Mondino and Fissore, 2022). Equation below shows the PPI formulation, developed by Jin and Eklundh (2014).

$$PPI = -K \cdot ln\left(\frac{M - DVI}{M + DVI_S}\right) \tag{3.1}$$

where *K* is a gain factor, *DVI* is calculated using sun-sesnsor geometry corrected NIR and red reflectences, DVI_S is the *DVI* of the soil and *M* is a site-specific canopy maximum *DVI*. Details are given in Jin and Eklundh (2014).

Productivity is a phrase used to describe the growth of vegetation. It is frequently defined as either gross primary productivity (GPP), the growth resulting from photosynthesis, or net primary productivity (NPP), the GPP minus the respiration of the plant (European Union, 2022). Even though vegetation phenology and productivity may have a complicated relationship because of the local climate and other external factors (Wu et al., 2016), phenology metrics have been demonstrated to be potential indicators of productivity (Richardson et al., 2013; Piao et al., 2019; Zhou et al., 2021). Accordingly, several studies have been conducted on phenology and productivity of vegetation. However, most of the studies on vegetation phenology and productivity have been conducted in large areas and over long periods of time to investigate the impact of climate change on ecosystems. Particularly, the regions with minimum human disruptions to ecosystems, as well as distinct geographical location, temperature, and vegetation zone are thought to be suitable for determining the influence of climate change on vegetation phenology and productivity and its inter-annual changes (Bao et al., 2020). For example, studies were conducted in Tibetan

Plateau (Wu et al., 2016; Gao et al., 2016; Wang et al., 2017; Sun et al., 2022), Alaska (Kelsey et al., 2020), Greenland (Ellebjerg et al., 2008), Mongolia (Bao et al., 2020) and Namaqualand (Davis et. al, 2017) are among others. Furthermore, studies have been performed on the phenology and productivity of crops, including maize (Zhou et al., 2021) and winter wheat (Vavlas et al., 2020). However, studies on phenology and productivity of olive trees are limited. Hachicha et al. (2021) evaluated the potential of Sentinel-2 to monitor and estimate crop growth over various olive orchards in Sfax, Tunisia between 2016 and 2020. They utilized two independent statistical approaches, Markov chain (MC) and autoregressive (AR). Azpiroz et al. (2021) used MODIS satellite data and geophysical & climatic data to create a phenology prediction model, utilizing remote measurements of surface spectral reflectance, slope of the terrain, and weather data, in Tuscany, Italy. Oses et al. (2020) analysed Copernicus' ERA5 climate reanalysis data in Tuscany, Italy, utilizing temperature and ground phenology observation data for olive phenology phase estimation. Milicevic et al. (2020) investigated the feasibility of employing machine learning and deep learning techniques to observe and capture the phenological stages of olive trees using ground cameras in a olive orchard in Croatia. Nevertheless, none of these studies investigated the interannual variability of phenology of olive trees. In addition to phenology-based studies abovementioned, two researches have been conducted on estimation of productivitity of olive trees. Maselli et al. (2012) presented a methodology using remotely sensed and ancillary data to estimate olive fruit yield in Tuscany, Italy. They used IKONOS, Landsat ETM+ and MODIS images to predict daily gross primary productivity (GPP) for ten years, and simulate net primary productivity (NPP) using a bio-geochemical model. Similarly, Brilli et al. (2013) created and evaluated an approach that combined multi-sensor satellite data (IKONOS, Landsat ETM+ and MODIS) with climate data and ground data to estimate the gross primary productivity in Tuscany, Italy. However, no research has been evaluated the relationships between productivity of olive trees and external factors, such as climate and elevation on a regional scale. Furthermore, no research was performed on phenology and productivity of olive trees using satellite sensor data in Türkiye. To address this gap, this chapter of the thesis investigates: (i) the interannual variability of phenology metrics (i.e. SOSD, EOSD), (ii) the effects of elevation to the phenology and total productivity, (iii) the effects of climatic conditions to the total productivity and (iv) the relationship between crop yield and total productivity of olive trees in Izmir province between 2017 and 2021 using Copernicus Land Monitoring Service’s (CLMS) High Resolution Vegetation Phenology and Productivity (HR-VPP) parameters derived from Sentinel-2 data.

3.2 Materials and Methods

3.2.1 Data preparation and analysis

In this research, CLMS HR-VPP products including start of season date (SOSD), end of season date (EOSD) and total productivity (TPROD) were used. HR-VPP data can be accessed and downloaded from WEkEO (https://www.wekeo.eu/), the European Union's Copernicus Data and Information Access Service (DIAS) platform for environmental data, virtual processing environments, and expert user assistance.

In addition to climate data such as precipitation, surface soil moisture and land surface temperature, elevation data was used to evaluate the effects of external factors to the productivity of olive trees.

Google Earth Engine was utilized as the data source for climate data and the platform to process and analyse all the data used in this research.

3.2.1.1 Olive tree map

In Chapter 2 of the thesis, the distribution of olive trees of Izmir Province was determined and defined as the “final olive map” (Figure 2.4b). This map was used as the base map and the study area of this research.

3.2.1.2 Vegetation phenology and productivity metrics

CLMS HR-VPP products are derived from Sentinel-2 satellites and have a five-day frequency with 10-metre spatial resolution. HR-VPP has three product groups and 35 product types. The vegetation indices (VI) group includes plant phenology index (PPI), leaf area index (LAI), fraction of absorbed photosynthetically active radiation (FAPAR), and normalized difference vegetation index (NDVI). Seasonal trajectories (ST) group consists time series of PPI and quality flag. The vegetation phenology and productivity (VPP) group has 13 metrics for up to two seasons each year, including the PPI value and date at the season's start, end, and peak, season length, seasonal and total productivity. They are extracted from seasonal trajectories and are also created yearly (European Union, 2022). In this research, vegetation phenology and productivity products including SOSD, EOSD and total productivity were used.

The purpose of this research was not to validate HR-VPP metrics in terms of value. Thus, the accuracy values stated in the HR-VPP user's manual (European Union, 2022) was considered as proper (Borgogno-Mondino and Fissore, 2022). The manual states that:

> The accuracy of phenology metrics (SOSD, EOSD) as compared with ground observations shows a slight positive bias of 4 days for SOSD, and negative bias of –11 days (anticipated end of season) for EOSD. The shorter seasons is the main issue observed which was confirmed as compared to other datasets, resulting in a shorter length of the season of 15 (MR-VPP) and 36 (MCD12Q2) days. Users should consider with caution (due to a possible anticipation) the end of the season dates. Large variability can be found in phenology metrics for bare areas where no clear temporal variations are expected (European Union, 2022, pp. 32).

Start of season date and end of season date

The start of season date (SOSD) and end of the season date (EOSD) are phenology metrics, determined by searching seasonal trajectories from minimum to peak levels, with the start and end of the season occurring when the amplitude exceeds a user-defined threshold. The threshold values are set at 15% for the end of the season and 25% of the seasonal amplitude for the start of the season after a detailed study using PhenoCam photos from 32 locations, carbon flux data from 49 sites, and manually recorded phenology observations from 1321 sites across Europe (Tian et al., 2021; European Union, 2022).

Izmir Province was covered by six Sentinel-2 L2A scenes. Covering the five-year period between 2017 and 2021, thirty SOSD and EOSD scenes for each were obtained from WEkEO platform and uploaded to GEE environment for further analysis. The final olive map was used to mask out non-olive pixels and produce annual maps of SOSD (Figure C.1 – C.5) and EOSD (Figure D.1 – D.5). SOSD and EOSD maps of 2017, 2018, 2019, 2020, and 2021 were produced separately. For district-level statistical analysis, median values of SOSD and EOSD were used to exclude outlier values. Average of annual median SOSD and EOSD values are used for province-level analysis.

Total productivity

Total productivity (TPROD), also described as the integral of growing season, is the sum of all daily PPI values (PPI × day) (European Union, 2022). The PPI values range between 0 and 3 while the day value is 365. Thus, physical TPROD values range between 0 and 1095. However, the digital value range is scaled with 10 (between 0 and 10950) and defined as digital number (DN). The value of each pixel represents the total productivity of that year. Total productivity data covering a five-year period between 2017 and 2021 were obtained from WEkEO platform and uploaded to GEE environment for further analysis. In order to compare the total produvtivity and TUIK crop yield data, cumulative total productivity of all pixels covering the final olive map was considered because the crop yield data represents the cumulative amount of olive crop yield. The final olive map was used to mask out non-olive pixels and produce annual TPROD maps (Figure E.1 – E.5). TPROD maps of 2017, 2018, 2019, 2020, and 2021 were produced separately.

3.2.1.3 Climate data

Climate is the main driver affecting the world ecosystems (Gang et al., 2017; Wang et al., 2018). In this research, the effects of precipitation, soil moisture and land surface temperature to the phenology and productivity of olive trees covering a five-year period between 2017 and 2021 was investigated.

Precipitation data

Precipitation, the primary water resource of the vegetation, has a significant effect on productivity (Beer et al., 2010; Bao et al., 2016) because it is essential for soil moisture and enables nutritient absorption and photosynthesis. Thus, it is crucial to investigate the effect of precipitation to the phenology and productivity of olive trees. Climate Hazards Group InfraRed Precipitation with Station data (CHIRPS) (Funk et al., 2015) was utilized for precipitation data since it has the highest spatial resolution (5566 m) among other datasets such as the Tropical Rainfall Measuring Mission (TRMM) (Adler et al., 2003) and the Global Precipitation Measurement (GPM) (Huffman et al., 2019). CHIRPS, a quasi-global rainfall dataset that spans more than 30 years, combines 0.05° resolution satellite images with in-situ station data to provide gridded rainfall time series for trend analysis and seasonal drought monitoring. The daily CHIRPS precipitation data is built-in GEE. Total annual, spring, summer, autumn precipitation was generated and evaluated with total productivity of olive trees. Furthermore, the precipitation of last three months before EOSD was considered to investigate the impact of precipitation to the EOSD and length of season.

Surface soil moisture data

Surface soil moisture (SSM), the water content of the top few centimetres of soil (Taylor et al., 2012), is a key environmental variable and crucial to understand global energy, carbon, and water cycles (Seneviratne et al., 2010). It is listed as an essential climate variable (ECV) by the Global Climate Observing System (GCOS) (Blunden and Arndt, 2012). The Copernicus daily Surface Soil Moisture (SSM) data, the first 1-km-resolution soil moisture monitoring data, utilise Sentinel-1 IW GRDH products (Bauer-Marschallinger et al., 2018). Copernicus daily SSM data were accessed and downloaded from WEkEO (https://www.wekeo.eu). 586 SSM images between 2017 and 2021 covering Izmir province were acquired. Since SSM products are presented in NetCDF4 file format, they converted to GeoTIFF before uploading to GEE environment for analysis. The unit of the daily SSM data is digital number (DN), range between 0 and 200.

Land surface temperature data

Land surface temperature (LST) has a substantial influence on plants, influencing photosynthesis, transpiration, vegetation health, phenology, and ecosystems. Monitoring LST gives useful insights into vegetation dynamics, water stress, and ecosystem functioning, hence assisting in sustainable management practises, climate research, and precision agricultural applications. The Moderate Resolution Imaging Spectroradiometer (MODIS) land surface temperature product provides daily land surface temperature with a spatial resolution of 1 km in a grid of 1200 × 1200 km. MODIS day-time and night-time LST products were accessed and processed on GEE platform. In order to investigate the impact of land surface temperature to the total productivity, spring, summer, autumn and annual land surface temperatures were considered for each year between 2017 and 2021.

3.2.1.4 Elevation data

Elevation is one of the main factors influence the growth of vegetation. The effects of the elevation to the phenology and the productivity of olive trees were investigated using European Digital Elevation Model (EU-DEM). It is derived using SRTM, ASTER GDEM and Russian topographic maps and presented in a format of Geotiff 32 bits. It is a contiguous dataset divided into 100 × 100 km tiles with a 25 m spatial resolution (Copernicus DEM, 2023). The vertical accuracy is +/- 7 metres of RMSE. EU-DEM was downloaded from https://land.copernicus.eu/imagery-in-situ/eu-dem/eu-dem-v1.1, the website of Copernicus Land Monitoring Service (CLMS). DEM data was uploaded to GEE platform and the effects of elevation to SOSD, EOSD and total productivity was investigated.

3.2.1.5 Crop yield data

District-level and province-level total crop yield statistics of Izmir province between 2017 and 2021 were obtained from TUIK website (TUIK 2022). Note that, the crop yield data represent the total amount of olive crop yield per year and per district/province. Therefore, crop yield data need to be related with annual cumulative TPROD and climate data to sustain the consistency between them. For example, annual cumulative TPROD and annual cumulative daily SSM data were considered for the correlation analyses.

3.3 Results

The seasonality and productivity of olive trees were examined and annual maps of SOSD, EOSD and TPROD were produced. The effects of climatic conditions and elevation to the productivity were evaluated. Furthermore, relationships between total productivity and crop yield were investigated.

3.3.1 Interannual variability of phenology

District-level and province-level seasonality of olive trees of Izmir were evaluated. It was observed that district level SOSD trend had less variation than EOSD. Both district-level (Figure 3.1 and Figure 3.2) and province-level (Figure 3.3) phenology metrics demonstrated that olive trees in 2018 have advanced SOSD and EOSD.

Furthermore, EOSD of all districts except Narlıdere was significantly delayed in 2018, resulted in shorter length of season (Figure 3.3).

Due to extraordinary decrease on EOSD of 2018, potential external factors were considered. For example, increasing precipitation is linked to advanced EOSD (Wu et al., 2021). Therefore, the cumulative precipitation during three months before EOSD were examined. In this regard, three months before the earliest EOSD across olive growing regions were considered. It was observed that increased precipitation in 2018 significantly shortened the growing season and resulted in advanced EOSD (Figure 3.4).

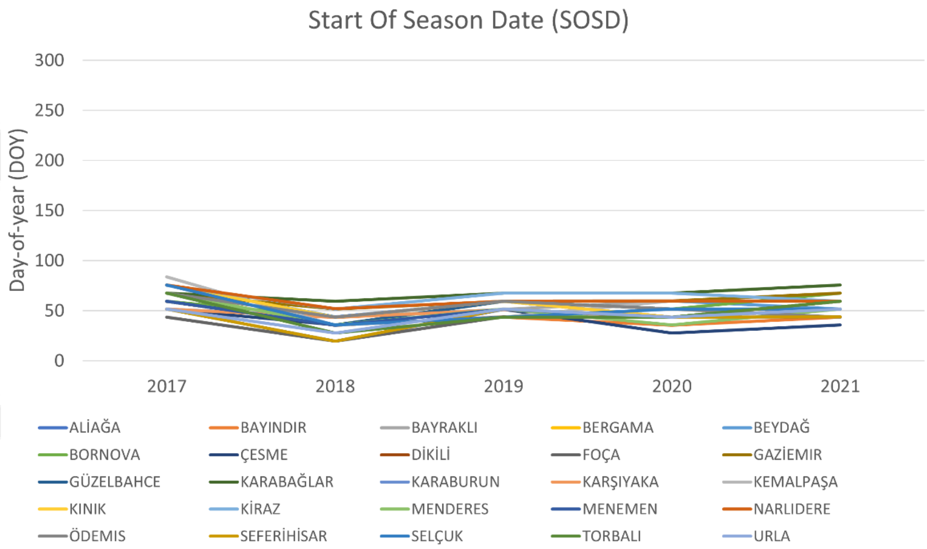

Figure 3.1 : District-level start of season dates of olive trees between 2017 and 2021. Y axis represents day of year (DOY) while X axis depicts years.

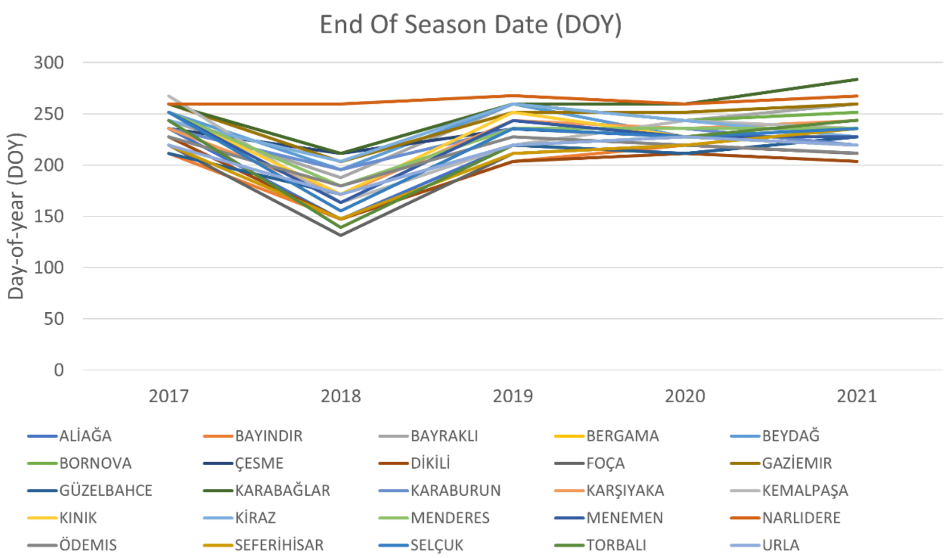

Figure 3.2 : District-level end of season dates of olive trees between 2017 and 2021. Y axis represents day of year (DOY) while X axis depicts years.

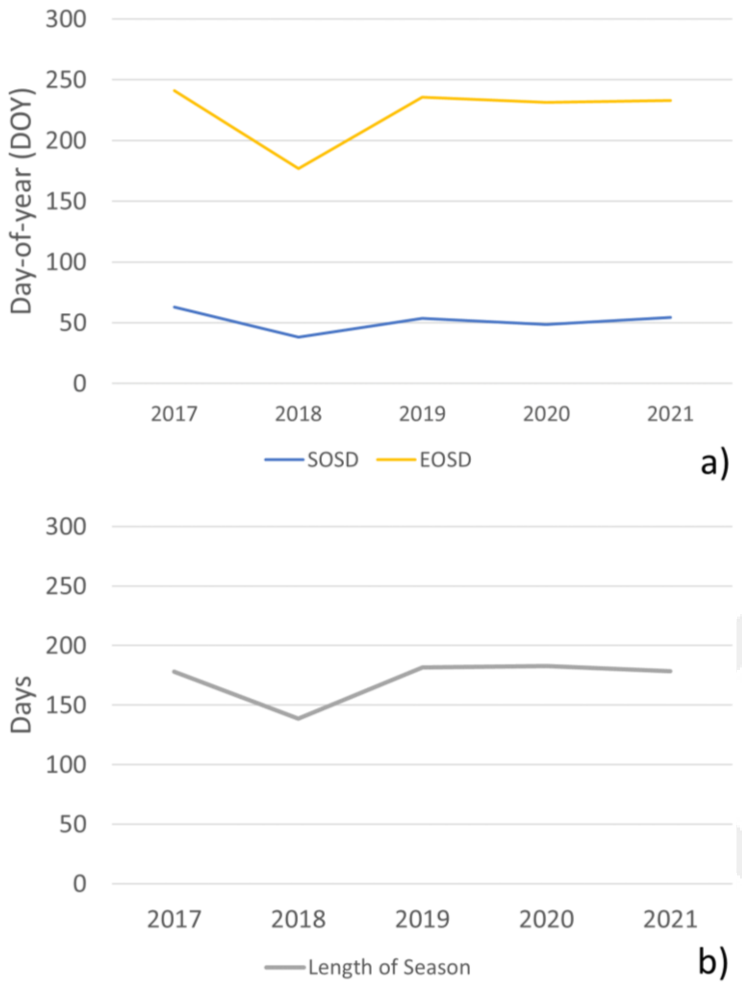

Figure 3.3 : a) Province-level 5-year average SOSD and EOSD of olive trees between 2017 and 2021. b) Province-level 5-year average length of season. SOSD and EOSD describe the start of season date and end of season date respectively.

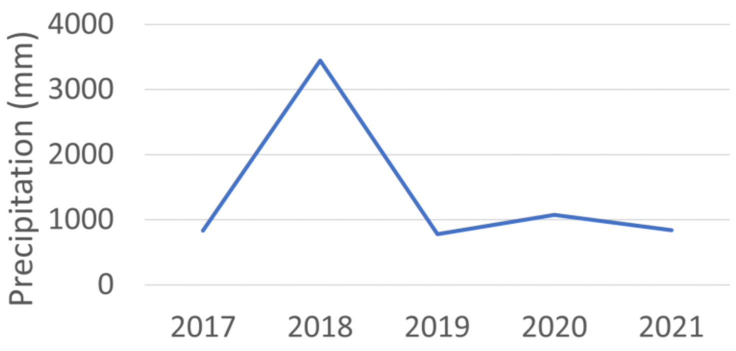

Figure 3.4 : Cumulative precipitation during three months before the end of season date (EOSD).

3.3.2 Phenology by elevation

Results indicated that SOSD and EOSD was delayed consistently until 1000-metre elevation. In addition, advancing EOSD trend slowed after 1000 m elevation. SOSD consistently delayed until 2000 m elevation. Advancing trend slowed after 2000 m elevation. Accordingly, as elevation increased, SOSD and EOSD of olive trees were delayed and the length of the season was shortened slightly (Figure 3.5). In addition, it was observed that the correlation between SOSD and elevation (R^2 = 0.43) was significantly higher than the correlation between EOSD and elevation (R^2 = 0.22) (Figure 3.6).

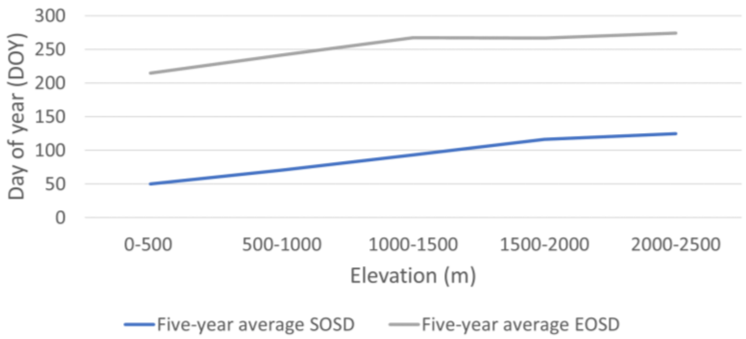

Figure 3.5 : Province-level 5-year average SOSD and EOSD of olive trees (2017-2021). SOSD and EOSD describe start of season date and end of season date respectively.

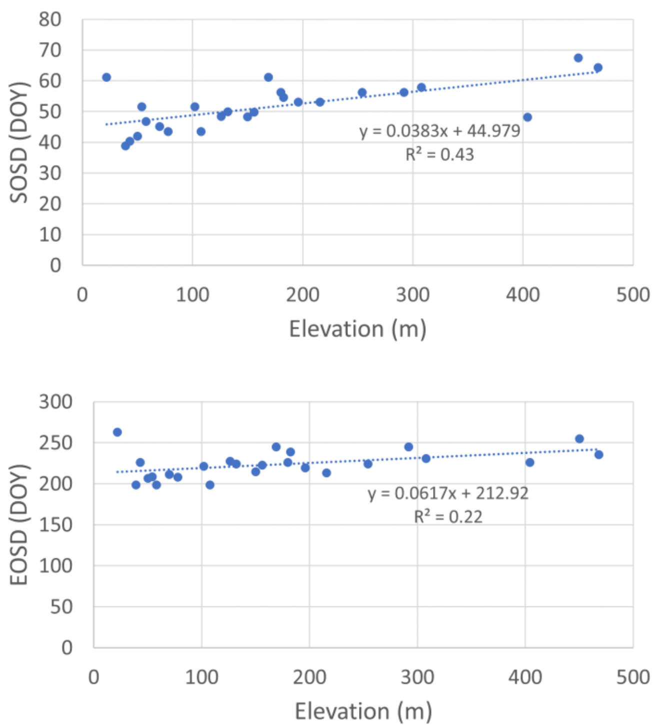

Figure 3.6 : District-level correlation between 5-year average phenology metrics (2017-2021) and elevation. SOSD and EOSD describe start of season date and end of season date respectively. Y axis represents Day of Year (DOY) while X axis depicts elevation (metre).

3.3.3 Total productivity by elevation

As the elevation was increased, the total productivity of olive trees was decreased (Figure 3.7). However, it was observed that the province-level five-year average mean TPROD between 500 and 800-metre elevations slightly fluctuated. Above this elevation, the decrease trend continued consistently over 800-metre elevations (Figure 3.7a). Furthermore, province-level five-year average cumulative TPROD decreased rapidly up to 600-metre elevation. Thereafter, the decline trend sustained but diminished (Figure 3.7b).

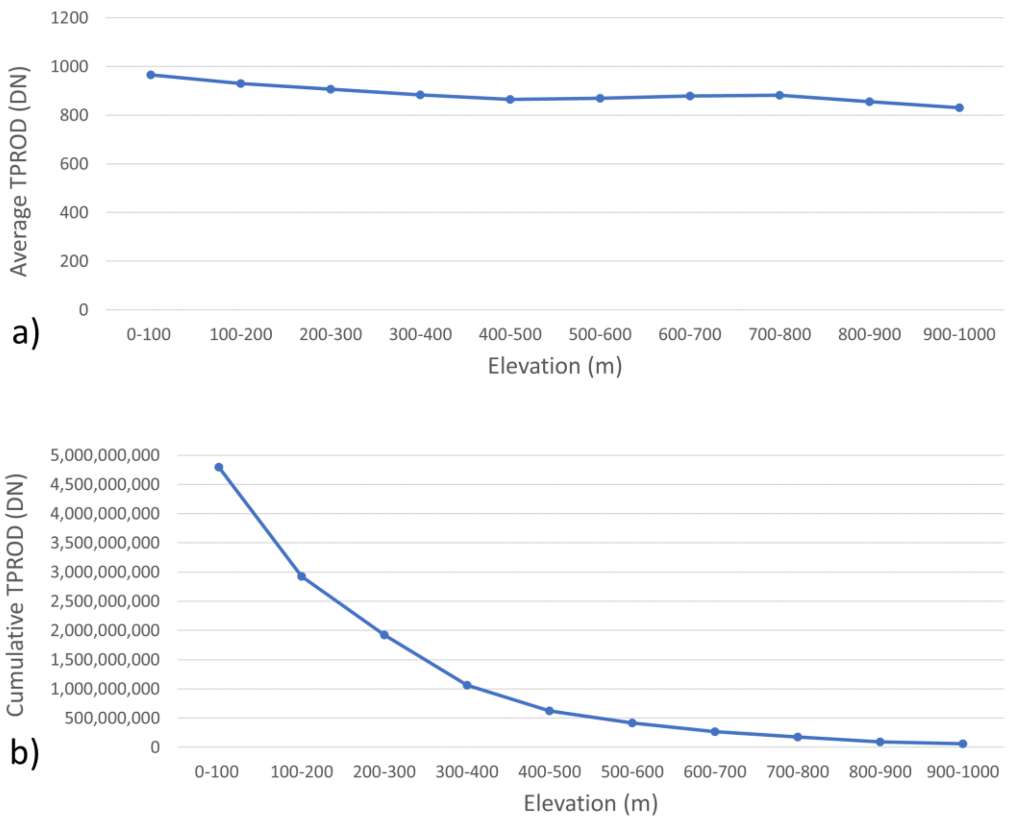

Figure 3.7 : a) Province-level five-year average mean TPROD; and b) Province-level five-year average cumulative TPROD according to elevations. TPROD defines total productivity while DN demonstrate digital number.

3.3.4 Relationships between total productivity and crop yield

As aforementiend in the Chapter 2, the total area covered by olive trees in Bayındır and Bergama districts were underestimated and overestimated, respectively. Therefore, field observations were conducted in these districts, explained in detail in Chapter 4 of the thesis. Therefore, the relationship between total productivity and crop yield were investigated both by including and excluding these districts. It was observed that TUIK crop yield had a good agreement with total productivity (R^2 = 0.58) when

Bayındır and Bergama districts were included (Figure 3.8a). Furthermore, a strong correlation ($R^2 = 0.77$) with total productivity was succeded (Figure 3.8b) when these two districts were excluded.

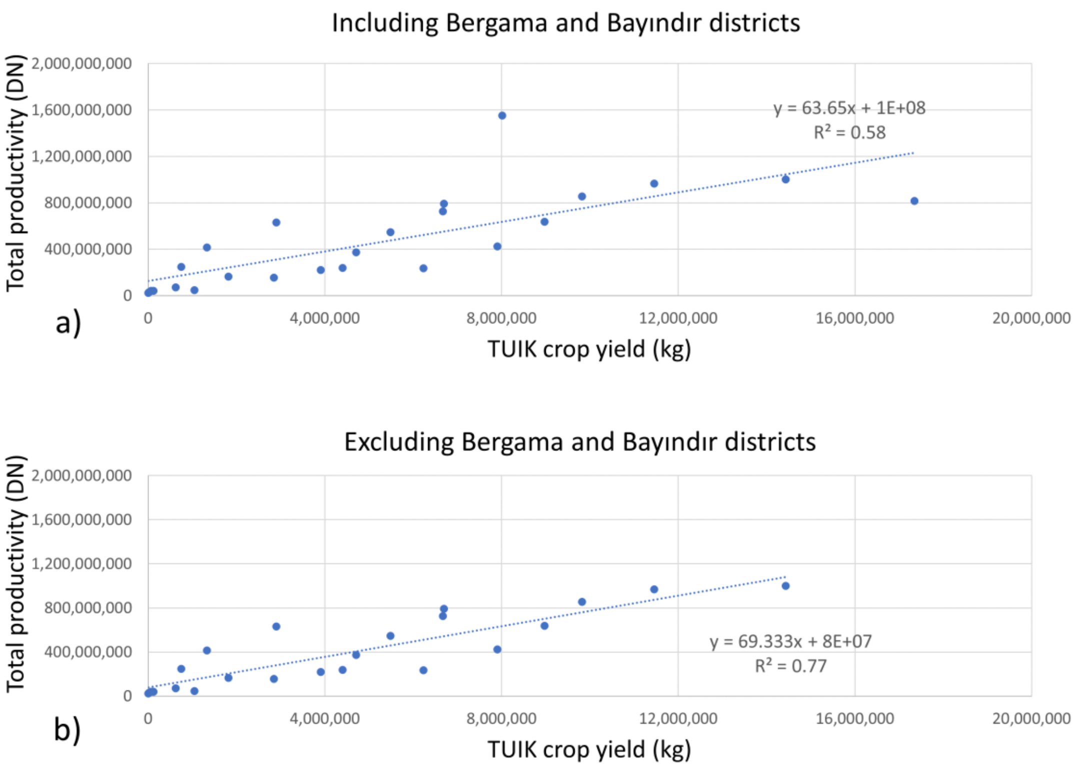

Figure 3.8 : District-level correlation between TUIK 5-year average annual total crop yield a) including Bayındır and Bergama districts; and b) excluding Bayındır and Bergama districts

3.3.5 Relationships between total productivity and climatic conditions

Total productivity corresponds to the cumulative daily productivity of the vegetation during the year. Therefore, in order to correlate TPROD and climatic condistions, total precipitation and total surface soil moisture were considered.

3.3.5.1 Relationships between total productivity and precipitation

Spring, summer, autumn as well as annual precipitation were considered to investigate the effects of precipitation on productivity in different phenological periods. Results demonstrated that the precipitation was strongly correlated to total productivity (TPROD) (Figure 3.9 – 3.12). Furthermore, spring (Figure 3.10) and autumn (Figure 3.12) precipitation was more correlated with total productivity than summer precipitation (Figure 3.11).

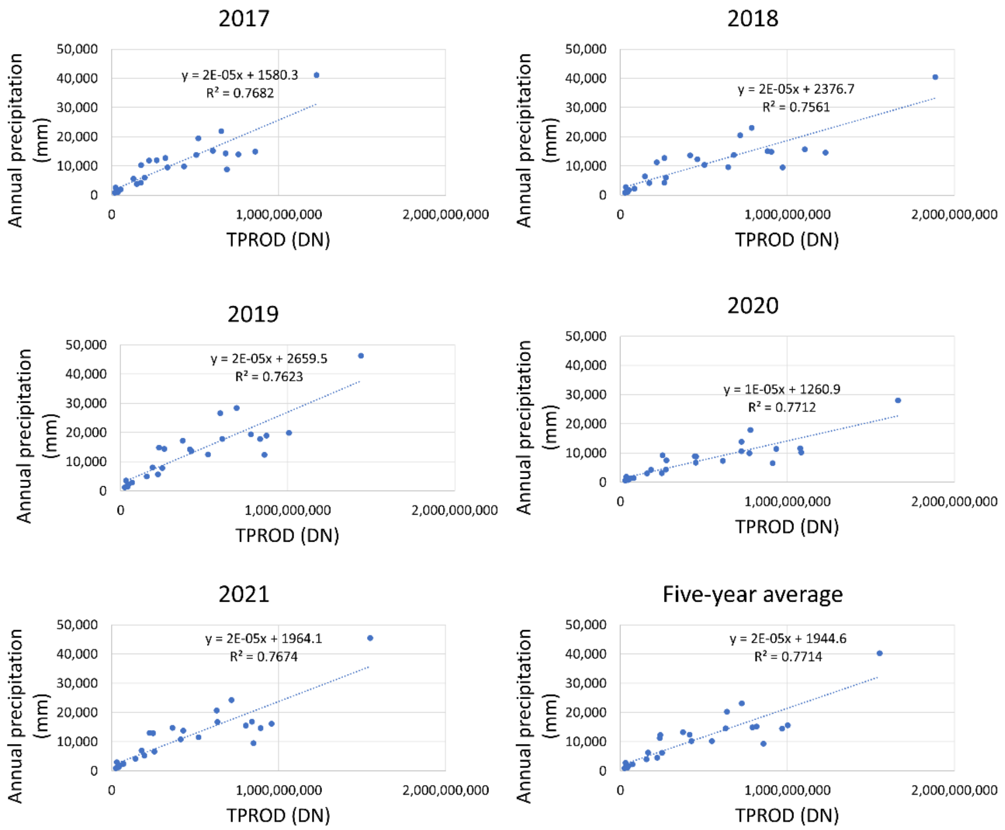

Figure 3.9 : District-level correlation between annual precipitation and TPROD.

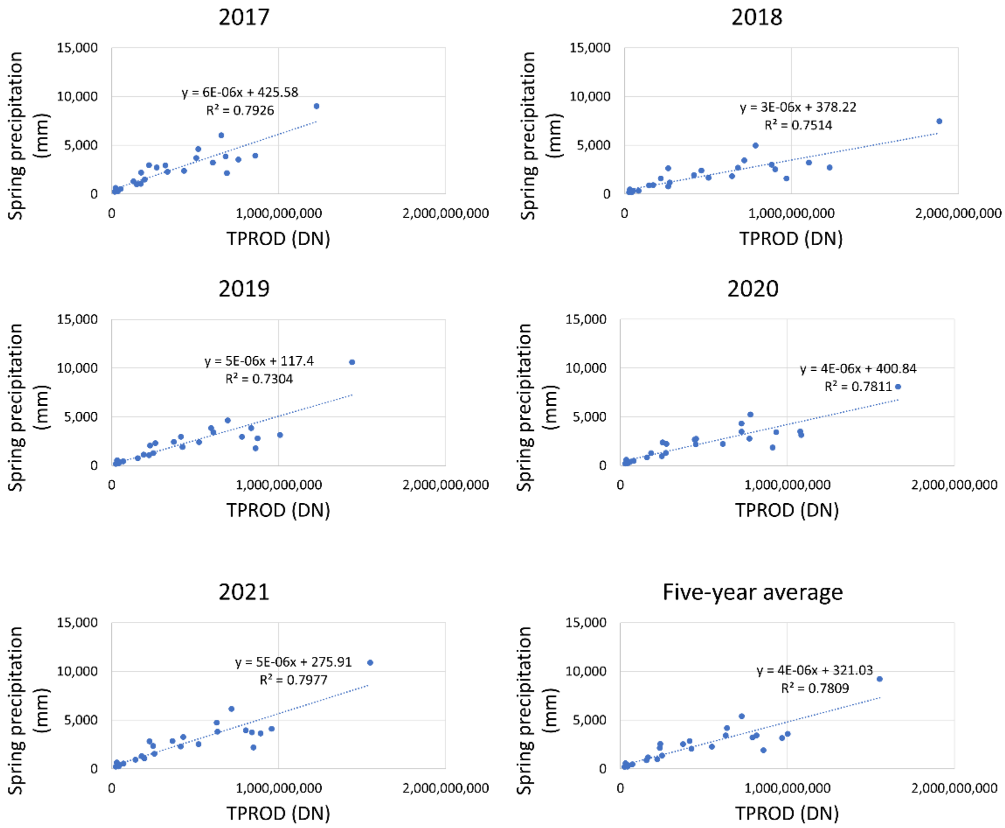

Figure 3.10 : District-level correlation between spring precipitation and TPROD.

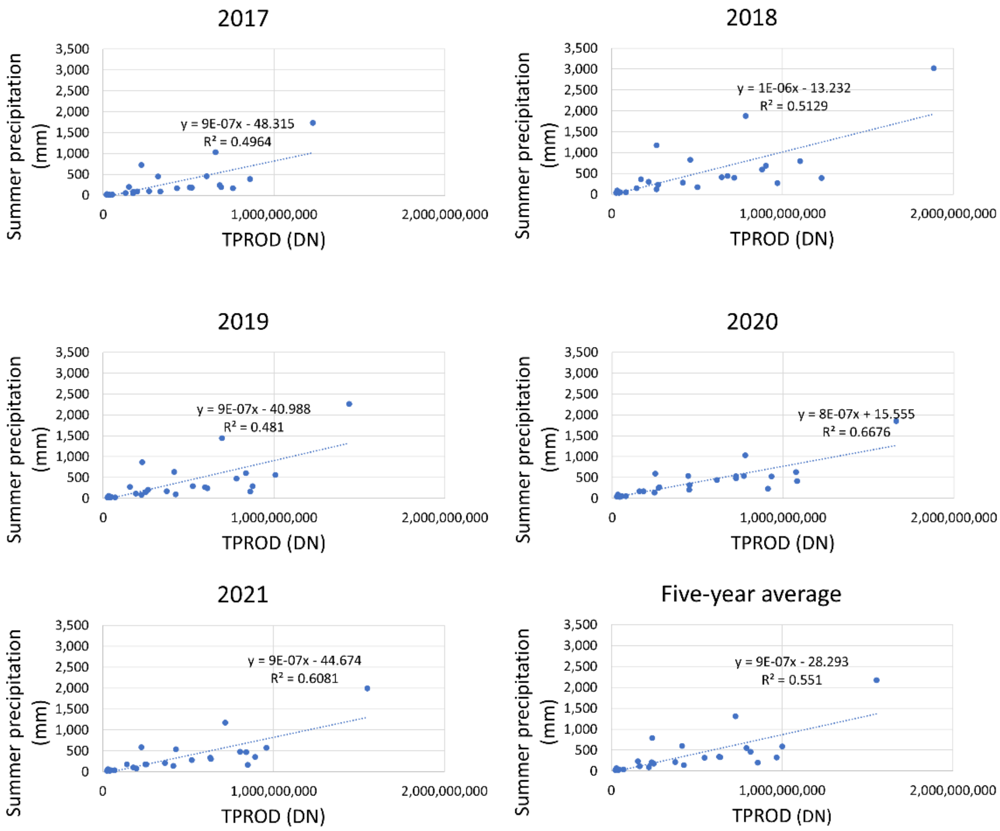

Figure 3.11 : District-level correlation between summer precipitation and TPROD.

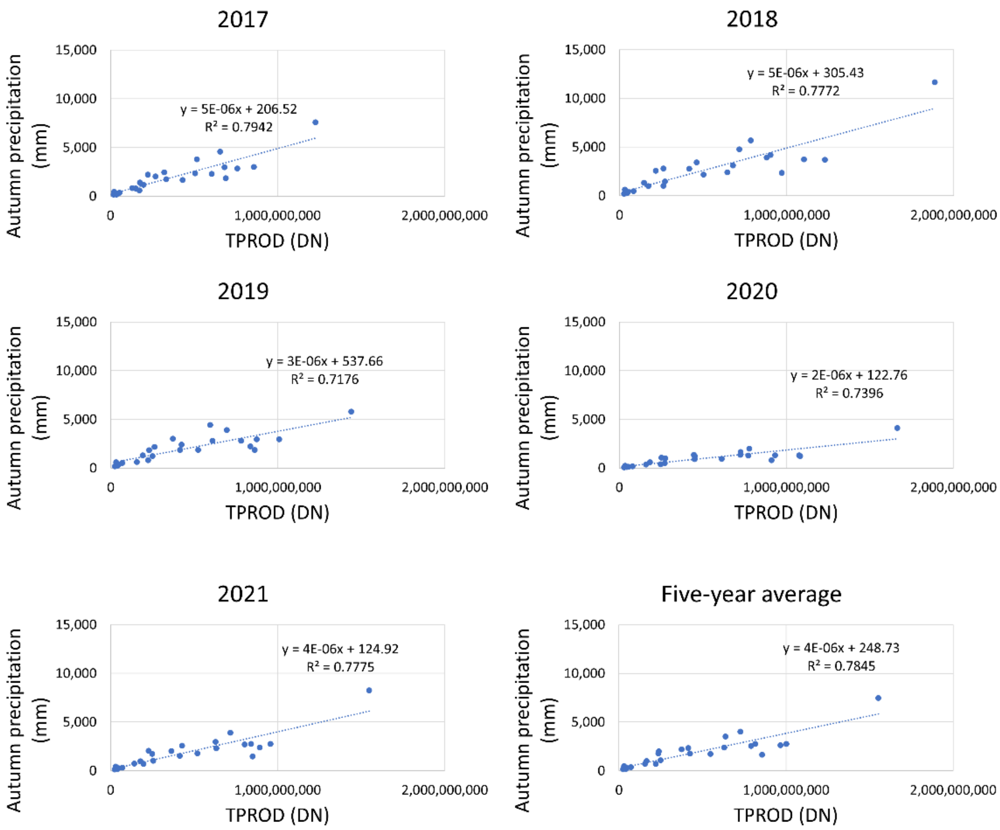

Figure 3.12 : District-level correlation between autumn precipitation and TPROD.

3.3.5.2 Relationships between total productivity and surface soil moisture

In addition to annual surface soil moisture, spring, summer and autumn surface soil moisture were considered to investigate the effects of SSM to the total productivity of olive trees in different phenological periods (Figure 3.13 – 3.16). Results showed that TPROD had strong correlation with surface soil moisture. According to five-year average statistics, the correlation between TPROD and spring surface soil moisture (R^2 =0.62) were higher than the summer (R^2 =0.51) and autumn (R^2 =0.51).

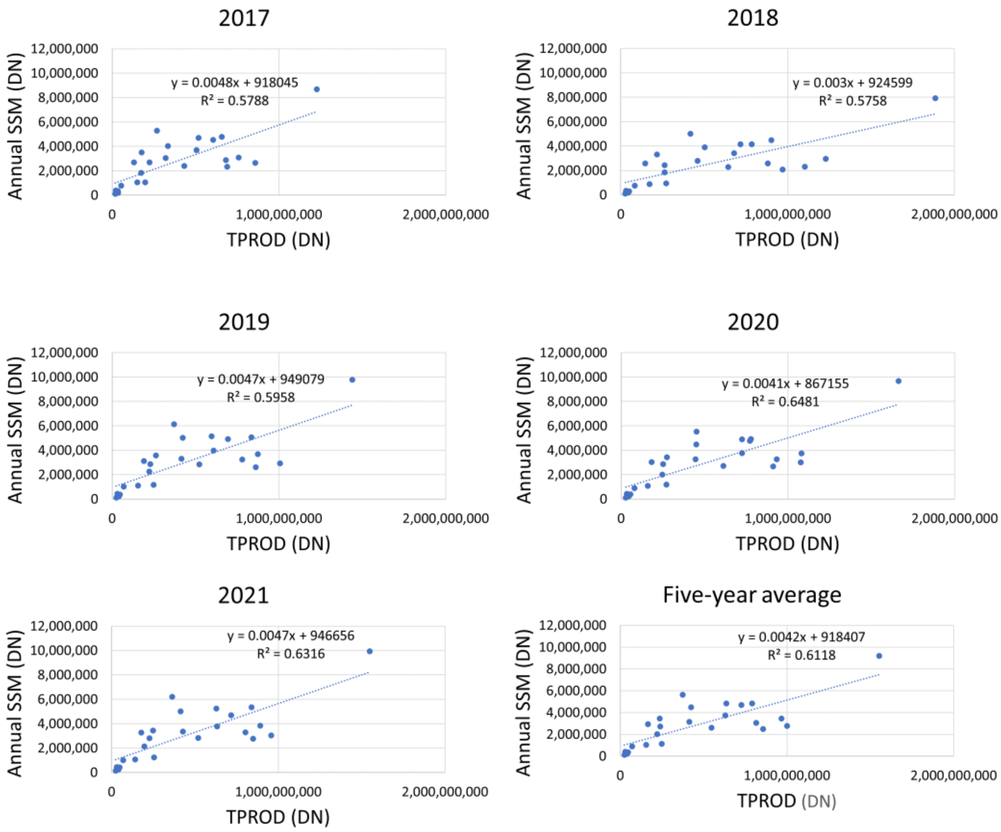

Figure 3.13 : District-level correlation between annual SSM and TPROD.

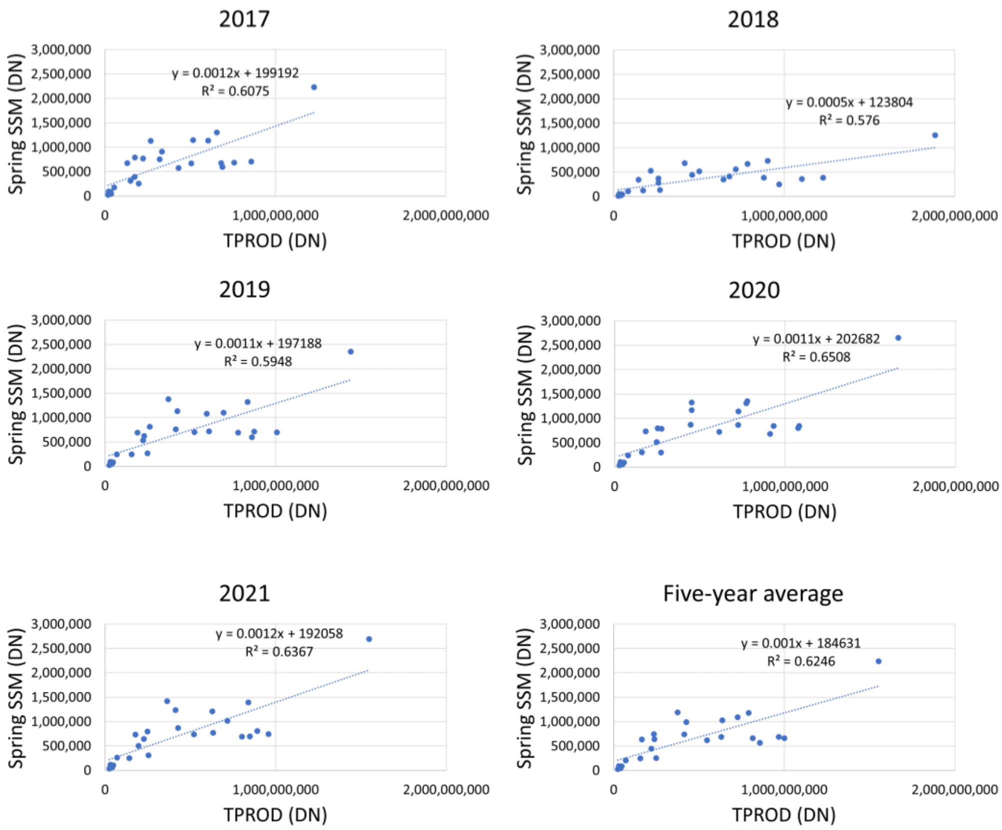

Figure 3.14 : District-level correlation between spring SSM and TPROD.

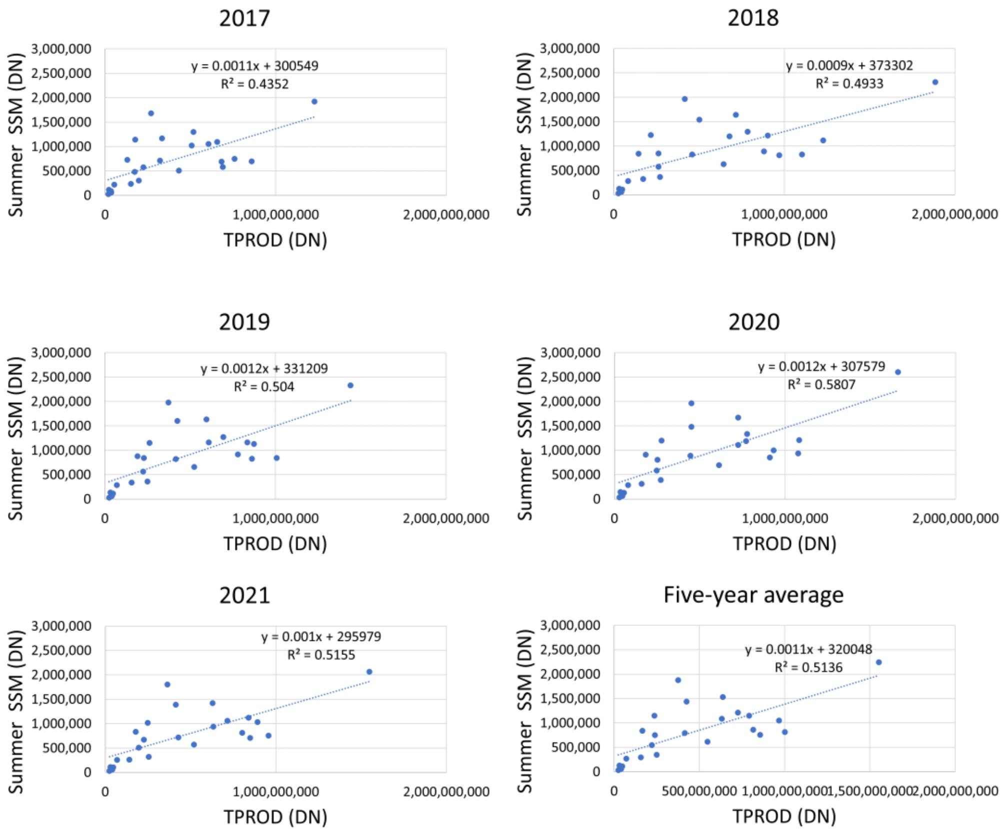

Figure 3.15 : District-level correlation between summer SSM and TPROD.

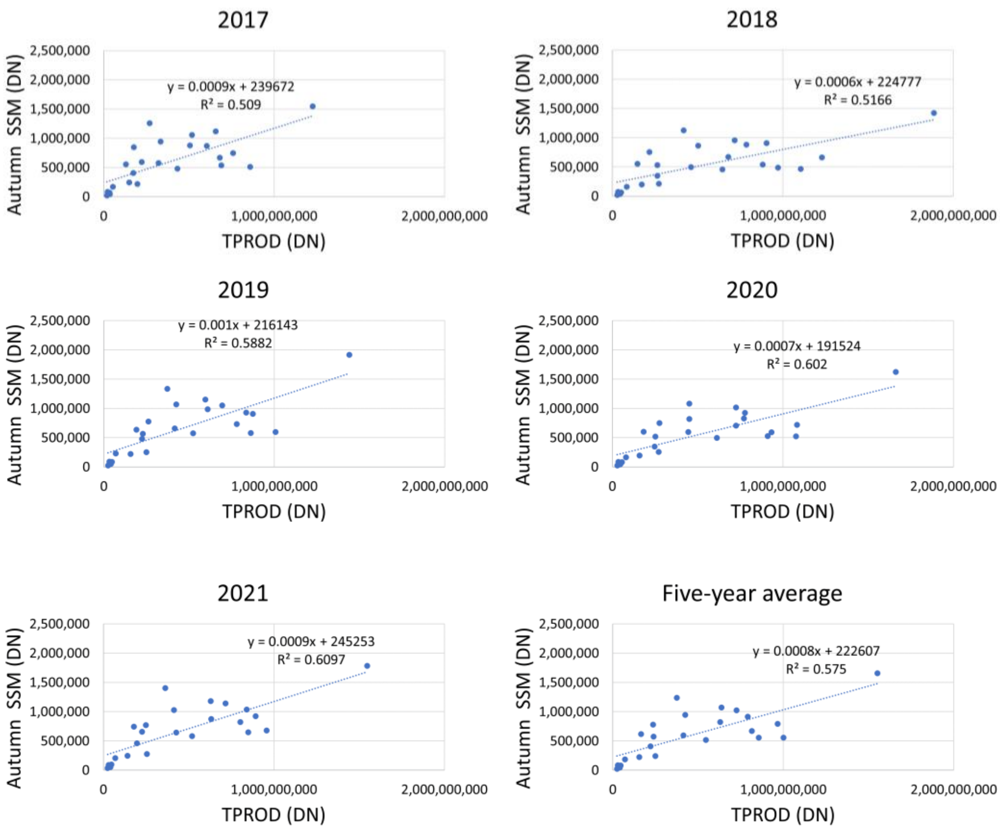

Figure 3.16 : District-level correlation between summer SSM and TPROD.

3.3.5.3 Relationships between total productivity and land surface temperature

In order to understand the relationships between the total productivity and land surface temperature, both day-time and night-time LST were used. In addition to annual LST, spring, summer and autumn LST were also investigated. This procedure was conducted separately for years 2017, 2018, 2019, 2020, 2021. However, no correlation found between total productivity and land surface temperature.

3.3.6 Start of season date and end of season date maps

The phenology metrics are expressed with day-of-year (DOY) values range between 1 and 365. In order to create comparable and consistent phenology maps, the earliest and latest DOYs covering a five-year-period (2017-2021) were selected as the minimum and maximum values for map representation threshold values.

3.3.6.1 Start of season date maps

The earliest start of season DOY in a five-year peried (2017-2021) was 19 while the latest one was 84. SOSD maps of olive trees were produced separately for years 2017, 2018, 2019, 2020 and 2021 using this procedure (Figure C.1 – C.5).

3.3.6.2 End of season date maps

The earliest end of season DOY in a five-year peried (2017-2021) was 131 while the latest one was 284. EOSD maps of olive trees were produced separately for years 2017, 2018, 2019, 2020 and 2021 using this procedure (Figure D.1 – D.5).

3.3.7 Total productivity maps

The lowest and highest total productivity value across “final olive map” covering a five-year-period (2017-2021) were 0 and 4786, respectively. However, the threshold values of TPROD map determined as 200 and 1800 for a better contrast visual representation. TPROD maps of olive trees were produced separately for years 2017, 2018, 2019, 2020 and 2021 (Figure E.1 – E.5).

3.4 Discussion

The phenology and productivity of olive trees in Izmir province were investigated. To the best knowledge, this research is the first attempt to use Copernicus Land Monitoring Service’s High-Resolution Vegetation Phenology and Productivity (HR-VPP) products derived from Sentinel-2 satellites to investigate the phenology and productivity of olive trees on a regional scale. It is also the first research on phenology of produtivity of olive trees in Türkiye using satellite remote sensing data. The cloud infrustructere of WEkEO and GEE enabled this research to exploit time-series of satellite-derived data. Most of other large-scale studies on vegetation phenology and productivity (VPP) were mainly concentrated on the regions with minimum human disruptions to understand the impact of climate change on ecosystems. Furthermore, VPP studies on agricultural crops are mainly focused on estimating phenological stages and yield estimation. In addition, several studies investigated the relationships between productivity and external factors but mostly focused on water availability (e.g. irrigation, water content). However, studies on phenology of productivity of olive trees using satellite remote sensing are limited but increasing over time. Most studies focused on estimating the crop growth/phenological phases of olive trees (Milicevic et al., 2020; Oses et al., 2020; Azpiroz et al., 2021; Hachicha et al., 2021). Furthermore, only two studies concetrated on productivity of olive trees. For example, Maselli et al. (2012) and Brilli et al. (2013) worked on gross primary productivity (GPP) prediction models. Apart these, this research have contributed to this research series with investigating the inter-annual variability of phenology and effects of climatic conditions and elevation to the productivity of olive trees on a regional-scale. The findings of this research are evaluated in the following paragraphs.

EOSD was reported to be positively linked to SOSD, implying that an advanced SOSD may be associated with an advanced EOSD (Wu et al., 2016). Accordingly, temporal SOSD and EOSD of olive trees had similar trends. For example, advanced SOSD in 2018 and 2021 resulted in advanced EOSD. Furthermore, delayed SOSD in 2017, 2019 and 2021 resulted in delayed EOSD (Figure 3.3a). However, SOSD trend had less variation than EOSD. This can be explained with the sensitivity of olive trees to external factors (e.g. local geographic, climatic, and environmental factors as well as human disturbance) during growing season.

An interesting outcome of this research is that EOSD of olive trees in Narlıdere had less variation in 2018 than other districts. Given that Narlıdere's seasonality was akin to that of other districts in 2017, 2019, 2020, and 2021, this result needs further investigations. Because Narlıdere has similar precipitation and surface soil moisture patterns to other districts, it may be inferred that unexpected factors impacted EOSD of olive trees in 2018. According to information obtained from Izmir Olive Research Institute (https://arastirma.tarimorman.gov.tr/izmirzae), several factors, including pruning and fertilization, have significinat impacts to the phenology and productivity of olive trees. For example, the following year of the pruning may significantly lower the crop yield. Furthermore, irrigation is considered as another significant driver. Wu et al. (2021) reported that EOSD is advanced by increasing precipitation. Likewise, increased precipitation in the three months before EOSD significantly advanced the EOSD of olive trees in 2018 (Figure 3.4).

Elevation is one of the significant parameters affects the vegetation phenology and productivity. Increasing elevation is linked to delayed SOSD, advanced EOSD and shortened length of season (Wu et al., 2021). However, some studies linked advanced SOSD with longer length of season (Myneni et al., 1997; Julien and Sobrino, 2009; Wu et al., 2012, Wu et al., 2016). In the case of this research, as elevation increased, SOSD and EOSD of olive trees were delayed and the length of the season was shortened. However, no significant decrease on the length of season was observed up to 1000-metre elevation. Apart these, the correlation between SOSD and elevation (R^2 = 0.43) was significantly higher than the EOSD and elevation (R^2 = 0.22) (Figure 3.6).

Considering the less sensitivity than EOSD, higher correlation of SOSD and elevation can be explained with the higher dependency of SOSD to the elevation.

Increasing elevation is linked to decline in soil nutrients (Sun et al., 2022) which adversely affects the organic matter absorption of the plant (Demers et al., 1998). Moreover, as elevation increased, physiological characteristics such as leaf area, biomass of roots and stomatal conductance are reported to decrease (Frank et al., 2015) which may result in decline of productivity. Likewise, total productivity of olive trees was decreased as the elevation increased. Nevertheless, it was slightly fluctuated between 500 and 800-metre elevations. Aforementined olive forests mixed with other vegetation in hillsides as well as shrubs, grass and weeds among olive groves are more likely to be denser in higher elevations that can potentially distort the spectral reflectance in higher elevations. These can explain the fluctuations on total productivity between 500 and 800-metre elevations. Nevertheless, this result needs further investigations because productivity shows discrepancies based on the specific locations (Wu et al., 2016). Apart these, Ayaz and Varol (2014) reported that the ecologies that are most suited for olive farming is up to 600-metre elevation which may explain the shrink of cumulative TPROD above 600-metre elevations (Figure 3.7b).

Crop yield and total productivity are closely related concepts in the context of agriculture. Crop yield refers to the amount of a specific crop harvested from a given area of land. It focuses on the productivity of cultivated plants, such as grains, fruits, or vegetables, and is measured in terms of weight or quantity per unit area/tree. However, total productivity represents the productivity of all vegetation within a given area (per pixel). It includes not only cultivated crops but also natural vegetation, such as weed, grass, trees, shrubs, and other plants inside the pixel. Therefore, a good correlation between these two is expected, even though not perfect. Accordingly, a strong correlation ($R^2 = 0.77$) with total productivity was achieved (Figure 3.8b) when Bayındır and Bergama districts were excluded (due to underestimation and overestimation issues). This result also demonstrated the importance of the field observations in agricultural studies.

Studies reported the vitality of water for the productivity of vegetation (Churkina and Running, 1998; Aguirre-García et al., 2021). Similarly, increased water availability is linked to increased crop yield of olive trees (Caruso et al., 2022) even though their water resistant capability. For example Aguilera et al. (2019) reported precipitation as one of the main drivers of the fluctuations on olive crop yield. They stated that precipitation before and after flowering stages has strong impact on fruit productivity. Likewise, it was observed that the correlation between five-year average total productivity and spring precipitation between 2017 and 2021 was quite strong (R^2 = 0.78). Summer and autumn precipitation were also reported to be positive driver for the higher olive crop yield. Accordingly, even though not as good as spring and autumn precipitation, summer precipitation was well correlated with total productivity (R^2 = 0.55).

Soil moisture is described as the key parameter (Zribi et al., 2011) for the water, energy and carbon cycle (Bauer-Marschallinger et al., 2018). Its influence on vegetation productivity was reported to be significant, particularly in dry seasons (Cleverly et al., 2016). In the case of this research, surface soil moisture was well correlated with total productivity (Figure 3.9 – 3.12). It was observed that five-year average spring correlation (R^2 = 0.62) between SSM and TPROD was higher than that between annual (R^2 = 0.61), autumn (R^2 = 0.58) and summer (R^2 = 0.51) surface soil moisture. This finding supports the previous studies' indication on water requirements of olive trees in flowering stage.

One of the significant outcome of this research was the correlation between precipitation and total productivity was stronger than that between surface soil moisture and total productivity. This can be explained with the contribution of water stored under the soil surface (Ren et al., 2022b) to the productivity of olive trees. This is because even after the surface soil moisture is evaporated, olive tree roots may able to absorb the water from under the surface.

In addition to the precipitation and surface soil moisture, the effects of land surface temperature to the productivity of olive trees were investigated. Annual, spring, summer and autumn day-time and night-time mean temperatures were considered but no significant correlation was observed. This can be due to the adverse effects of background vegetation among olive trees, particularly in hillsides which might distort the land surface temperature data. Moreover, daily minimum and maximum temperatures (Wu et. al., 2021) may also be considered in the future researches because studies reported the vitality of minimum temperature during the winter chilling period of olive trees (Efe et al., 2013). Apart from these, higher spatial-resolution data as well as thermal imagery may be considered to have better results.

As described in details in Chapter 2, olive trees of Izmir were classified very well despite limitations may caused misclassification particularly in hillsides. This issue has been confirmed by field observations in Bayındır and Bergama districts, explained in detail in Chapter 4. Therefore, all limitations described in Chapter 2 need to be considered for this chapter as well, because the olive map produced in Chapter 2 was used as the base map in this chapter. However, despite all these limitations, very good agreements between total productivity and climatic conditions (precipitation and surface soil moisture) were succeded. Moreover, interannual variability of phenology of olive trees and the impacts of elevation to the phenology and productivity was sufficiently evaluated and potential drivers were explained.

3.5 Conclusion

In this research, the phenology and productivity of olive trees in Izmir province were investigated on a regional scale. The results demonstrated that phenology of olive trees in Izmir province were significantly influenced by precipitation and elevation. Moreover, findings demonstrated that the total productivity has close relationships with external factors such as climatic conditions (i.e. precipitation and surface soil moisture) and elevation. This research is one of the first attempts to exploit the CLMS HR-VPP products utilising the power and opportunities of cloud infrastractures of WEkEO and GEE. In addition, this is the first regional satellite based phenology and productivity study on olive trees in Izmir Province and Türkiye. The method presented is a scalable approach to other tree crops regionally and globally. This method's expansion to other regions of Türkiye will open the door to the first country-scale research of olive trees.

4. FIELD OBSERVATIONS

In Chapter 2 of the thesis, olive trees covering the Izmir province were classified and the total area computed on district basis. Then, calculated olive tree area was validated with official TUIK statistics (https://www.tuik.gov.tr). The results showed that the classification led to a slight overestimation. However, the classification underestimated and overestimated in Bayındır and Bergama districts, respectively. This resulted in distortion in the correlation between TUIK data and final olive map (Figure 2.5).

In the Chapter 3 of the thesis, the total productivity of olive trees covering the Izmir province were investigated on district basis. Total productivity was compared with TUIK crop yield statistics. The results demonstrated that two districts distorted the correlation between total productivity and TUIK crop yield. It was observed that total productivity of olive trees in Bayındır district was less than it should be due to the underestimation while total productity of olive trees in Bergama district was more than it should be due to overestimation.

Based on the findings in Chapter 2 and Chapter 3, olive trees in Bayındır and Bergama districts were decided to be investigated with field observations in order to understand the reasons of underestimation and overestimation. In this regard, first of all, final olive map was overlaped with Google Earth high-resolution image and locations of potential misclassified olive tree areas in Bergama and Bayındır districts were determined. As aforementioned in the Chapter 2 (Figure 2.1), olive trees in hilly areas are more likely to be misclassified due to mixed vegetation. When determining the locations for the field observations, this issue was considered.

4.1 Field Observations in Bayındır

More than half of Bayındır district consists of hills and mountains. In addition to the homogeneous distribution of olive trees in flat areas, they are distributed among mixed vegetation in hilly areas and adjacent to forests (Figure 4.1). Olive trees in hilly areas are likely to be misclassified as non-olive (e.g. shrubland, forest).

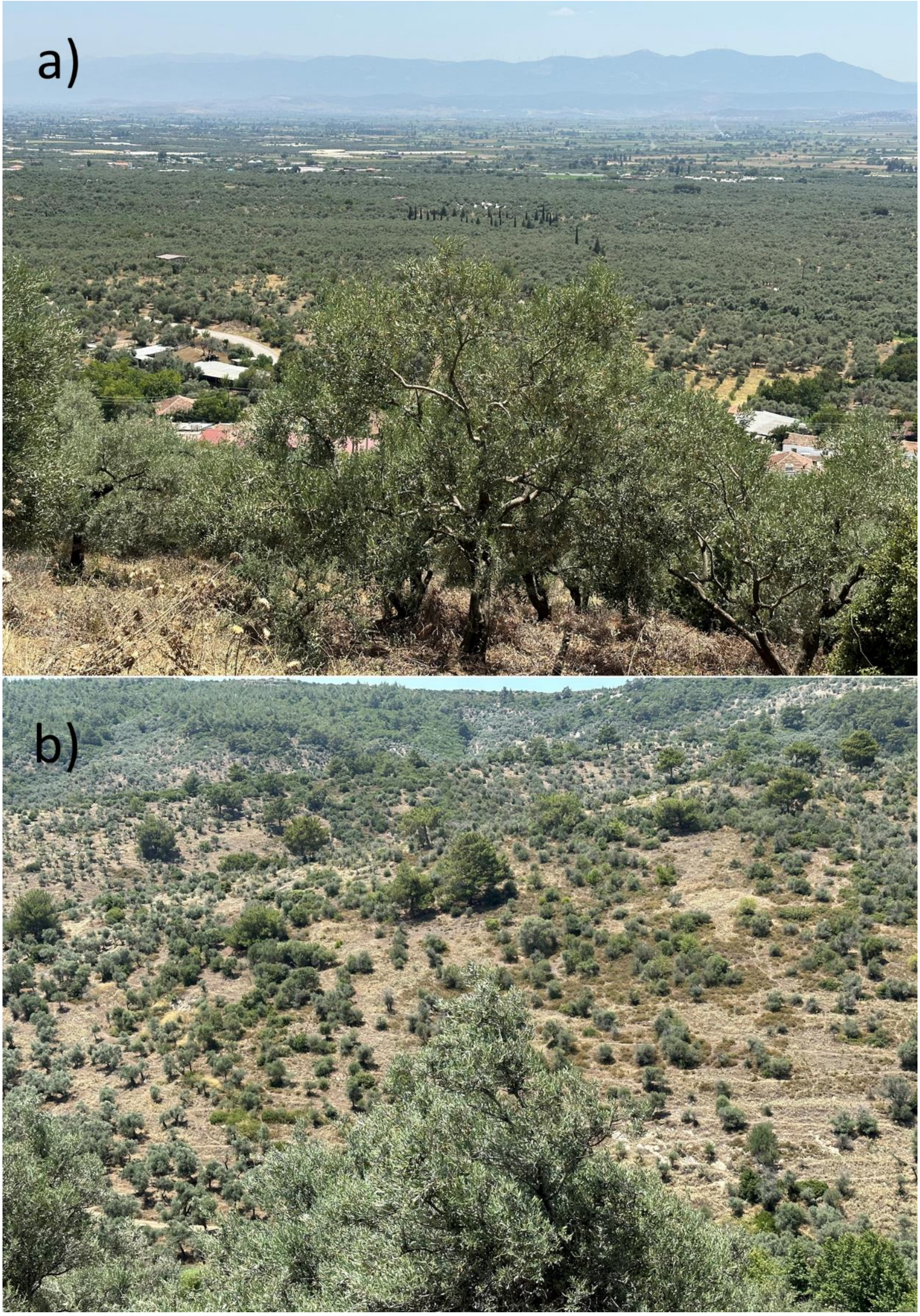

Figure 4.1 : a) Homogeneous olive tree distribution in a flat area and b) Olive trees in an heterogenous hilly area of Bayındır district.

Three different misclassifed regions were observed in Bayındır district. In the first region, olive trees were sparsely scattered to the region and mixed with other vegetation. The first zone of the first region was mostly distributed with olive trees and correctly classified as olive. However, the second and the third zones were sparsely vegetated and consisted of olive trees and mixed vegetation including pine trees and weed. These two zones were misclassified as non-olive (Figure 4.2).

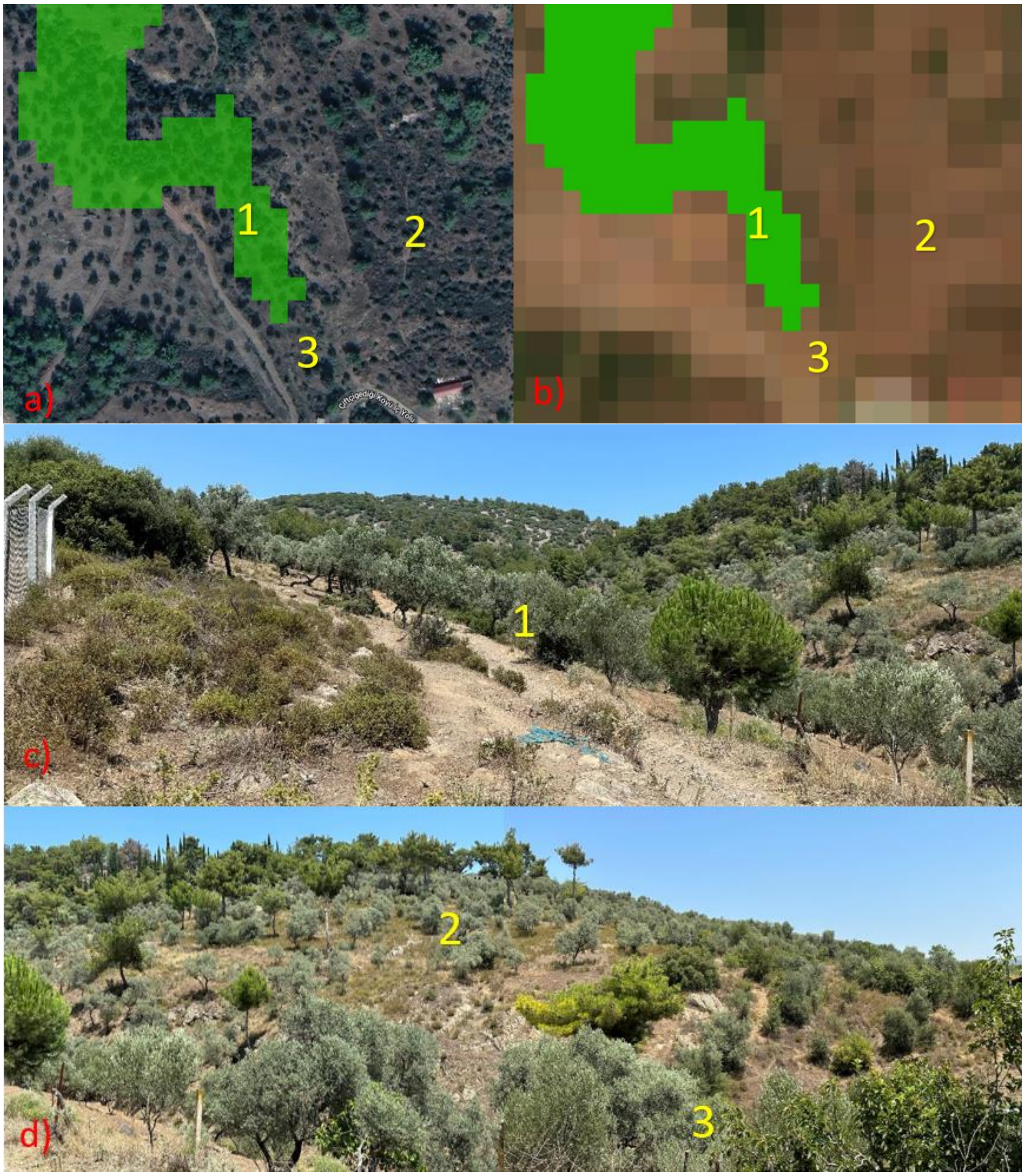

Figure 4.2 : Olive classified areas in green colour and three zones of the first observation region on a) Google Earth high-resolution image; and b) Sentinel-2 L2A RGB image; c) photo of the first zone; d) photo of the second and third zones.

Five zones were observed in the the second observation region (Figure 4.3). The first, second, third, and fourth zones were misclassified as non-olive. The first zone mostly consisted of olive trees. However, in addition to pine trees, dense background vegetation such as weed and soil among olive trees were considered as the main factors for misclassification.

Figure 4.3 : a) Olive classified areas in green colour and five zones of the second observation region on a) Google Earth high-resolution image; and b) Sentinel-2 L2A RGB image; c), d), e), f) and g) are the photos of the first, second, third, fourth and fifth zones, respectively.

In the second, third and fourth zones of the second observation region, olive trees were mostly mixed with background vegetation such as weed. Furthermore, pine trees and shrubs were also other factors for misclassification in these zones. The fifth zone was mostly covered with olive trees. Eventhough the existence of pine trees and weed among olive trees, this zone was correctly classified as olive.

Three zones were observed in the third observation region of Bayındır district (Figure 4.4). Olive trees in the third observation region were formed by the expansion of olive groves towards the forest area. Therefore, olive trees in this region were adjacent to forest area and mixed with pine trees. Thus, in addition to pine trees, background vegetation and soil among olive trees were main factors for the misclassification of these zones as non-olive.

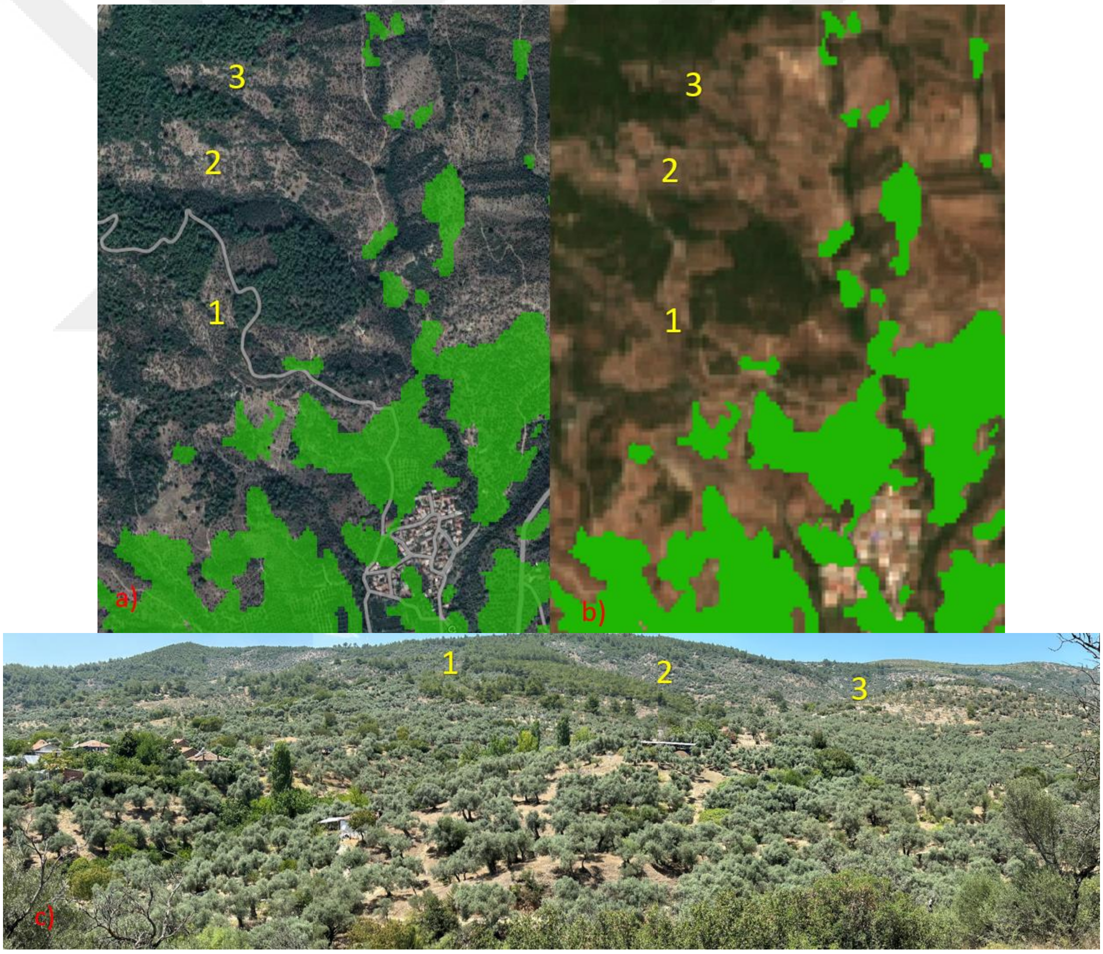

Figure 4.4 : Olive classified areas in green colour and three zones of the third observation region on a) Google Earth high-resolution image; and b) Sentinel-2 L2A RGB image; b) the photo of the three zones in the region.

4.2 Field Observations in Bergama

Bergama is the largest district in Izmir Province in terms of surface area, and it is mostly made up of hills. Olive trees are distributed across both flat and hilly areas of the district. Furthermore, they were also observed in densely heterogeneous areas, the vast majority of which consisted of other vegetation including shrubs, holm oak, as well as bare soil, stones and rocks (Figure 4.5).

Figure 4.5 : Olive trees in hilly heterogenous canopies of Bergama district.

Apart these, regions with holm oak tree (*Quercus ilex*) distribution were observed. In addition to its morphological structure, the colour of the leaves of the holm oak resemble that of the olive tree (Figure 4.6). These similarities were considered to be a potential basis for misclassification as olive, which might be the main driver of Bergama district's overestimation in olive area and total productivity.

Figure 4.6 : The morphological structures of a) holm oak (*Quercus ilex*); and b) olive tree (*Olea europaea*).

Accordingly, three different misclassified regions were observed in Bergama district. Field observations in the first and the second regions of Bergama district were validated that the misclassification of holm oak trees as olive resulted in overestimation in classification area and total prouductivity.

The first observation region was mostly covered with holm oaks with background vegetation and soil among them. Even though the region was located in higher elevation, it was mostly flat. Therefore, the resemblance of the canopy to the olive groves in flat areas was considered as the main driver for the misclassification. Figure 4.7 demonstrates the location and photos of the first region.

In the second region, holm oak trees were sparsely distributed in the first zone while they were denser in the second zone. Therefore, the first zone was correctly classified as non-olive but the second zone was misclassified as olive. Figure 4.8 shows the location and the photos of the second region.

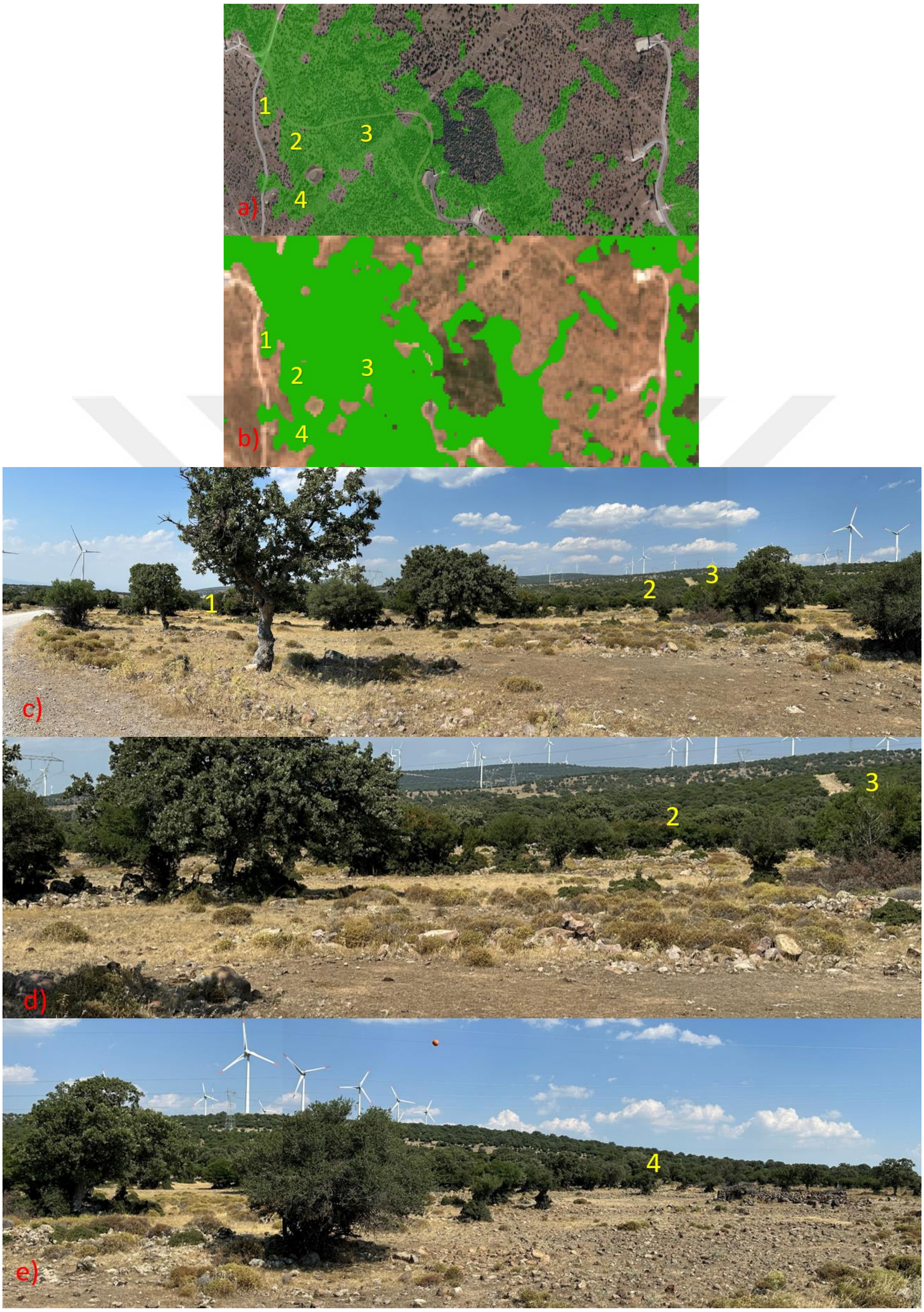

Figure 4.7 : Olive classified areas in green colour and four zones of the first observation region on a) Google Earth high-resolution image; and b) Sentinel-2 L2A RGB image; c) the photo of the first, second and third zones; d) closer look at second and third zones; e) the photo of the fourth zone.

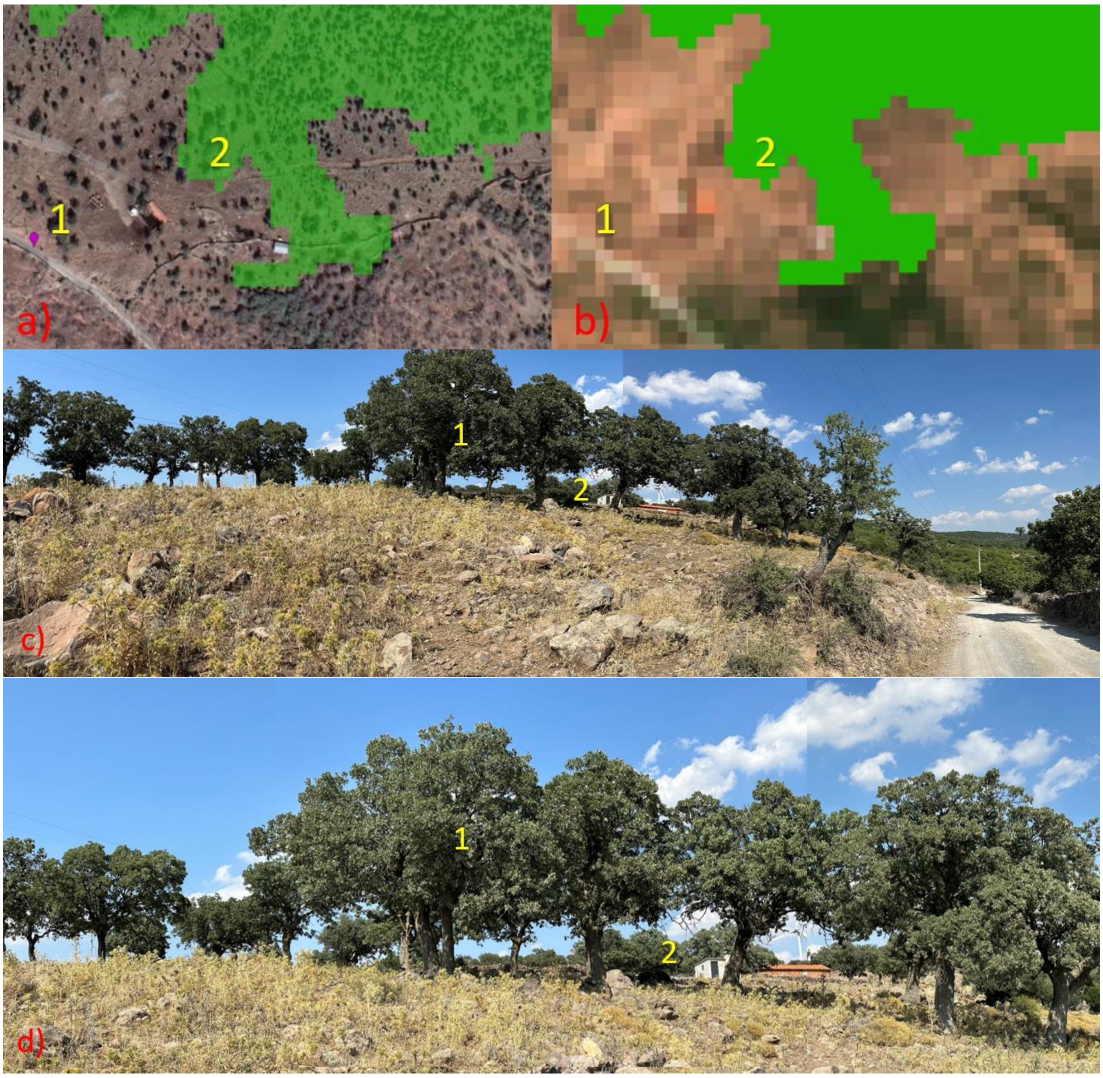

Figure 4.8 : Olive classified areas in green colour and two zones of the second observation region on a) Google Earth high-resolution image; and b) Sentinel-2 L2A RGB image; c) the photo of the first and the second zones; d) closer look at first and second zones.

As aforementioned in the Chapter 2, historical images and street view capability of Google Earth was used for determining the locations of olive tree samples across Izmir province. The lack of street view opportunity in hilly areas resulted in taking very limited amount of olive samples. As a result, sparsely vegetated trees in hilly regions were likely to be misclassified as olive since their canopy structure resembled that of olive trees. This condition was seen to occur in the first zone of Bergama's third observation region. The second zone, on the other hand, which was densely vegetated with pine trees, was correctly classified as non-olive (Figure 4.9).

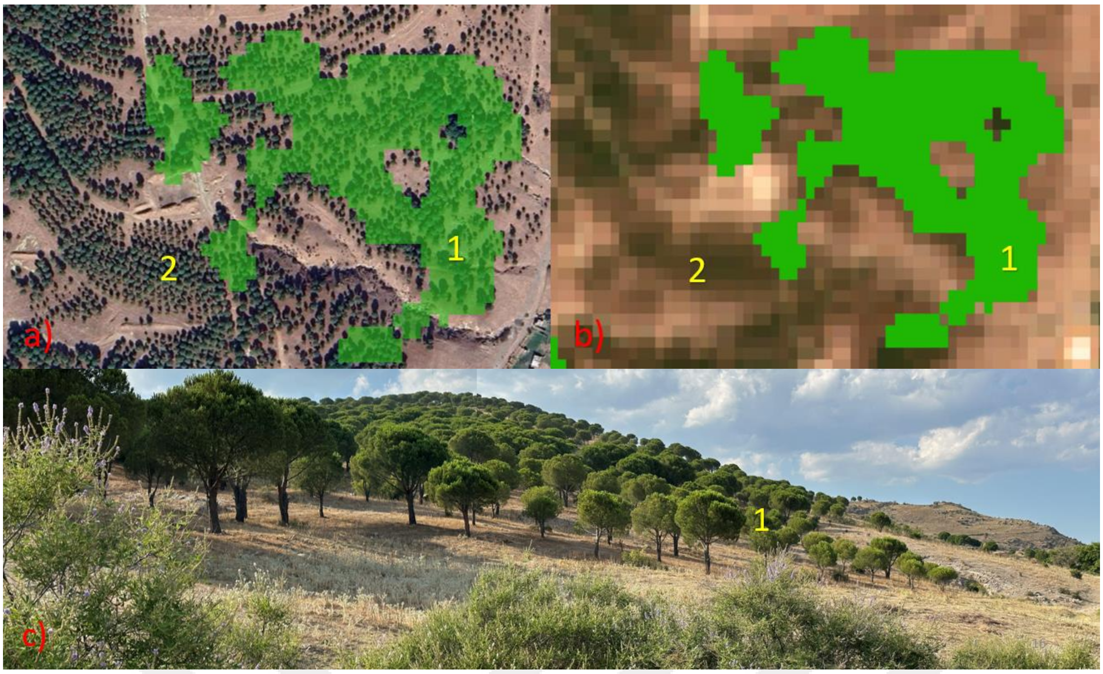

Figure 4.9 : Olive classified areas in green colour and two zones of the third observation region on a) Google Earth high-resolution image; and b) Sentinel-2 L2A RGB image; c) the photo of the first zone.

5. DISCUSSION AND CONCLUSION

This thesis is one of the first attempts to utilise the power and potential of WEkEO and GEE cloud infrastructures using Sentinel-1 and Sentinel-2 data as well as CLMS HR-VPP products. This study evaluated the potential of regional olive tree mapping and investigated their phenology and productivity using Sentinel-1 and -2 derived data. As studies using VHR images are still expensive and challanging, the availability of Sentinel-derived data is crucial for regional to global scale studies.

In Chapter 2, the efficacy of multitemporal Sentinel-1 and -2 data for olive tree classification was assessesd using random forest classifier. As the aim of this study was not to evaluate different classification algorithms, only the random forest classifier was used because it has shown high accuracy and low bias by voting from several decision trees (Sun et al., 2021), which makes it widely usable, especially for extensive and diverse datasets (Bargiel, 2017). According to the findings, none of the Sentinel-1 data combinations exceeded 70% producer accuracy for the olive class in any year, implying less textural variability among the different land cover classes. It was observed that GLCM textures and speckle filtering had more positive influence than VH/VV and RVI on the accuracy of the classifier. This explains why textural information are important in SAR data (Mishra et al., 2019; Maskell et al., 2021), and may account for the considerable plant structural information included in SAR backscatter amplitudes (Van Tricht et al., 2018). Studies have demonstrated that utilising Sentinel-2 variables results in classification accuracies ranging from 70% to 90% when mapping crops on a landscape scale (Mudereri et al., 2022). In the case of this study, the combination of Sentinel-2 with the spectral indices dataset resulted in up to 90% producer accuracy for the olive class, revealing the clear advantages of Sentinel-2 data for olive tree mapping. Furthermore, seasonal trends in optical data and textural information from radar data contribute to classification (Maskell et al., 2021). Several researches have examined the role of optical and radar data fusion in crop mapping (Jin et al., 2019; Poortinga et al., 2019). Similarly, in this study, the combination of Sentinel-1 and Sentinel-2 data succeded the highest classification accuracy, with an overall accuracy of up to 90% and a producer accuracy of more than 90% for olive class. This exemplifies the advantage of using radar and optical data fusion for tree crop mapping.

Although olive trees grow on Mediterranean hills with other vegetation, the majority of the samples for training and validation were limited to the main road because that was the only data accessible in Google Street View. This limited the ability to gather samples from diverse geographical locations. Furthermore, ground vegetation such as grass, weeds, planted plants, and bare soil among olive trees can affect spectral reflectance (Fig 2.1b). This problem has also been identified in object-based classification studies that used a blob-detection approach with VHR images (Messina et al., 2022). Other vegetation cover within olive groves might vary by place and year. This results in different spectral/radar signatures and, in turn, different overall classification accuracies in different years. In addition, the spectral reflectance curve of olive trees was similar to that of shrublands (Figure 2.6), which could cause misclassifications.

In Chapter 3, the phenology and productivity of olive trees were investigated on a regional scale using CLMS HR-VPP parameters. Studies on phenology of productivity of olive trees using satellite remote sensing are limited but increasing over time. The majority of studies focused on estimating crop growth/phenological phases (Milicevic et al., 2020; Oses et al., 2020; Azpiroz et al., 2021; Hachicha et al., 2021). Moreover, a few studies focused on the yield estimation of olive trees (Maselli et al., 2012; Brilli et al., 2013). This study contributes to this research series by exploring the inter-annual variability of phenology and the impacts of climatic conditions and elevation to the productivity of olive trees on a regional scale. The findings indicated that multi-temporal EOSD trend has more variation than SOSD trend. This can be explained by considering that olive trees are more sensitive to external factors (local geographic, climatic, and environmental conditions as well as human disturbance) throughout the growing season. According to studies, increasing precipitation advances EOSD (Wu et al., 2021). Similarly, higher precipitation in the three months before EOSD advanced the EOSD of olive trees in 2018 (Figure 3.4). Increasing elevation is associated with delayed SOSD, advanced EOSD, and a shorter length of season (Wu et al., 2021). Similarly, when elevation increased, SOSD and EOSD of olive trees were delayed, resulting in a shorter length of season. Crop yield and productivity are closely associated terms in agriculture. This study showed a strong correlation (R^2 = 0.77) between crop yield and total productivity (Figure 3.8b). Apart these, higher water availability is associated with enhanced crop yield of olive trees (Caruso et al., 2022). Likewise, it was observed that the correlation between five-year average total productivity and average annual precipitation between 2017 and 2021 was strong (R^2 = 0.77). One notable finding of this study was that the relationship between precipitation and total productivity was higher than that between surface soil moisture and total productivity. This can be explained by the contribution of water held below the soil surface (Ren et al., 2022b) after surface soil moisture is evaporated.

In Chapter 4, field visits to Bayındır and Bergama districts were conducted to investigate the reasons of underestimation and overestimation issues explained in Chapter 2 and Chapter 3. Results demonstrated that olive trees are likely to be misclassified in hilly areas because the background vegetation among olive trees are denser and olive forests in mountains are mixed with other trees. The findings also demonstrated the importance of field observations.

Chapter 2 of the thesis includes the first regional-scale olive tree distribution map for the province of Izmir, and it is an essential resource for establishing an effective management plan. However, the olive tree distribution map produced in this study needs to be updated in the following years because spatial distribution of olive trees in Izmir province shows variation due to forest fires and/or human activities. Chapter 3 of the thesis includes one of the first attempts to use the CLMS HR-VPP products. Furthermore, it is the first regional satellite-based phenology and productivity research on olive trees in the province of Izmir and Türkiye. This study can be considered as the first step for a country scale study and can be extended/enriched with future studies. For example, the findings can be validated with district/province level reference phenology metrics.

The first country-scale research on olive trees will be possible if the method used in this thesis is expanded to other regions of Türkiye. Future studies on the phenology and productivity of olive trees in Türkiye can leverage the olive and olive oil industry which is mainly a family business. Therefore, a developed olive cultivation plan can significantly contribute to the economy of Türkiye. For the future of olive cultivation globally, olive trees need to be mapped and monitored continuously on regional to global scales due to severe wheather events and climate change. Thus, in the long term, the effects of climate change to the phenology and productivity of olive trees can be investigated and potential drivers and/or adaptations of olive trees can be identified.

REFERENCES

Adler, R.F., Huffman, G.J., Chang, A., Ferraro, R., Xie, P.P., Janowiak, J., Rudolf, B., Schneider, U., Curtis, S., Bolvin, D. and Gruber, A. (2003). The version-2 global precipitation climatology project (GPCP) monthly precipitation analysis (1979–present). *Journal of Hydrometeorology, 4*(6), pp.1147-1167.

Aguirre-García, S.D., Aranda-Barranco, S., Nieto, H., Serrano-Ortiz, P., Sánchez-Cañete, E.P. and Guerrero-Rascado, J.L. (2021). Modelling actual evapotranspiration using a two source energy balance model with Sentinel imagery in herbaceous-free and herbaceous-cover Mediterranean olive orchards. *Agricultural and Forest Meteorology, 311*, p.108692.

Akcay, H., Kaya, S., Sertel, E., Alganci, U. and Aksoy, S. (2021). Sentinel-1 and-2 time-series data-fusion for olive tree identification in heterogeneous land surfaces using Google Earth Engine. *Intercontinental Geoinformation Days*, 2, pp.159-162.

Aksoy, S., Yildirim, A., Gorji, T., Hamzehpour, N., Tanik, A. and Sertel, E. (2022). Assessing the performance of machine learning algorithms for soil salinity mapping in Google Earth Engine platform using Sentinel-2A and Landsat-8 OLI data. *Advances in Space Research, 69*(2), pp.1072-1086.

Alganci, U., Sertel, E. and Kaya, S. (2018). Determination of the olive trees with object based classification of Pleiades satellite image. *International Journal of Environment and Geoinformatics, 5*(2), pp.132-139.

Anastasiou, E., Balafoutis, A.T. and Fountas, S. (2023). Trends in remote sensing technologies in olive cultivation. *Smart Agricultural Technology, 3*, p.100103.

Avola, G., Di Gennaro, S.F., Cantini, C., Riggi, E., Muratore, F., Tornambè, C. and Matese, A. (2019). Remotely sensed vegetation indices to discriminate field-grown olive cultivars. *Remote Sensing, 11*(10), p.1242.

Ayaz, M. and Varol, N. (2015). The effect of climatic parameters changing (heat, raining, snow, relative humidity, fog, hail, and wind) on olive growing. *Zeytin Bilimi, 5*, pp.33-40.

Azpiroz, I., Oses, N., Quartulli, M., Olaizola, I.G., Guidotti, D. and Marchi, S. (2021). Comparison of climate reanalysis and remote-sensing data for predicting olive phenology through machine-learning methods. *Remote Sensing, 13*(6), p.1224**.**

Badeck, F.W., Bondeau, A., Böttcher, K., Doktor, D., Lucht, W., Schaber, J. and Sitch, S. (2004). Responses of spring phenology to climate change. *New Phytologist, 162*(2), pp.295-309.

Bao, G., Bao, Y., Qin, Z., Xin, X., Bao, Y., Bayarsaikan, S., Zhou, Y. and Chuntai, B. (2016). Modeling net primary productivity of terrestrial ecosystems in the semi-arid climate of the Mongolian Plateau using LSWI-based CASA ecosystem model. *International Journal of Applied Earth Observation and Geoinformation, 46*, pp.84-93.

Bao, G., Tuya, A., Bayarsaikhan, S., Dorjsuren, A., Mandakh, U., Bao, Y., Li, C. and Vanchindorj, B. (2020). Variations and climate constraints of terrestrial net primary productivity over Mongolia. *Quaternary International, 537*, pp.112-125.

Barata, T. and Pina, P. (2003). Morphological recognition of olive grove patterns. In Pattern Recognition and Image Analysis: *First Iberian Conference, IbPRIA 2003, Puerto de Andratx, Mallorca, Spain, JUne 4-6, 2003. Proceedings 1* (pp. 89-96). Springer Berlin Heidelberg.

Bargiel, D. (2017). A new method for crop classification combining time series of radar images and crop phenology information. *Remote Sensing of Environment, 198*, pp.369-383.

Bauer-Marschallinger, B., Freeman, V., Cao, S., Paulik, C., Schaufler, S., Stachl, T., Modanesi, S., Massari, C., Ciabatta, L., Brocca, L. and Wagner, W. (2018). Toward global soil moisture monitoring with Sentinel-1: Harnessing assets and overcoming obstacles. *IEEE Transactions on Geoscience and Remote Sensing, 57*(1), pp.520-539.

Beer, C., Reichstein, M., Tomelleri, E., Ciais, P., Jung, M., Carvalhais, N., Rödenbeck, C., Arain, M.A., Baldocchi, D., Bonan, G.B. and Bondeau, A. (2010). Terrestrial gross carbon dioxide uptake: global distribution and covariation with climate. *Science, 329*(5993), pp.834-838.

Blunden, J. and Arndt, D.S. (2012). State of the climate in 2011. *Bulletin of the American Meteorological Society, 93*(7), pp.S1-S282.

Borgogno-Mondino, E. and Fissore, V. (2022). Reading Greenness in Urban Areas: Possible Roles of Phenological Metrics from the Copernicus HR-VPP Dataset. *Remote Sensing, 14*(18), p.4517.

Braun, A. (2020) “SAR-based landcover classification with Sentinel-1 GRD products” ESA, Available online: http://step.esa.int/docs/tutorials/ S1TBX%20 Landcover%20classification%20with%20Sentinel-1%20 GRD.pdf (accessed on 08 February 2023).

Breiman, L. (2001). Random forests. *Machine learning, 45*, pp.5-32.

Brilli, L., Chiesi, M., Maselli, F., Moriondo, M., Gioli, B., Toscano, P., Zaldei, A. and Bindi, M. (2013). Simulation of olive grove gross primary production by the combination of ground and multi-sensor satellite data. *International Journal of Applied Earth Observation and Geoinformation, 23*, pp.29-36.

Caruso, G., Palai, G., Gucci, R. and Priori, S. (2022). Remote and proximal sensing techniques for site-specific irrigation management in the olive orchard. *Applied Sciences, 12*(3), p.1309.

Castillejo-González, I.L. (2018). Mapping of olive trees using pansharpened quickbird images: an evaluation of pixel-and object-based analyses. *Agronomy, 8*(12), p.288.

Charbonneau, F., Trudel, M. and Fernandes, R. (2005). Use of Dual Polarization and Multi-Incidence SAR for soil permeability mapping. In *Proceedings of the 2005 advanced synthetic aperture radar (ASAR) workshop, St-Hubert, QC, Canada* (pp. 15-17).

Churkina, G. and Running, S.W. (1998). Contrasting climatic controls on the estimated productivity of global terrestrial biomes. *Ecosystems, 1*, pp.206-215.

Cleverly, J., Eamus, D., Coupe, N.R., Chen, C., Maes, W., Li, L., Faux, R., Santini, N.S., Rumman, R., Yu, Q. and Huete, A. (2016). Soil moisture controls on phenology and productivity in a semi-arid critical zone. *Science of the Total Environment, 568*, pp.1227-1237.

Conners, R.W., Trivedi, M.M. and Harlow, C.A. (1984). Segmentation of a high-resolution urban scene using texture operators. *Computer Vision, Graphics, and Image Processing, 25*(3), pp.273-310.

Copernicus DEM (2023). Available online: https://spacedata.copernicus.eu/collecti-ons/copernicus-digital-elevation-model (accessed on 4 April 2023)

Daliakopoulos, I.N., Grillakis, E.G., Koutroulis, A.G. and Tsanis, I.K. (2009). Tree crown detection on multispectral VHR satellite imagery. *Photogrammetric Engineering & Remote Sensing, 75*(10), pp.1201-1211.

Dash, J., and Curran, P. J. (2004). The MERIS Terrestrial Chlorophyll Index. *International Journal of Remote Sensing 25* (23). Taylor & Francis: 5403–5413.

Davis, C.L., Hoffman, M.T. and Roberts, W. (2017). Long-term trends in vegetation phenology and productivity over Namaqualand using the GIMMS AVHRR NDVI3g data from 1982 to 2011. *South African Journal of Botany, 111*, pp.76-85.

Defourny, P., Bontemps, S., Bellemans, N., Cara, C., Dedieu, G., Guzzonato, E., Hagolle, O., Inglada, J., Nicola, L., Rabaute, T. and Savinaud, M. (2019). Near real-time agriculture monitoring at national scale at parcel resolution: Performance assessment of the Sen2-Agri automated system in various cropping systems around the world. *Remote Sensing of Environment, 221*, pp.551-568.

Demers, J.D., Lee, T.D. and Barrett, J.P. (1998). Substrate type and the distribution of sugar maple at its elevational limit in the White Mountains, New Hampshire. *Canadian Journal of Forest Research, 28*(3), pp.494-498.

Djamai, N., Fernandes, R., Weiss, M., McNairn, H. and Goïta, K. (2019). Validation of the Sentinel Simplified Level 2 Product Prototype Processor (SL2P) for mapping cropland biophysical variables using Sentinel-2/MSI and Landsat-8/OLI data. *Remote Sensing of Environment, 225,* pp.416-430.

Doraiswamy, P.C., Hatfield, J.L., Jackson, T.J., Akhmedov, B., Prueger, J. and Stern, A. (2004). Crop condition and yield simulations using Landsat and MODIS. *Remote Sensing of Environment, 92*(4), pp.548-559.

Doygun, H. (2009). Effects of urban sprawl on agricultural land: a case study of Kahramanmaraş, Turkey. *Environmental Monitoring and Assessment, 158,* pp.471-478.

Duarte, L., Teodoro, A.C., Monteiro, A.T., Cunha, M. and Gonçalves, H. (2018). QPhenoMetrics: An open source software application to assess vegetation phenology metrics. Computers and Electronics in Agriculture, 148, pp.82-94.

Efe, R., Soykan, A., Cürebal, I. and Sönmez, S. (2013) Olive and Olive Oil; Edremit Municipality: Balıkesir, Turkey: ISBN 978-605-62253-3-8

Efe, R., Soykan, A., Cürebal, I., Sönmez, S., Efe, R., Öztürk, M. and Ghazanfar, S. (2011). Olive and olive oil culture in the Mediterranean Basin. *Environment and Ecology in the Mediterranean Region*, pp.54-64.

Ellebjerg, S.M., Tamstorf, M.P., Illeris, L., Michelsen, A. and Hansen, B.U. (2008). Inter-annual variability and controls of plant phenology and productivity at Zackenberg. *Advances in Ecological Research, 40,* pp.249-273.

EL-Magd, I. and Tanton, T.W. (2003). Improvements in land use mapping for irrigated agriculture from satellite sensor data using a multi-stage maximum likelihood classification. *International Journal of Remote Sensing, 24*(21), pp.4197-4206.

Ertin, G. (2000). Edremit Körfezi Çevresinde Zeytin Üretimi [Olive Production Around The Edremit Gulf] *Türk Coğrafya Dergisi Sayı: 35*, İstanbul, s. 228

ESA (2022). Mission ends for Copernicus Sentinel-1B satellite. Available online: https://www.esa.int/Applications/Observing_the_Earth/Copernicus/Sentinel-1/Mission_ends_for_Copernicus_Sentinel-1B_satellite (accessed on 07 February 2023).

ESA (2012). Sentinel-1 ESA's Radar Observatory Mission for GMES Operational Services. Available online: https://sentinel.esa.int/documents/ 247904/ 349449/s1_sp-1322_1.pdf (accessed on 07 February 2023).

ESA (2015). Sentinel-2 User Handbook. Available online: https://sentinel. esa.int/documents/247904/685211/Sentinel-2_User_Handbook (accessed on 07 February 2023).

European Commission (n.d.). The Mediterranean Region. https:// ec.europa.eu. Available online: https://ec.europa.eu/environment/nature/natura2000/ biogeog_regions/mediterranean/index_en.htm (accessed on 07 February 2023).

European Union (2022). Copernicus Land Monitoring Service. European Environment Agency (EEA).

FAO (2022). Food and Agriculture Organization of the United Nations. https://www.fao.org/ (accessed on 07 June 2022).

Frank, D., Reichstein, M., Bahn, M., Thonicke, K., Frank, D., Mahecha, M.D., Smith, P., Van der Velde, M., Vicca, S., Babst, F. and Beer, C. (2015). Effects of climate extremes on the terrestrial carbon cycle: concepts, processes and potential future impacts. *Global Change Biology, 21*(8), pp.2861-2880.

Funk, C., Peterson, P., Landsfeld, M., Pedreros, D., Verdin, J., Shukla, S., Husak, G., Rowland, J., Harrison, L., Hoell, A. and Michaelsen, J. (2015). The climate hazards infrared precipitation with stations—a new environmental record for monitoring extremes. *Scientific data, 2*(1), pp.1-21.

Gandhi, U. (2021). Temporal Interpolation (Gap-Filling Masked Pixels), Available online: https://code.earthengine.google.co.in/536d8fc3b031365e6d4f75d38131682e (accessed on 07 February 2023).

Gao, Q., Guo, Y., Xu, H., Ganjurjav, H., Li, Y., Wan, Y., Qin, X., Ma, X. and Liu, S. (2016). Climate change and its impacts on vegetation distribution and net primary productivity of the alpine ecosystem in the Qinghai-Tibetan Plateau. *Science of the total Environment, 554,* pp.34-41.

García Torres, L., Peña-Barragán, J.M., López-Granados, F., Jurado-Expósito, M. and Fernández-Escobar, R. (2008). Automatic assessment of agro-environmental indicators from remotely sensed images of tree orchards and its evaluation using olive plantations. *Computers and Electronics in Agriculture, 61*(2), pp.179-191.

General Directorate of Traders, Artists and Cooperatives of Türkiye (2020). 2019 Olive and Olive Oil Report (in Turkish: Yılı Zeytin ve Zeytin Yağı Raporu). Available online: https://esnafkoop.ticaret.gov.tr/data/5d44168e13b876433065544f/2019%20Zeytinya%C4%9F%C4%B1%20Raporu.pdf (accessed on 4 December 2023).

Gilbertson, J.K., Kemp, J. and Van Niekerk, A. (2017). Effect of pan-sharpening multi-temporal Landsat 8 imagery for crop type differentiation using different classification techniques. *Computers and Electronics in Agriculture, 134,* pp.151-159.

Gitelson, A. and Merzlyak, M.N. (1994). Spectral reflectance changes associated with autumn senescence of Aesculus hippocastanum L. and Acer platanoides L. leaves. Spectral features and relation to chlorophyll estimation. *Journal of plant physiology, 143*(3), pp.286-292.

Global Climate Observing System (GCOS) (2016). The global observing system for climate: Implementation needs. In: GCOS Steering Committee at their 24th Meeting in Guayaquil, Ecuador, in October 2016, Available online: https://unfccc.int/sites/default/files/gcos_ip_10oct2016.pdf (accessed on 18 August 2021).

Gonzalez, J., Galindo, C., Arevalo, V. and Ambrosio, G. (2007). Applying image analysis and probabilistic techniques for counting olive trees in high-resolution satellite images. *In Advanced Concepts for Intelligent Vision Systems: 9th International Conference, ACIVS 2007, Delft, The Netherlands, August 28-31, 2007. Proceedings 9* (pp. 920-931). Springer Berlin Heidelberg.

Google (2022). Google Earth. https://earth.google.com/ (accessed 07 June 2022).

Gorelick, N., Hancher, M., Dixon, M., Ilyushchenko, S., Thau, D. and Moore, R. (2017). Google Earth Engine: Planetary-scale geospatial analysis for everyone. *Remote Sensing of Environment*, *202*, pp.18-27.

Griffiths, P., Nendel, C. and Hostert, P., (2019). Intra-annual reflectance composites from Sentinel-2 and Landsat for national-scale crop and land cover mapping. *Remote Sensing of Environment*, *220*, pp.135-151.

Gulcin, D. (2019). The influence of urban growth on surrounding mediterranean landscapes with particular reference to degradation of olive orchards. *Fresenius Environmental Bulletin*, *28*(5), 3854–3864.

Haboudane, D., Miller, J.R., Tremblay, N., Zarco-Tejada, P.J. and Dextraze, L. (2002). Integrated narrow-band vegetation indices for prediction of crop chlorophyll content for application to precision agriculture. *Remote Sensing of Environment*, *81*(2-3), pp.416-426.

Hachicha, M., Kallel, A. and Louati, M. (2021). Prediction of plant growth based on statistical methods and remote sensing data. *Journal of Applied Remote Sensing*, *15*(4), pp.042410-042410.

Haralick, R.M., Shanmugam, K. and Dinstein, I.H. (1973). Textural features for image classification. *IEEE Transactions on systems, man, and cybernetics*, *(6)*, pp.610-621.

Heupel, K., Spengler, D. and Itzerott, S. (2018). A progressive crop-type classification using multitemporal remote sensing data and phenological information. *PFG–Journal of Photogrammetry, Remote Sensing and Geoinformation Science*, *86*, pp.53-69.

Huete, A. R. (1988). A soil-adjusted vegetation index (SAVI). *Remote Sensing of Environment 25*(3), pp.295-309.

Huffman, G.J., Stocker E.F., Bolvin D.T., Nelkin E.J., Jackson T. (2019). GPM IMERG Final Precipitation L3 Half Hourly 0.1 degree x 0.1 degree V06, Greenbelt, MD, Goddard Earth Sciences Data and Information Services Center (GES DISC). (accessed on 15 June 2023)

Ivits, E., Cherlet, M., Horion, S. and Fensholt, R. (2013). Global biogeographical pattern of ecosystem functional types derived from earth observation data. *Remote Sensing*, *5*(7), pp.3305-3330.

Izmir Development Agency (2022). İzmir'in Kadim Üretim Havzaları [Ancient Production Basins of Izmir]. Available online: https://izka.org.tr/wp-content/uploads/2022/02/IZMIRIN-KADIM-URETIM-HAVZALA-RI.pdf (accessed on 5 February 2023)

Izmir Governership (n.d.). İzmir Hakkında [About Izmir]. Available online: http://izmir.gov.tr (accessed on 14 January 2023).

Izmir Municipality (n.d.). İzmir'in Coğrafyası [Geography of Izmir]. Available online: https://www.izmir.bel.tr/tr/IzmirinCografyasi/220/255 (accessed on 15 June 2023)

Jin, Z., Azzari, G., You, C., Di Tommaso, S., Aston, S., Burke, M. and Lobell, D.B. (2019). Smallholder maize area and yield mapping at national scales with Google Earth Engine. *Remote Sensing of Environment, 228,* pp.115-128.

Julien, Y. and Sobrino, J.A. (2009). Global land surface phenology trends from GIMMS database. *International Journal of Remote Sensing, 30*(13), pp.3495-3513.

Kang, S., Running, S.W., Lim, J.H., Zhao, M., Park, C.R. and Loehman, R. (2003). A regional phenology model for detecting onset of greenness in temperate mixed forests, Korea: an application of MODIS leaf area index. *Remote Sensing of Environment, 86*(2), pp.232-242.

Karydas, C., Gewehr, S., Iatrou, M., Iatrou, G. and Mourelatos, S. (2017). Olive plantation mapping on a sub-tree scale with object-based image analysis of multispectral UAV data; Operational potential in tree stress monitoring. *Journal of Imaging, 3*(4), p.57.

Kelsey, K.C., Pedersen, S.H., Leffler, A.J., Sexton, J.O., Feng, M. and Welker, J.M. (2021). Winter snow and spring temperature have differential effects on vegetation phenology and productivity across Arctic plant communities. *Global Change Biology, 27*(8), pp.1572-1586.

Khan, A., Khan, U., Waleed, M., Khan, A., Kamal, T., Marwat, S.N.K., Maqsood, M. and Aadil, F. (2018). Remote sensing: an automated methodology for olive tree detection and counting in satellite images. *IEEE Access, 6*, pp.77816-77828.

Lin, C., Jin, Z., Mulla, D., Ghosh, R., Guan, K., Kumar, V. and Cai, Y. (2021). Toward large-scale mapping of tree crops with high-resolution satellite imagery and deep learning algorithms: A case study of olive orchards in Morocco. *Remote Sensing, 13*(9), p.1740.

Ma, X., Huete, A., Yu, Q., Coupe, N.R., Davies, K., Broich, M., Ratana, P., Beringer, J., Hutley, L.B., Cleverly, J. and Boulain, N. (2013). Spatial patterns and temporal dynamics in savanna vegetation phenology across the North Australian Tropical Transect. *Remote sensing of Environment*, *139*, pp.97-115.

Maponya, M.G., Van Niekerk, A. and Mashimbye, Z.E. (2020). Pre-harvest classification of crop types using a Sentinel-2 time-series and machine learning. *Computers and electronics in agriculture, 169*, p.105164.

Maselli, F., Chiesi, M., Brilli, L. and Moriondo, M. (2012). Simulation of olive fruit yield in Tuscany through the integration of remote sensing and ground data. *Ecological Modelling, 244*, pp.1-12.

Maskell, G., Chemura, A., Nguyen, H., Gornott, C. and Mondal, P. (2021). Integration of Sentinel optical and radar data for mapping smallholder coffee production systems in Vietnam. *Remote Sensing of Environment, 266*, p.112709.

Masson, J., Soille, P. and Mueller, R. (2004). Tests with VHR images for the identification of olive trees and other fruit trees in the European Union. *Remote Sensing for Agriculture, Ecosystems, and Hydrology VI (Vol. 5568*, pp. 23-36). SPIE.

Mathworks (2023). Texture Analysis Using the Gray-Level Co-Occurrence Matrix (GLCM). Available online: https://www.mathworks.com/help/images/texture-analysis-using-the-gray-level-co-occurrence-matrix-glcm.html (accessed on 03 January 2023).

McNairn, H. and Brisco, B. (2004). The application of C-band polarimetric SAR for agriculture: A review. *Canadian Journal of Remote Sensing, 30*(3), pp.525-542.

Messina, G. and Modica, G. (2022). The role of remote sensing in olive growing farm management: a research outlook from 2000 to the present in the framework of precision agriculture applications. *Remote Sensing, 14*(23), p.5951.

Milicevic, M., Zubrinic, K., Grbavac, I. and Obradovic, I. (2020). Application of deep learning architectures for accurate detection of olive tree flowering phenophase. *Remote Sensing, 12*(13), p.2120.

Mishra, V.N., Prasad, R., Rai, P.K., Vishwakarma, A.K. and Arora, A. (2019). Performance evaluation of textural features in improving land use/land cover classification accuracy of heterogeneous landscape using multi-sensor remote sensing data. *Earth Science Informatics, 12*, pp.71-86.

Modica, G., De Luca, G., Messina, G. and Praticò, S. (2021). Comparison and assessment of different object-based classifications using machine learning algorithms and UAVs multispectral imagery: A case study in a citrus orchard and an onion crop. *European Journal of Remote Sensing, 54*(1), pp.431-460.

Modica, G., Messina, G., De Luca, G., Fiozzo, V. and Praticò, S. (2020). Monitoring the vegetation vigor in heterogeneous citrus and olive orchards. A multiscale object-based approach to extract trees' crowns from UAV multispectral imagery. *Computers and Electronics in Agriculture, 175*, p.105500.

Morisette, J.T., Richardson, A.D., Knapp, A.K., Fisher, J.I., Graham, E.A., Abatzoglou, J., Wilson, B.E., Breshears, D.D., Henebry, G.M., Hanes, J.M. and Liang, L. (2009). Tracking the rhythm of the seasons in the face of global change: phenological research in the 21st century. *Frontiers in Ecology and the Environment, 7*(5), pp.253-260.

Mudereri, B.T., Abdel-Rahman, E.M., Ndlela, S., Makumbe, L.D.M., Nyanga, C.C., Tonnang, H.E. and Mohamed, S.A. (2022). Integrating the Strength of Multi-Date Sentinel-1 and-2 Datasets for Detecting Mango (Mangifera indica L.) Orchards in a Semi-Arid Environment in Zimbabwe. *Sustainability, 14*(10), p.5741.

Mullissa, A., Vollrath, A., Odongo-Braun, C., Slagter, B., Balling, J., Gou, Y., Gorelick, N. and Reiche, J. (2021). Sentinel-1 sar backscatter analysis ready data preparation in google earth engine. *Remote Sensing, 13*(10), p.1954.

Myneni, R.B., Keeling, C.D., Tucker, C.J., Asrar, G. and Nemani, R.R. (1997). Increased plant growth in the northern high latitudes from 1981 to 1991. *Nature, 386*(6626), pp.698-702.

Nihal, C.; Ediz, U.; Masson, J. A. Case Study of Developing An Olive Tree Database for Türkiye. Photogramm. Eng. Remote Sens. 2009, 75, 1397–1405.

Oses, N., Azpiroz, I., Marchi, S., Guidotti, D., Quartulli, M. and G. Olaizola, I. (2020). Analysis of Copernicus' ERA5 climate reanalysis data as a replacement for weather station temperature measurements in machine learning models for olive phenology phase prediction. *Sensors*, *20*(21), p.6381.

Ozen, F. and Bolca, M. (2020). The Compare of Olive Tree Counting Methods. *Fresenius Environ. Bull. 29*, 1655–1667

Parmesan, C., (2006). Ecological and evolutionary responses to recent climate change. Annu. Rev. Ecol. Evol. Syst. 37, 637–669.

Pelletier, C., Valero, S., Inglada, J., Champion, N. and Dedieu, G. (2016). Assessing the robustness of Random Forests to map land cover with high resolution satellite image time series over large areas. *Remote Sensing of Environment*, *187*, pp.156-168.

Peña, J.M., Gutiérrez, P.A., Hervás-Martínez, C., Six, J., Plant, R.E. and López-Granados, F. (2014). Object-based image classification of summer crops with machine learning methods. *Remote sensing, 6*(6), pp.5019-5041.

Peña-Barragán, J.M., Jurado-Expósito, M., López-Granados, F., Atenciano, S., Sánchez-De la Orden, M., Garcıa-Ferrer, A. and Garcıa-Torres, L. (2004). Assessing land-use in olive groves from aerial photographs. *Agriculture, ecosystems & environment*, *103*(1), pp.117-122.

Peña-Barragán, J.M., López-Granados, F., García-Torres, L., Jurado-Expósito, M., Sánchez de la Orden, M. and García-Ferrer, A. (2008). Discriminating cropping systems and agro-environmental measures by remote sensing. *Agronomy for Sustainable Development*, *28*, pp.355-362.

Peng, D., Zhang, X., Wu, C., Huang, W., Gonsamo, A., Huete, A.R., Didan, K., Tan, B., Liu, X. and Zhang, B. (2017). Intercomparison and evaluation of spring phenology products using National Phenology Network and AmeriFlux observations in the contiguous United States. *Agricultural and Forest Meteorology*, *242*, pp.33-46.

Peters, J., Van Coillie, F., Westra, T. and De Wulf, R. (2011). Synergy of very high resolution optical and radar data for object-based olive grove mapping. *International Journal of Geographical Information Science*, *25*(6), pp.971-989.

Piao, S., Liu, Q., Chen, A., Janssens, I.A., Fu, Y., Dai, J., Liu, L., Lian, X.U., Shen, M. and Zhu, X. (2019). Plant phenology and global climate change: Current progresses and challenges. *Global Change Biology*, *25*(6), pp.1922-1940.

Poortinga, A., Tenneson, K., Shapiro, A., Nquyen, Q., San Aung, K., Chishtie, F. and Saah, D. (2019). Mapping plantations in Myanmar by fusing Landsat-8, Sentinel-2 and Sentinel-1 data along with systematic error quantification. *Remote sensing*, *11*(7), p.831.

Qader, S.H., Dash, J. and Atkinson, P.M. (2018). Forecasting wheat and barley crop production in arid and semi-arid regions using remotely sensed primary productivity and crop phenology: A case study in Iraq. *Science of the Total Environment*, *613*, pp.250-262.

Ramezan, C., A. Warner, T. and E. Maxwell, A. (2019). Evaluation of sampling and cross-validation tuning strategies for regional-scale machine learning classification. *Remote Sensing*, *11*(2), p.185.

Ranghetti, L., Boschetti, M., Nutini, F. and Busetto, L. (2020). “sen2r”: An R toolbox for automatically downloading and preprocessing Sentinel-2 satellite data. *Computers & Geosciences*, *139*, p.104473.

Ren, S., Chen, X. and Pan, C. (2022a). Temperature-precipitation background affects spatial heterogeneity of spring phenology responses to climate change in northern grasslands (30° N-55° N). *Agricultural and Forest Meteorology*, *315*, p.108816.

Ren, T., Xu, H., Cai, X., Yu, S. and Qi, J. (2022b). Smallholder crop type mapping and rotation monitoring in mountainous areas with Sentinel-1/2 imagery. *Remote Sensing*, *14*(3), p.566.

Richardson, A.D., Braswell, B.H., Hollinger, D.Y., Jenkins, J.P. and Ollinger, S.V. (2009). Near-surface remote sensing of spatial and temporal variation in canopy phenology. *Ecological Applications*, *19*(6), pp.1417-1428.

Richardson, A.D., Keenan, T.F., Migliavacca, M., Ryu, Y., Sonnentag, O. and Toomey, M. (2013). Climate change, phenology, and phenological control of vegetation feedbacks to the climate system. *Agricultural and Forest Meteorology*, *169*, pp.156-173.

Robbez-Masson, J.M. and Foltête, J.C. (2005). Localising missing plants in squared-grid patterns of discontinuous crops from remotely sensed imagery. *Computers & geosciences*, *31*(7), pp.900-912.

Rodriguez-Galiano, V.F., Ghimire, B., Rogan, J., Chica-Olmo, M. and Rigol-Sanchez, J.P. (2012). An assessment of the effectiveness of a random forest classifier for land-cover classification. *ISPRS Journal of Photogrammetry and Remote Sensing*, *67*, pp.93-104.

Roma, E. and Catania, P. (2022). Precision Oliviculture: Research Topics, Challenges, and Opportunities—A Review. *Remote Sensing*, *14*(7), p.1668.

Rouse, J.W., Haas, R.H., Schell, J.A. and Deering, D.W. (1974). Monitoring vegetation systems in the Great Plains with ERTS. *NASA Spec. Publ*, *351*(1), p.309.

Roy, P.S., Sharma, K.P. and Jain, A. (1996). Stratification of density in dry deciduous forest using satellite remote sensing digital data—An approach based on spectral indices. *Journal of Biosciences, 21*, pp.723-734.

Salamí, E., Gallardo, A., Skorobogatov, G. and Barrado, C. (2019). On-the-fly olive tree counting using a UAS and cloud services. *Remote Sensing, 11*(3), p.316.

Sarabia, R., Aquino, A., Ponce, J.M., López, G. and Andújar, J.M. (2020). Automated identification of crop tree crowns from uav multispectral imagery by means of morphological image analysis. *Remote Sensing, 12*(5), p.748.

Seneviratne, S.I., Corti, T., Davin, E.L., Hirschi, M., Jaeger, E.B., Lehner, I., Orlowsky, B. and Teuling, A.J. (2010). Investigating soil moisture–climate interactions in a changing climate: A review. *Earth-Science Reviews, 99*(3-4), pp.125-161.

Šiljeg, A., Panđa, L., Domazetović, F., Marić, I., Gašparović, M., Borisov, M. and Milošević, R. (2022). Comparative assessment of pixel and object-based approaches for mapping of olive tree crowns based on UAV multispectral imagery. *Remote Sensing, 14*(3), p.757.

Solano, F., Di Fazio, S. and Modica, G. (2019). A methodology based on GEOBIA and WorldView-3 imagery to derive vegetation indices at tree crown detail in olive orchards. *International Journal of Applied Earth Observation and Geoinformation, 83*, p.101912.

Sun, C., Li, J., Liu, Y., Liu, Y. and Liu, R. (2021). Plant species classification in salt marshes using phenological parameters derived from Sentinel-2 pixel-differential time-series. *Remote Sensing of Environment, 256*, p.112320.

Sun, H., Chen, Y., Xiong, J., Ye, C., Yong, Z., Wang, Y., He, D. and Xu, S. (2022). Relationships between climate change, phenology, edaphic factors, and net primary productivity across the Tibetan Plateau. *International Journal of Applied Earth Observation and Geoinformation, 107*, p.102708.

Taylor, C.M., de Jeu, R.A., Guichard, F., Harris, P.P. and Dorigo, W.A. (2012). Afternoon rain more likely over drier soils. *Nature, 489*(7416), pp.423-426.

Temuçin, E. (1993). Türkiye'de Zeytin Yetişen Alanların Sıcaklık Değişkenine Göre İncelenmesi [Investigation of Olive Growing Areas in Türkiye According to Temperature Variable] *Ege Coğ. Der. Sayı: 7*, İzmir. s. 117-131.

Thenkabail, P.S., Biradar, C.M., Noojipady, P., Dheeravath, V., Li, Y., Velpuri, M., Gumma, M., Gangalakunta, O.R.P., Turral, H., Cai, X. and Vithanage, J. (2009). Global irrigated area map (GIAM), derived from remote sensing, for the end of the last millennium. *International journal of remote sensing, 30*(14), pp.3679-3733.

Tiktak, A., van der Linden, A.M. and van der Pas, L.J. (1998). Application of the pesticide transport assessment model to a field study in a humic sandy soil in Vredepeel, The Netherlands. *Pesticide Science, 52*(4), pp.321-336.

Torres, R., Snoeij, P., Geudtner, D., Bibby, D., Davidson, M., Attema, E., Potin, P., Rommen, B., Floury, N., Brown, M. and Traver, I.N. (2012). GMES Sentinel-1 mission. *Remote Sensing of Environment, 120*, pp.9-24.

Tucker, C.J. (1979). Red and photographic infrared linear combinations for monitoring vegetation. *Remote Sensing of Environment, 8*(2), pp.127-150.

TUIK (2019). Turkish Statistical Institute. Available online: https://www.tuik.gov.tr/ (accessed 05 May 2020).

TUIK (2022). Turkish Statistical Institute, Available online: https://www.tuik.gov.tr/ (accessed 06 June 2022).

Ulaş, M. (2012). Bahçe Tesisi ve Modern Plantasyonlar Zeytin Yetiştiriciliği kursu [Garden Plant and Modern Plantations Olive Cultivation course] T.C. *Gıda Tarım ve Hayvancılık Bakanlığı, Zeytincilik Araştırma İstasyonu, Kurs notları* (basılmamış).

Van Deventer, A.P., Ward, A.D., Gowda, P.H. and Lyon, J.G. (1997). Using thematic mapper data to identify contrasting soil plains and tillage practices. *Photogrammetric Engineering and Remote Sensing, 63*, pp.87-93.

Van Tricht, K., Gobin, A., Gilliams, S. and Piccard, I. (2018). Synergistic use of radar Sentinel-1 and optical Sentinel-2 imagery for crop mapping: A case study for Belgium. *Remote Sensing, 10*(10), p.1642.

Vavlas, N.C., Waine, T.W., Meersmans, J., Burgess, P.J., Fontanelli, G. and Richter, G.M. (2020). Deriving wheat crop productivity indicators using sentinel-1 time series. *Remote Sensing*, *12*(15), p.2385.

Vos, R. and Bellu, L.G., (2019). Global trends and challenges to food and agriculture into the 21st century. *Sustainable food and agriculture*, pp.11-30.

Waleed, M., Um, T.W., Khan, A. and Ahmad, Z. (2020a). An automated method for detection and enumeration of olive trees through remote sensing. *IEEE Access, 8*, pp.108592-108601.

Waleed, M., Um, T.W., Khan, A. and Khan, U. (2020b). Automatic detection system of olive trees using improved K-means algorithm. *Remote Sensing*, *12*(5), p.760.

Wang, S., Zhang, B., Yang, Q., Chen, G., Yang, B., Lu, L., Shen, M. and Peng, Y. (2017). Responses of net primary productivity to phenological dynamics in the Tibetan Plateau, China. *Agricultural and Forest Meteorology, 232*, pp.235-246.

Wang, Q., Zeng, J., Leng, S., Fan, B., Tang, J., Jiang, C., Huang, Y., Zhang, Q., Qu, Y., Wang, W. and Shui, W. (2018). The effects of air temperature and precipitation on the net primary productivity in China during the early 21st century. *Frontiers of Earth Science, 12*, pp.818-833.

Weiss, M., Jacob, F. and Duveiller, G. (2020). Remote sensing for agricultural applications: A meta-review. *Remote Sensing of Environment, 236*, p.111402.

White, M.A., de Beurs, K.M., Didan, K., Inouye, D.W., Richardson, A.D., Jensen, O.P., O'keefe, J., Zhang, G., Nemani, R.R., van Leeuwen, W.J. and Brown, J.F. (2009). Intercomparison, interpretation, and assessment of spring phenology in North America estimated from remote sensing for 1982–2006. *Global Change Biology, 15*(10), pp.2335-2359.

Wu, C., Hou, X., Peng, D., Gonsamo, A. and Xu, S. (2016). Land surface phenology of China's temperate ecosystems over 1999–2013: Spatial–temporal patterns, interaction effects, covariation with climate and implications for productivity. *Agricultural and Forest Meteorology, 216*, pp.177-187.

Wu, C., Peng, D., Soudani, K., Siebicke, L., Gough, C.M., Arain, M.A., Bohrer, G., Lafleur, P.M., Peichl, M., Gonsamo, A. and Xu, S. (2017). Land surface phenology derived from normalized difference vegetation index (NDVI) at global FLUXNET sites. *Agricultural and Forest Meteorology, 233*, pp.171-182.

Wu, L., Ma, X., Dou, X., Zhu, J. and Zhao, C. (2021). Impacts of climate change on vegetation phenology and net primary productivity in arid Central Asia. *Science of the Total Environment, 796*, p.149055.

Xu, Q., Yang, G., Long, H., Wang, C., Li, X. and Huang, D. (2014). Crop information identification based on MODIS NDVI time-series data. *Transactions of the Chinese Society of Agricultural Engineering, 30*(11), pp.134-144.

Ye, Z., Wei, J., Lin, Y., Guo, Q., Zhang, J., Zhang, H., Deng, H. and Yang, K. (2022). Extraction of olive crown based on uav visible images and the u2-net deep learning model. *Remote Sensing, 14*(6), p.1523.

Zanaga, D., Van De Kerchove, R., De Keersmaecker, W., Souverijns, N., Brockmann, C., Quast, R., Wevers, J., Grosu, A., Paccini, A., Vergnaud, S. and Cartus, O. (2021). ESA WorldCover 10 m 2020 v100.

Zeng, L., Wardlow, B.D., Xiang, D., Hu, S. and Li, D. (2020). A review of vegetation phenological metrics extraction using time-series, multispectral satellite data. *Remote Sensing of Environment, 237*, p.111511.

Zha, Y., Gao, J. and Ni, S. (2003). Use of normalized difference built-up index in automatically mapping urban areas from TM imagery. *International Journal of Remote Sensing, 24*(3), pp.583-594.

Zhang, X., Friedl, M.A., Schaaf, C.B., Strahler, A.H., Hodges, J.C., Gao, F., Reed, B.C. and Huete, A. (2003). Monitoring vegetation phenology using MODIS. *Remote Sensing of Environment, 84*(3), pp.471-475.

Zhao, D., Hou, Y., Zhang, Z., Wu, Y., Zhang, X., Wu, L., Zhu, X. and Zhang, Y. (2022). Temporal resolution of vegetation indices and solar-induced chlorophyll fluorescence data affects the accuracy of vegetation phenology estimation: A study using in-situ measurements. *Ecological Indicators*, *136*, p.108673.

Zhong, L., Hawkins, T., Biging, G. and Gong, P. (2011). A phenology-based approach to map crop types in the San Joaquin Valley, California. *International Journal of Remote Sensing*, *32*(22), pp.7777-7804.

Zhou, L., Wang, Y., Jia, Q. and Zhou, G. (2021). Increasing temperature shortened the carbon uptake period and decreased the cumulative net ecosystem productivity in a maize cropland in Northeast China. *Field Crops Research*, *267*, p.108150.

Zribi, M., Chahbi, A., Shabou, M., Lili-Chabaane, Z., Duchemin, B., Baghdadi, N., Amri, R. and Chehbouni, A. (2011). Soil surface moisture estimation over a semi-arid region using ENVISAT ASAR radar data for soil evaporation evaluation. *Hydrology and Earth System Sciences*, *15*(1), pp.345-358.

Zupanc, A. (2020). Improving Cloud Detection with Machine Learning. Available online: https: //medium.com/sentinel-hub/improving-cloud-detection-with-machine-learning-c09dc5d7cf13 (accessed on 26 December 2022).

APPENDICES

APPENDIX A: Confusion matrices of dataset “g”
APPENDIX B: Datasets
APPENDIX C: Start of season date maps
APPENDIX D: End of season date maps
APPENDIX E: Total productivity maps

APPENDIX A: Confusion matrices of dataset “g”

Table A.1 : Confusion matrices of dataset “g”

Year	Class	Olive	Cropland	Forest	Barren-land	Built-up	Grassland	Shrubland	Producer's Acc.	kappa
2017	Olive	438	4	26	0	3	10	43	83.6%	0.85
	Cropland	11	521	15	8	6	20	24	86.1%	
	Forest	0	0	481	0	0	0	1	99.8%	
	Barren-land	0	15	0	62	17	21	4	52.1%	
	Built-up	0	1	0	18	252	0	5	91.3%	
	Grassland	0	0	0	0	0	291	58	83.4%	
	Shrubland	43	2	1	0	1	4	485	90.5%	
	User's Acc.	89.0%	95.9%	92.0%	70.5%	90.3%	84.1%	78.2%	87.5%	
2018	Class	Olive	Cropland	Forest	Barren-land	Built-up	Grassland	Shrubland	Producer's Acc.	kappa
	Olive	453	9	7	0	14	5	36	86.5%	0.84
	Cropland	70	471	4	8	1	19	32	77.9%	
	Forest	1	0	476	0	0	0	3	99.2%	
	Barren-land	0	9	0	82	17	5	6	68.9%	
	Built-up	0	1	0	10	260	0	5	94.2%	
	Grassland	3	2	0	2	1	286	55	81.9%	
	Shrubland	43	3	1	0	5	3	481	89.7%	
	User's Acc.	79.5%	95.2%	97.5%	80.4%	87.2%	89.9%	77.8%	86.8%	
2019	Class	Olive	Cropland	Forest	Barren-land	Built-up	Grassland	Shrubland	Producer's Acc.	kappa
	Olive	471	10	13	0	3	2	25	89.9%	0.87
	Cropland	11	516	19	2	0	14	43	85.3%	
	Forest	0	0	479	0	0	0	2	99.6%	
	Barren-land	0	6	0	82	15	13	3	68.9%	
	Built-up	0	3	0	23	248	0	2	89.9%	
	Grassland	0	3	0	0	0	289	57	82.8%	
	Shrubland	25	7	0	0	0	1	505	93.9%	
	User's Acc.	92.9%	94.7%	93.7%	76.6%	93.2%	90.6%	79.3%	89.6%	
2020	Class	Olive	Cropland	Forest	Barren-land	Built-up	Grassland	Shrubland	Producer's Acc.	kappa
	Olive	457	13	5	0	1	2	46	87.2%	0.87
	Cropland	28	515	25	3	1	9	24	85.1%	
	Forest	0	2	479	0	0	0	1	99.4%	
	Barren-land	0	18	0	68	24	9	0	57.1%	
	Built-up	0	3	0	11	262	0	0	94.9%	
	Grassland	8	35	0	0	0	283	23	81.1%	
	Shrubland	29	0	2	0	0	0	507	94.2%	
	User's Acc.	87.5%	87.9%	93.7%	82.9%	91.0%	93.4%	84.4%	88.9%	
2021	Class	Olive	Cropland	Forest	Barren-land	Built-up	Grassland	Shrubland	Producer's Acc.	kappa
	Olive	464	3	21	0	1	2	33	88.5%	0.85
	Cropland	21	533	9	4	6	10	22	88.1%	
	Forest	0	0	482	0	0	0	0	100.0%	
	Barren-land	0	20	0	58	28	13	0	48.7%	
	Built-up	0	2	0	20	254	0	0	92.0%	
	Grassland	3	26	0	3	0	247	70	70.8%	
	Shrubland	33	0	0	0	0	0	505	93.9%	
	User's Acc.	89.1%	91.3%	94.1%	68.2%	87.9%	90.8%	80.2%	87.9%	

APPENDIX B: Datasets

Table B.1 : Datasets

Months	Dataset Code	Dataset	Number of Layers	Year	Producer's Acc. of Olive	Consumer's Acc. of Olive	Overall Accuracy	Kappa
July + October	a	S1	2 layers	2017	46.6%	37.4%	43.4%	0.32
July + October	b	S1 (speckle filtered)	2 layers	2017	58.4%	49.0%	54.1%	0.45
July + October	c	S1+ VV/VH + Angle (speckle filtered)	8 layers	2017	43.5%	38.5%	50.2%	0.40
July + October	d	S1 + VH/VV + RVI + GLCM textures	80 layers	2017	68.3%	35.7%	46.9%	0.36
July + October	e	S2	24 layers	2017	68.9%	85.1%	80.6%	0.77
July + October	f	S2 + 10 indices	44 layers	2017	78.1%	84.0%	84.2%	0.81
July + October	g	S1 + S2 + 10 indices	48 layers	2017	83.6%	89.0%	87.5%	0.85
July + October	h	S1 (speckle filtered) + S2 + 10 indices	48 layers	2017	82.6%	89.6%	87.8%	0.85
July + October	i	S1 (speckle filtered) + S2 + 10 indices + GLCM textures	120 layers	2017	81.9%	89.7%	87.8%	0.85
July + October	j	S1 + S2 + 10 indices + VH/VV + RVI + GLCM textures	124 layers	2017	82.6%	89.1%	87.3%	0.85
July + October	a	S1	2 layers	2018	50.6%	39.8%	45.6%	0.35
July + October	b	S1 (speckle filtered)	2 layers	2018	58.4%	53.0%	52.5%	0.43
July + October	c	S1+ VV/VH + Angle (speckle filtered)	8 layers	2018	46.0%	40.8%	48.5%	0.38
July + October	d	S1 + VH/VV + RVI + GLCM textures	80 layers	2018	67.7%	36.3%	45.7%	0.34
July + October	e	S2	24 layers	2018	67.4%	64.8%	77.2%	0.73
July + October	f	S2 + 10 indices	44 layers	2018	81.5%	73.2%	83.6%	0.80
July + October	g	S1 + S2 + 10 indices	48 layers	2018	86.5%	79.5%	86.8%	0.84
July + October	h	S1 (speckle filtered) + S2 + 10 indices	48 layers	2018	84.5%	77.0%	86.5%	0.84
July + October	i	S1 (speckle filtered) + S2 + 10 indices + GLCM textures	120 layers	2018	85.5%	79.2%	86.4%	0.84
July + October	j	S1 + S2 + 10 indices + VH/VV + RVI + GLCM textures	124 layers	2018	84.4%	78.4%	86.2%	0.84
July + October	a	S1	4 layers	2019	49.0%	41.6%	44.7%	0.33
July + October	b	S1 (speckle filtered)	4 layers	2019	56.5%	49.3%	52.4%	0.43
July + October	c	S1+ VV/VH + Angle (speckle filtered)	8 layers	2019	42.2%	42.5%	48.9%	0.39
July + October	d	S1 + VH/VV + RVI + GLCM textures	80 layers	2019	63.2%	37.5%	45.7%	0.34
July + October	e	S2	24 layers	2019	75.0%	92.3%	82.9%	0.80
July + October	f	S2 + 10 indices	44 layers	2019	90.6%	91.9%	88.4%	0.86
July + October	g	S1 + S2 + 10 indices	48 layers	2019	89.9%	92.9%	89.6%	0.87
July + October	h	S1 (speckle filtered) + S2 + 10 indices	48 layers	2019	91.4%	91.1%	90.7%	0.89
July + October	i	S1 (speckle filtered) + S2 + 10 indices + GLCM textures	120 layers	2019	91.2%	92.0%	90.8%	0.89
July + October	j	S1 + S2 + 10 indices + VH/VV + RVI + GLCM textures	124 layers	2019	89.9%	93.6%	89.6%	0.88

Table B.1(continued) : Datasets

Months	Dataset Code	Dataset	Number of Layers	Year	Producer's Acc. of Olive	Consumer's Acc. of Olive	Overall Accuracy	Kappa
July + October	a	S1	4 layers	2020	49.4%	40.5%	43.6%	0.32
July + October	b	S1 (speckle filtered)	4 layers	2020	60.5%	51.9%	53.1%	0.44
July + October	c	S1+ VV/VH + Angle (speckle filtered)	8 layers	2020	56.7%	47.6%	53.4%	0.44
July + October	d	S1 + VH/VV + RVI + GLCM textures	80 layers	2020	63.9%	35.8%	45.8%	0.34
July + October	e	S2	24 layers	2020	73.7%	81.3%	82.5%	0.79
July + October	f	S2 + 10 indices	44 layers	2020	82.1%	83.7%	85.5%	0.83
July + October	g	S1 + S2 + 10 indices	48 layers	2020	87.2%	87.5%	88.9%	0.87
July + October	h	S1 (speckle filtered) + S2 + 10 indices	48 layers	2020	86.6%	87.5%	89.4%	0.87
July + October	i	S1 (speckle filtered) + S2 + 10 indices + GLCM textures	120 layers	2020	84.5%	89.0%	88.9%	0.87
July + October	j	S1 + S2 + 10 indices + VH/VV + RVI + GLCM textures	124 layers	2020	85.9%	89.5%	88.5%	0.86
July + October	a	S1	4 layers	2021	53.1%	40.9%	43.9%	0.32
July + October	b	S1 (speckle filtered)	4 layers	2021	59.4%	54.4%	54.4%	0.45
July + October	c	S1+ VV/VH + Angle (speckle filtered)	8 layers	2021	38.5%	37.6%	41.4%	0.30
July + October	d	S1 + VH/VV + RVI + GLCM textures	80 layers	2021	63.5%	41.0%	50.1%	0.39
July + October	e	S2	24 layers	2021	80.9%	85.7%	82.9%	0.79
July + October	f	S2 + 10 indices	44 layers	2021	89.1%	86.5%	87.3%	0.85
July + October	g	S1 + S2 + 10 indices	48 layers	2021	88.5%	89.1%	87.9%	0.85
July + October	h	S1 (speckle filtered) + S2 + 10 indices	48 layers	2021	88.5%	93.4%	88.9%	0.87
July + October	i	S1 (speckle filtered) + S2 + 10 indices + GLCM textures	120 layers	2021	89.1%	92.7%	89.4%	0.87
July + October	j	S1 + S2 + 10 indices + VH/VV + RVI + GLCM textures	124 layers	2021	90.8%	89.8%	88.2%	0.86

Note: Note: S1 = VH and VV bands of Sentinel-1 GRD product; S2 = 12 spectral bands of Sentinel-2 level 2A; 10 indices = NDVI, MTCI, DVIR, DVI, NDVIre, (B+G+R)/3 ratio, NDTI, SAVI, NDBI, BSI; GLCM = 36 grey-level co-occurrence matrix textures

APPENDIX C: Start of season date maps

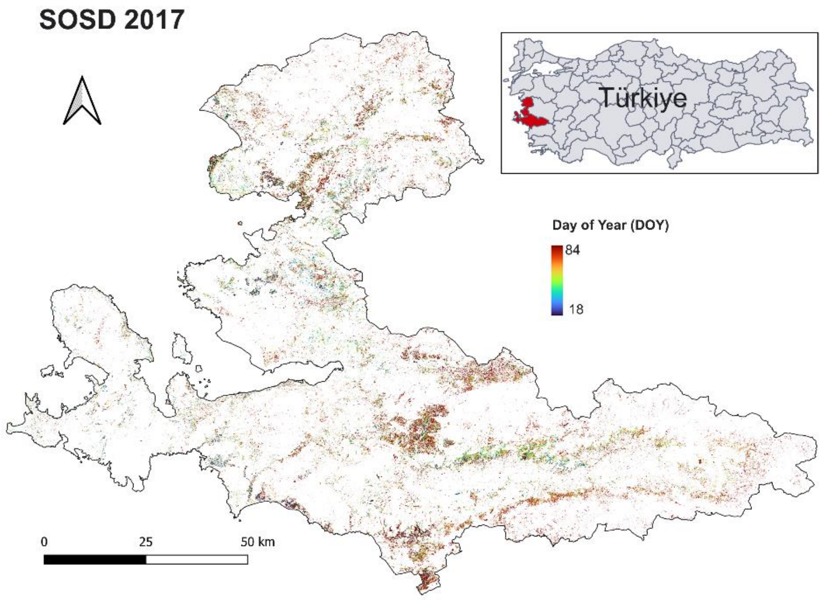

Figure C.1 : Start of season date (SOSD) map of 2017.

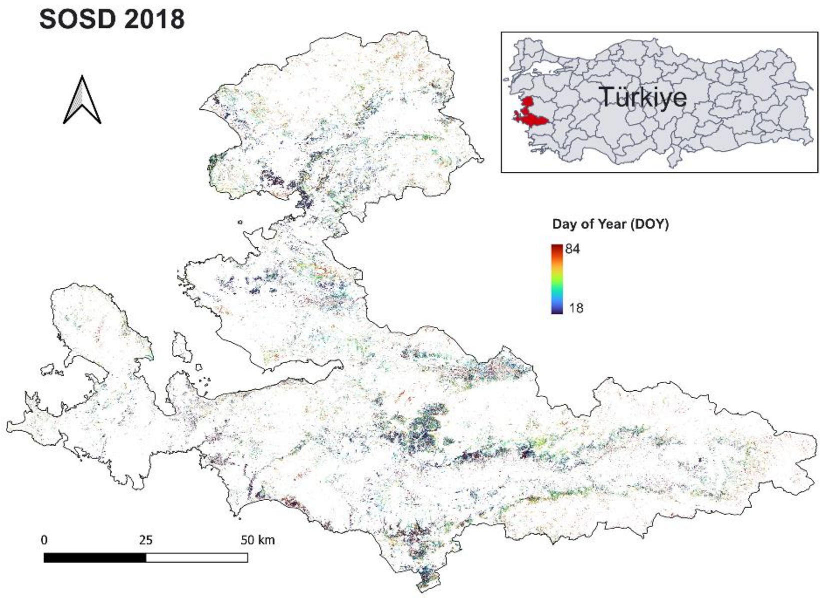

Figure C.2 : Start of season date (SOSD) map of 2018.

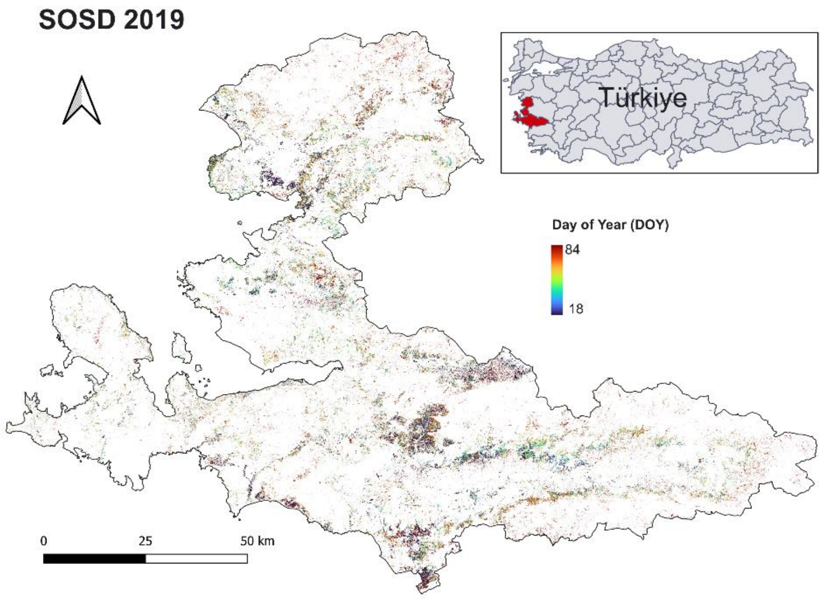

Figure C.3 : Start of season date (SOSD) map of 2019.

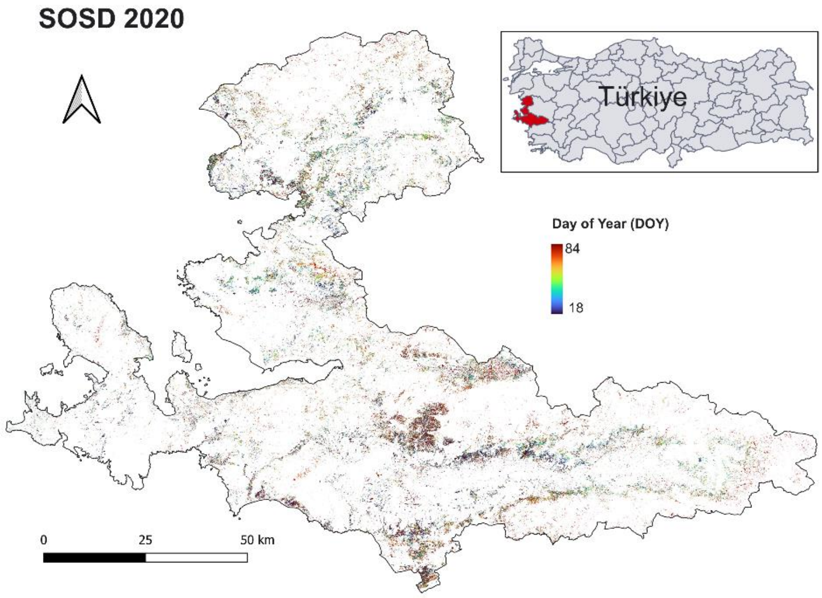

Figure C.4 : Start of season date (SOSD) map of 2020.

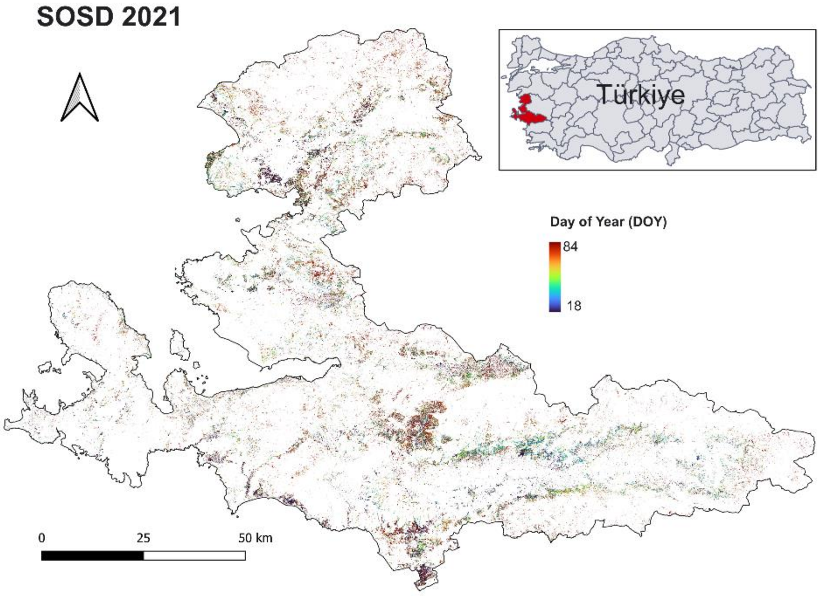

Figure C.5 : Start of season date (SOSD) map of 2021.

APPENDIX D: End of season date maps

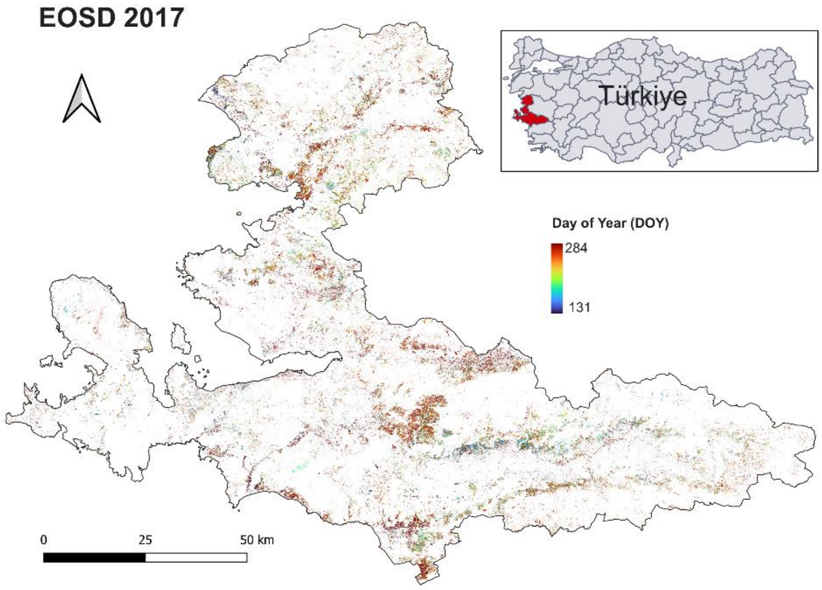

Figure D.1 : End of season date (EOSD) map of 2017.

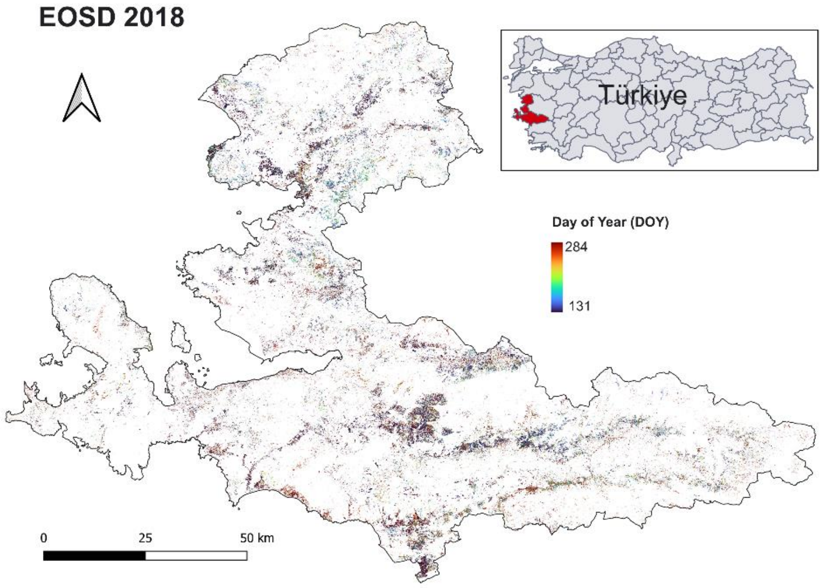

Figure D.2 : End of season date (EOSD) map of 2018.

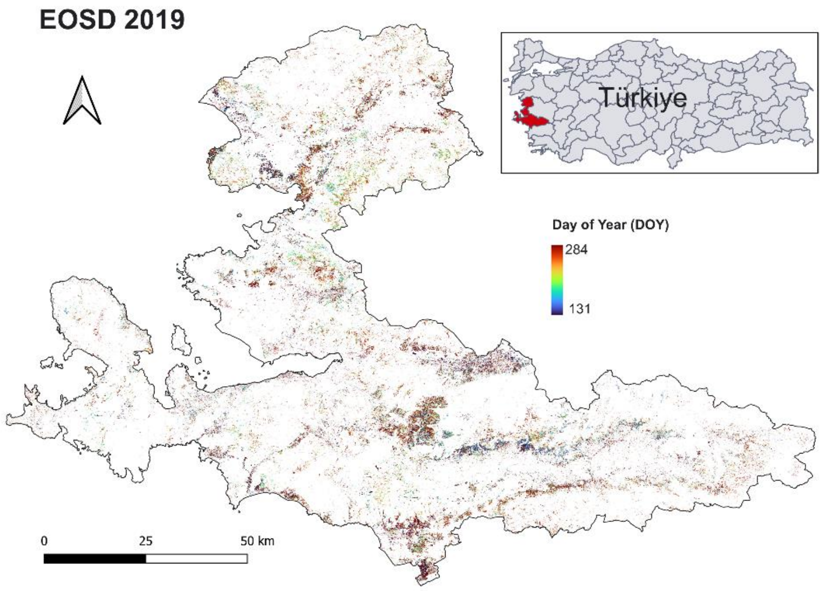

Figure D.3 : End of season date (EOSD) map of 2019.

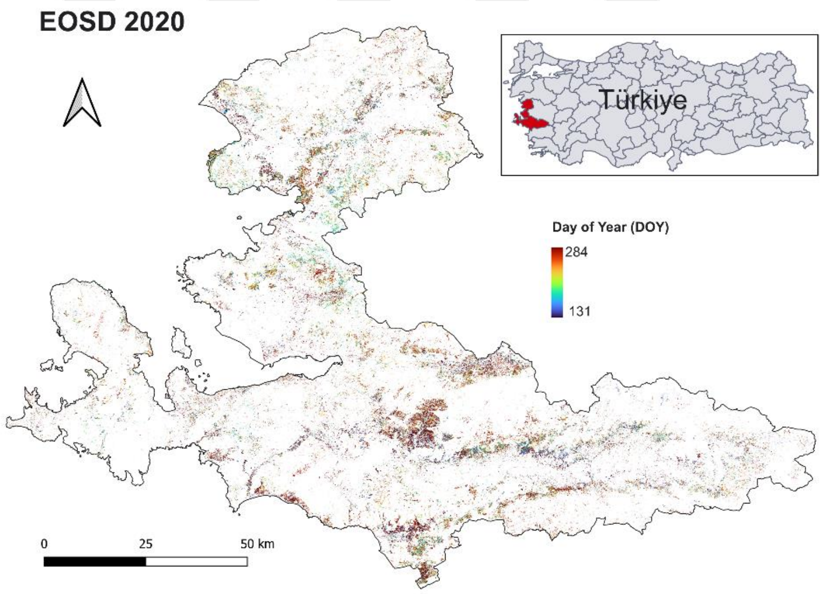

Figure D.4 : End of season date (EOSD) map of 2020.

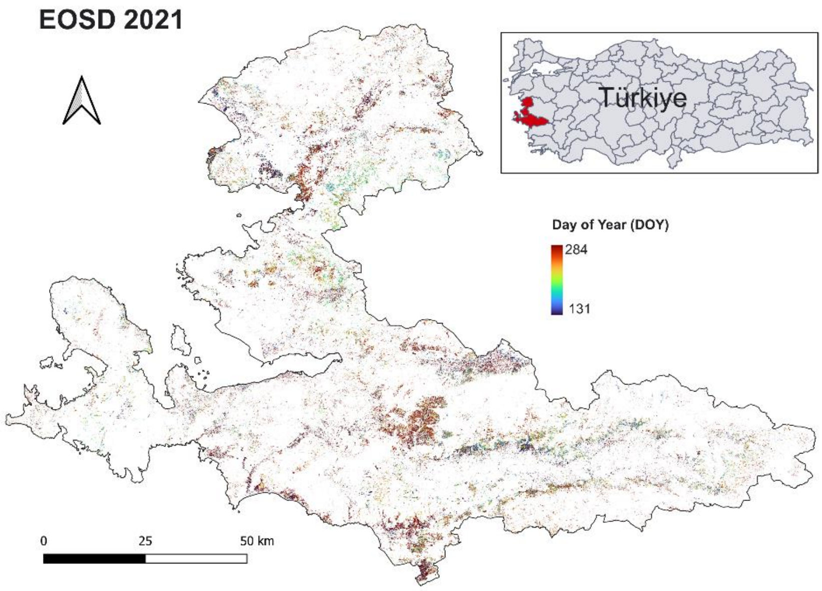

Figure D.5 : End of season date (EOSD) map of 2021.

APPENDIX E: Total productivity maps

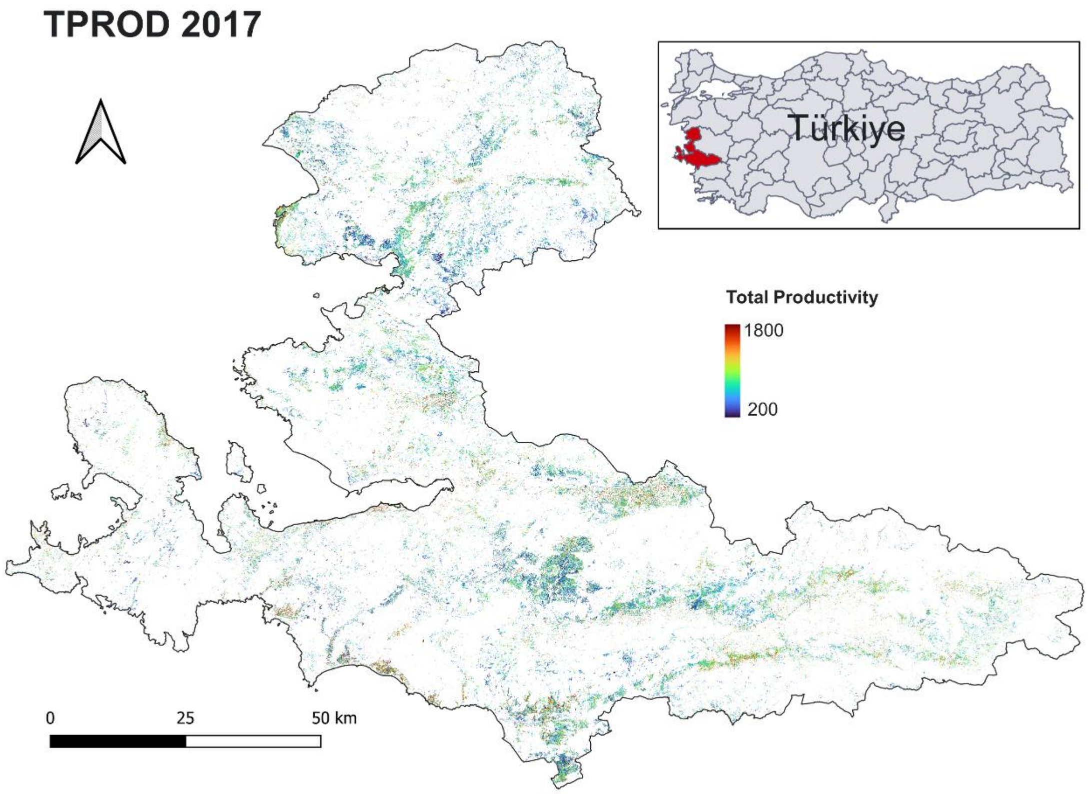

Figure E.1 : Total productivity (TPROD) map of 2017.

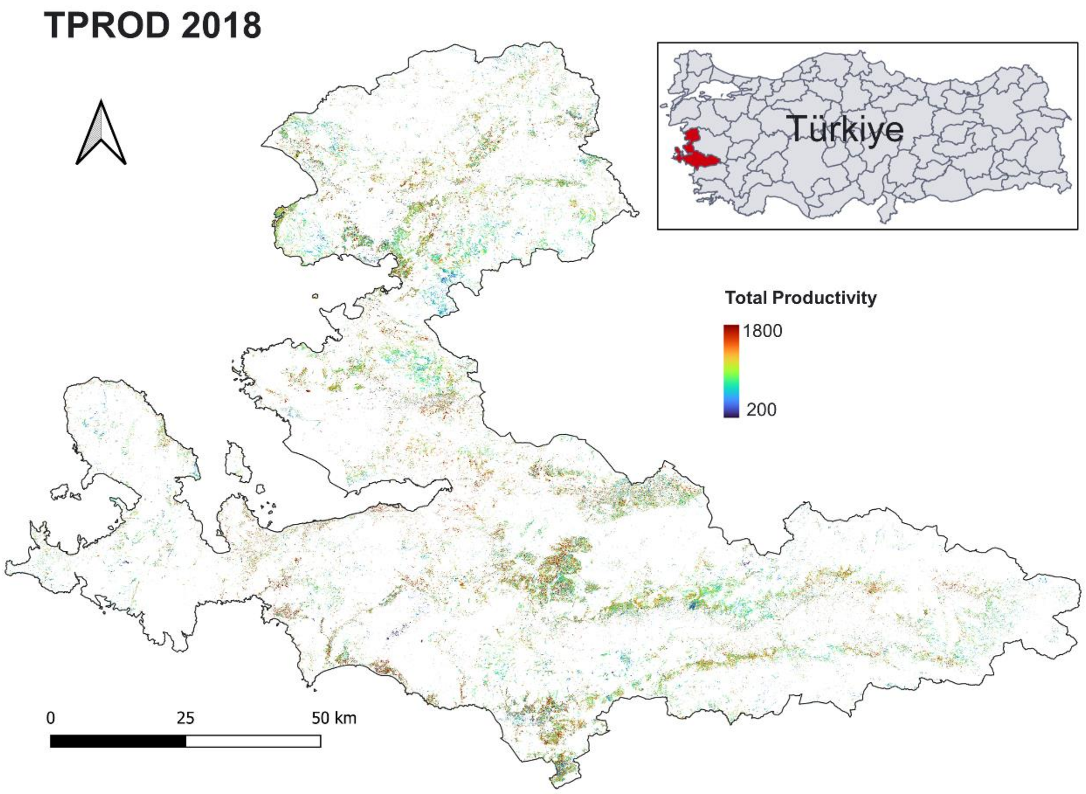

Figure E.2 : Total productivity (TPROD) map of 2018.

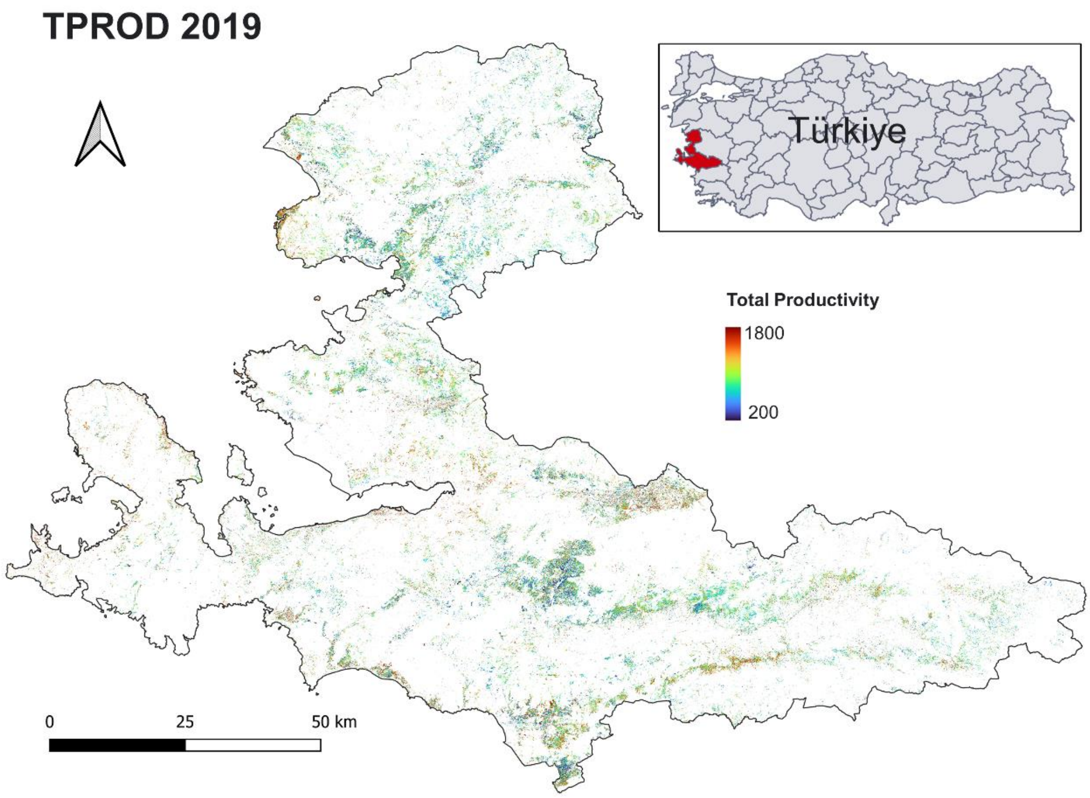

Figure E.3 : Total productivity (TPROD) map of 2019.

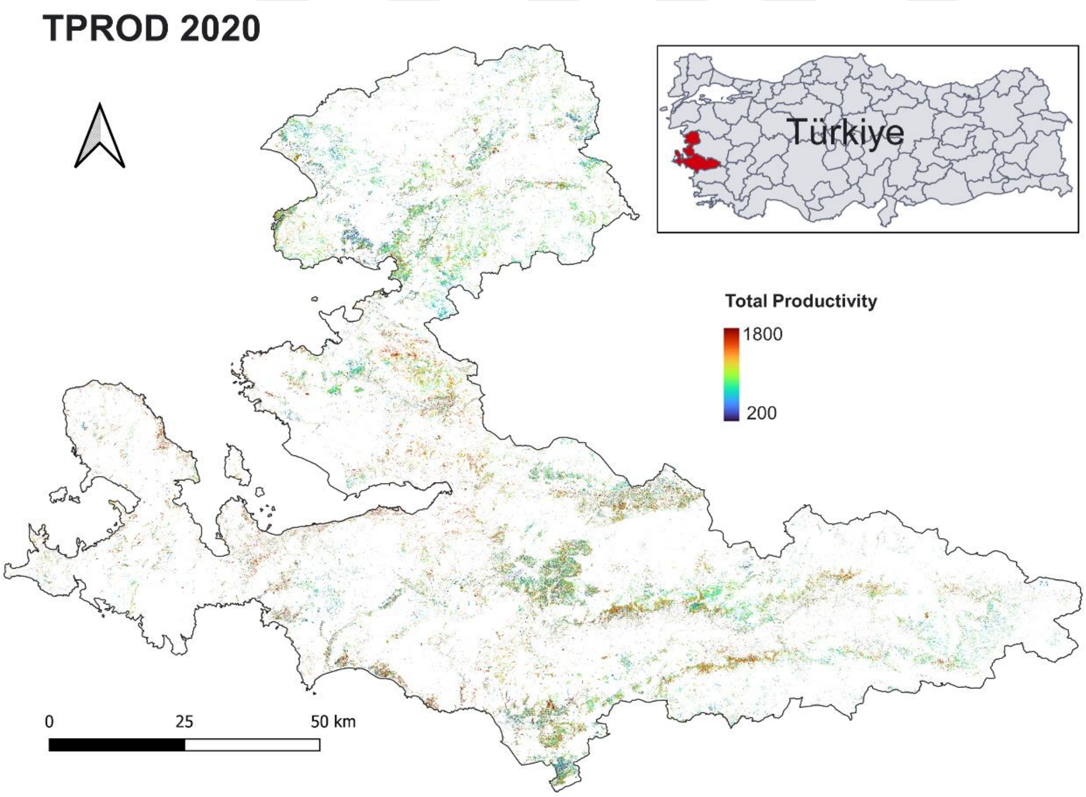

Figure E.4 : Total productivity (TPROD) map of 2020.

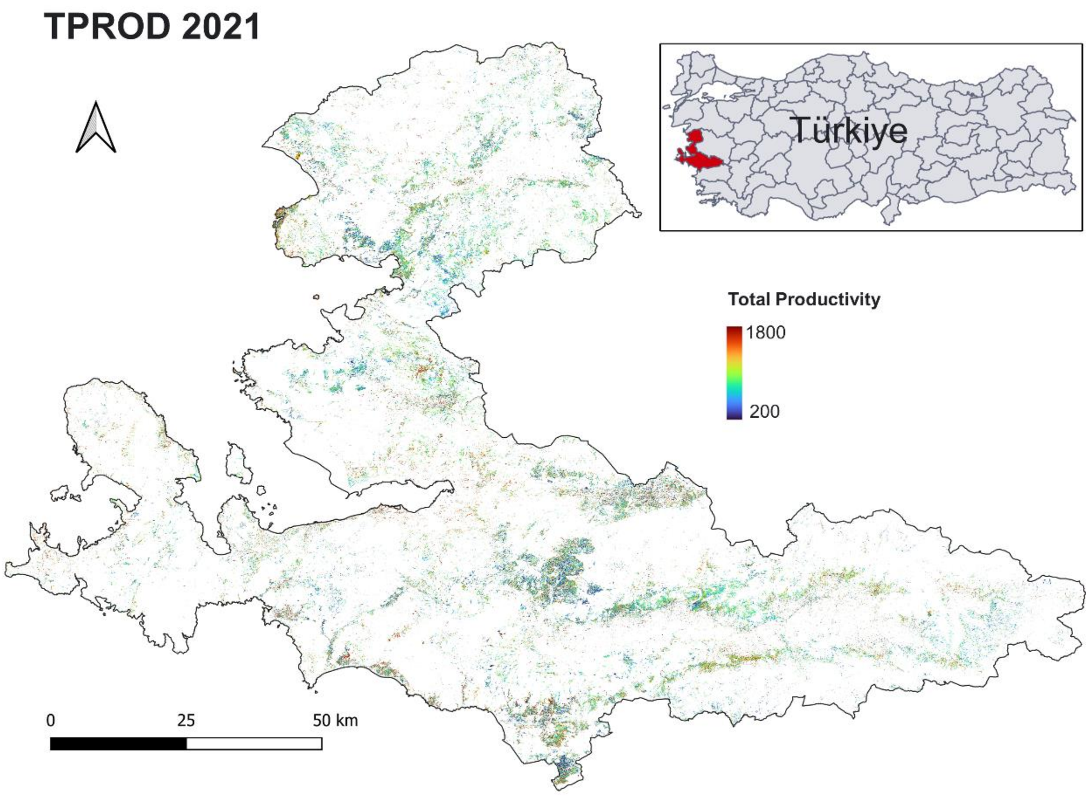

Figure E.5 : Total productivity (TPROD) map of 2021.

CURRICULUM VITAE

Name Surname : Haydar Muhammed AKÇAY

EDUCATION :

- **B.Sc.** : 2009, Istanbul Technical University, Civil Engineering Faculty, Geomatics Engineering
- **M.Sc.** : 2013, Istanbul Technical University, Graduate School, Geomatics Engineering

PUBLICATIONS, PRESENTATIONS AND PATENTS ON THE THESIS:

- **Akcay, H.,** Kaya, S., Sertel, E., and Alganci, U. (2019). Determination of olive trees with multi-sensor data fusion. 8th International Conference on Agro-Geoinformatics (Agro-Geoinformatics) (pp. 1-6). IEEE.
- **Akcay, H.,** Kaya, S., Sertel, E., and Alganci, U. (2019) Separating Olive Trees From Agricultıral Areas and Bare Lands By Using Spectral Indices With Multi-Temporal Sentinel-2 Images. International Symposium on Applied Geoinformatics 1 (1), 415-420
- **Akcay, H.,** Kaya, S., Sertel, E., Alganci, U., and Aksoy, S. (2021). Sentinel-1 and-2 time-series data-fusion for olive tree identification in heterogeneous land surfaces using Google Earth Engine. Intercontinental Geoinformation Days, 2, 159-162.
- **Akcay, H.,** Kaya, S., Sertel, E., Aksoy, S., and Dash, J. (2023) Evaluating the potential of multi-temporal Sentinel-1 and Sentinel-2 data for regional mapping of olive trees, *International Journal of Remote Sensing*, *44:23*, 7338-7364, DOI: 10.1080/01431161.2023.2282404

OTHER PUBLICATIONS, PRESENTATIONS AND PATENTS:

- Brown, L.A., Morris, H., Morrone, R., Sinclair, M., Williams, O., Hunt, M., Bandopadhyay, S., Guo, X., **Akcay, H.** and Dash, J. (2024). Near-infrared digital hemispherical photography enables correction of plant area index for woody material during leaf-on conditions. *Ecological Informatics, 79, p.102441*.